Thesis for the degree of Doctor of Philosophy

Observations of submillimeter galaxies and of the Sunyaev–Zeldovich effect toward clusters of galaxies

Daniel Johansson

Department of Earth and Space Sciences
CHALMERS UNIVERSITY OF TECHNOLOGY
Göteborg, Sweden 2011

Observations of submillimeter galaxies and of the Sunyaev–Zeldovich effect toward clusters of galaxies

DANIEL JOHANSSON
ISBN 978-91-7385-519-8

Doktorsavhandlingar vid Chalmers tekniska högskola
Ny serie nr 3200
ISSN: 0346-718X

Radio Astronomy & Astrophysics group
Department of Earth and Space Sciences
Chalmers University of Technology
SE–412 96 Göteborg, Sweden
Telephone: +46 (0)31–772 1000

Cover
Color image: LABOCA map of the Bullet Cluster. The dark spots are distant galaxies.
Spectrum: Detections of two rotational transitions of carbon monoxide in the brightest galaxy in the LABOCA map.

Printed in Sweden
Chalmers Reproservice
Göteborg, Sweden 2011

Observations of submillimeter galaxies and of the Sunyaev–Zeldovich effect toward clusters of galaxies

DANIEL JOHANSSON
Department of Earth and Space Sciences
Chalmers University of Technology

Abstract

This thesis describes observations of a population of high-redshift, dusty star-forming galaxies: the submillimeter (submm) galaxies. The submm galaxies detected so far are very massive and luminous systems, with huge star-formation-rates (SFR $> 100\,M_\odot\,\mathrm{yr}^{-1}$), large reservoirs of molecular gas ($M_{\mathrm{gas}} \sim 1 \times 10^{10}\,M_\odot$) and large dynamical masses ($M_{\mathrm{dyn}} > 10^{10}\,M_\odot$). The median redshift of detected submm galaxies is $z \sim 2.2$, which corresponds to a look-back time of 10 Gyr.

We have used the LABOCA bolometer camera mounted on the APEX telescope in Chile to search for gravitationally lensed submm galaxies behind massive galaxy clusters (with a total mass $M_{\mathrm{clust}} > 5 \times 10^{14}\,M_\odot$). The gravitational magnification induced by the galaxy clusters boosts the observed flux densities of the background submm galaxies and allows us to probe deeper into the faint galaxy population. The number counts of submm galaxies show that there are many more faint galaxies than bright ones, and thus the properties of the bright submm galaxies mainly studied so far may not be representative of the bulk of the population.

In two papers we present our results of the observations toward galaxy clusters. In paper I, we discuss a merging galaxy cluster: the Bullet Cluster at redshift $z \sim 0.3$. The huge mass concentration provides large magnification factors, and one of the background galaxies detected with LABOCA is gravitationally magnified ~ 100 times. The number of galaxies detected toward the Bullet Cluster is consistent with previously published number counts, and we probed the number counts to some of the lowest flux density levels so far. Paper I also includes a study of the multi-wavelength-properties of the LABOCA galaxies, where we identified counterparts in infrared Spitzer maps.

In paper II the study of submm galaxies lensed by clusters was extended with four additional clusters. The number of detected galaxies was more than doubled compared to paper I. A more sophisticated method was used to determine the magnification factors for each galaxy, and to correct the number counts for the effect of magnification differences across the map. The number counts agree with previous work but may indicate a flattening towards low flux densities. A study of the faint, unresolved background population was also included, via the stacking technique. We used the positions of all sources detected in Spitzer 24 μm maps across the observed LABOCA fields. The LABOCA flux was extracted at each 24 μm position and when added together this yielded a 14.5σ detection, and a signal 5 to 10 times lower than the adopted flux limit for extraction of significant sources in the maps. In combination with gravitational magnification, stacking makes it possible to probe deeper into the submm population, although only mean properties of the faint galaxies can be derived.

Having studied the observational properties of a sample of submm galaxies in paper III we focused on one particular galaxy behind the Bullet Cluster, SMM J0658, gravitationally magnified up to 100 times in total. The strong lensing caused by the total cluster potential and an elliptical galaxy within the cluster gives rise to three images of the same background galaxy. In our

observations with a radio/mm interferometer, the Australia Telescope Compact Array (ATCA), we detected two rotational transitions of the carbon monoxide (CO) molecule in SMM J0658. CO is commonly used as a tracer of the more abundant molecule H_2, which constitutes a large fraction of the molecular gas in galaxies. Because of the large magnification factor of this galaxy it is possible to probe the physical conditions in a system with ten times less molecular gas and a lower star formation rate than the bright submm galaxy population studied so far.

Finally, I have participated in the APEX-SZ project. APEX-SZ is a bolometer camera operating at 2 mm wavelength, designed with the aim of detecting the Sunyaev–Zeldovich decrement in clusters of galaxies. The Sunyaev–Zeldovich effect is a secondary anisotropy to the Cosmic Microwave Background (CMB) radiation. It is due to inverse Compton scattering of CMB photons by hot electrons in the cluster gas. At 2 mm the SZ effect gives rise to a lower temperature when compared to the 2.7 K radiation. I participated in six observing runs in Chile between 2008 and 2010. The scientific studies with APEX-SZ focus on the physical state of the intra-cluster gas in galaxy clusters. In two of the papers summarized in this thesis the APEX-SZ detection was used together with XMM-Newton X-ray observations to constrain non-parametric models for the distribution and temperature of the hot gas. The existence of dusty galaxies within high-redshift galaxy clusters is a possible explanation as to why several high-redshift galaxy clusters have eluded detection in Sunyaev–Zeldovich experiments.

List of appended papers

This thesis is based on the following research papers. References to the paper will be made using the Roman numbers associated with the paper.

I Johansson, D., Horellou, C., Sommer, M. W., Basu, K., Bertoldi, F., Birkinshaw, M., Lancaster, K., Lopez-Cruz, O., & Quintana, H., *Submillimeter galaxies behind the Bullet cluster (1E 0657-56)*, A&A, 2010, 514, A77

II Johansson, D., Sigurdarson, H., & Horellou, C., *A LABOCA survey of submillimeter galaxies behind galaxy clusters*, A&A, 2011, 527, A117

III Johansson et al, *Molecular gas and dust in a highly magnified galaxy at* $z \sim 2.8$, to be submitted to A&A

I have also participated in the following published papers, which are not appended. Summaries of these paper are included in Chapters 2 and 3 of this thesis.

A) Nord, M., Basu, K., Pacaud, F., Ade, P. A. R., Bender, A. N., Benson, B. A., Bertoldi, F., Cho, H.-M., Chon, G., Clarke, J., Dobbs, M., Ferrusca, D., Halverson, N. W., Holzapfel, W. L., Horellou, C., Johansson, D., Kennedy, J., Kermish, Z., Kneissl, R., Lanting, T., Lee, A. T., Lueker, M., Mehl, J., Menten, K. M., Plagge, T., Reichardt, C. L., Richards, P. L., Schaaf, R., Schwan, D., Spieler, H., Tucker, C., Weiss, A., & Zahn, O., *Multi-frequency imaging of the galaxy cluster Abell 2163 using the Sunyaev-Zel'dovich effect*, A&A, 2009, 506, 623-636

B) Reichardt, C. L., Zahn, O., Ade, P. A. R., Basu, K., Bender, A. N., Bertoldi, F., Cho, H.-M., Chon, G., Dobbs, M., Ferrusca, D., Halverson, N. W., Holzapfel, W. L., Horellou, C., Johansson, D., Johnson, B. R., Kennedy, J., Kneissl, R., Lanting, T., Lee, A. T., Lueker, M., Mehl, J., Menten, K. M., Nord, M., Pacaud, F., Richards, P. L., Schaaf, R., Schwan, D., Spieler, H., Weiss, A., & Westbrook, B., *Constraints on the High-ℓ Power Spectrum of Millimeter-Wave Anisotropies from APEX-SZ*, ApJ, 2009, 701, 1958-1964

C) Basu, K., Zhang, Y.-Y., Sommer, M. W., Bender, A. N., Bertoldi, F., Dobbs, M., Eckmiller, H., Halverson, N. W., Holzapfel, W. L., Horellou, C., Jaritz, V., Johansson, D., Johnson, B., Kennedy, J., Kneissl, R., Lanting, T., Lee, A. T., Mehl, J., Menten, K. M., Navarrete, F. P., Pacaud, F., Reichardt, C. L., Reiprich, T. H., Richards, P. L., Schwan, D., & Westbrook, B., *Non-parametric modeling of the intra-cluster gas using APEX-SZ bolometer imaging data*, A&A, 2010, 519, A29

D) Rex, M., Rawle, T. D., Egami, E., Pérez-González, P. G., Zemcov, M., Aretxaga, I., Chung, S. M., Fadda, D., Gonzalez, A. H., Hughes, D. H., Horellou, C., Johansson, D., Kneib, J.-P., Richard, J., Altieri, B., Fiedler, A. K., Pereira, M. J., Rieke, G. H., Smail, I., Valtchanov, I., Blain, A. W., Bock, J. J., Boone, F., Bridge, C. R., Clement, B., Combes, F., Dowell, C. D., Dessauges-Zavadsky, M., Ilbert, O., Ivison, R. J., Jauzac, M., Lutz, D., Omont, A., Pelló, R., Rodighiero, G., Schaerer, D., Smith, G. P., Walth, G. L., van der Werf, P., Werner, M. W., Austermann, J. E., Ezawa, H., Kawabe, R., Kohno, K., Perera, T. A., Scott, K. S., Wilson, G. W., & Yun, M. S., *The far-infrared/submillimeter properties of galaxies located behind the Bullet cluster*, A&A, 2010, 518, L13

E) Pérez-González, P. G., Egami, E., Rex, M., Rawle, T. D., Kneib, J.-P., Richard, J., Johansson, D., Altieri, B., Blain, A. W., Bock, J. J., Boone, F., Bridge, C. R., Chung, S. M., Clément, B., Clowe, D., Combes, F., Cuby, J.-G., Dessauges-Zavadsky, M., Dowell, C. D., Espino-Briones, N., Fadda, D., Fiedler, A. K., Gonzalez, A., Horellou, C., Ilbert, O., Ivison, R. J., Jauzac, M., Lutz, D., Pelló, R., Pereira, M. J., Rieke, G. H., Rodighiero, G., Schaerer, D., Smith, G. P., Valtchanov, I., Walth, G. L., van der Werf, P., Werner, M. W., & Zemcov, M., *Improving the identification of high-z Herschel sources with position priors and optical/NIR and FIR/mm photometric redshifts*, A&A, 2010, 518, L15

Acknowledgements

First I would like to say that I have had a wonderful time working as a PhD-student during these five years. I have met many interesting, smart, funny and friendly people, I have spent a lot of my time at the Onsala space observatory and enjoyed the beautiful surroundings and the hospitality of the people working there. I have travelled around the world to observe with different telescopes and to go to conferences. And the most important: I have had the privilege to work in scientific projects with the aim to understand how the Universe works!

First of all, I thank my supervisor Cathy Horellou for making this possible. I have learned so much from you over these years; from the physical laws of the Universe to how one writes a good paper. With her constant enthusiasm in the projects we have been working on she has been able to keep also my spirit up, also at times when the tasks have seemed overwhelmingly complicated. I am very glad that you have always taken the time to discuss our research and always kept your door open. Even at times when the answers to my questions have been obvious. I think that we have had a very positive collaboration over the years and I hope that it will continue.

During the last six months I have worked on the project which finally lead to Paper III in this thesis. While working on the interferometric data Sebastien Muller has been my guide through everything from technical problems with data reduction to the interpretation of our observations and scientific conclusions. Thanks Seb! A warm thank you goes to John Black, my examiner, who appears to always understand any of my research problems better than I do. That is an formidable quality in a researcher. John: it is always a great pleasure to discuss research and other things with you! Thanks also to Haukur for all the hard work on the lensing models in Paper II.

There are several other colleagues that I would like to thank. First, Camilla, Margareta, Paula, Vivi, Ingrid, Eva and Katarina for keeping track of me when needed and for many good times. Thanks to Rodrigo, Evert and Carina who, having started their PhD a few years before me, could share their eternal wisdom about how to make the life and work as a PhD student easier. A special thank you to my former office-mate Eva, with whom I shared offices during one year, for all the help. My new office mate Robert has a fantastically positive spirit and an ability to always find new explanations or suggestions for my many blob-like galaxies. He really manages to think outside the box. Thanks for all the help over the last year Robert! Thanks to Alessandro for interesting discussions, and a special thanks to Magnus Thomasson for reading this thesis and coming up with lots of suggestions on how to improve it. Thanks to Kirsten for interesting discussions about submm galaxies.

I have also worked in collaboration with the APEX-SZ team. I spent several weeks on observing runs in Chile and had a lot of fun there, both while observing in the late nights with James, as well as hanging out at the BBQ. Thank you Adrian, Amy, James, Arti, Filipe, Kaustuv, Nils,

Ben, Cathy, Brad and others. Thanks also to the APEX staff for all the help over the years and for creating such a nice atmosphere at the telescope. Those worth a special mention: Andreas, Rodrigo, Paco, Felipe, David, Giorgio, Claudio, Mauricio x 2.

To all my friends near and far, thanks for bearing with me at times when my work has been the only thing on my mind. First of all, thank you Niklas & Niklas. With your help, both as friends but also as my scientific likes, we've hopefully all learned something over the years, both about science but also about life. Thanks to Caroline, Sandra, Daniel, Jannicke, Robin, Sandra for your lovely company over the years. At first I was about to put my fellow Phd-students (and postdocs) in a separate paragraph, but I think that you are much more than colleagues: you have become some of my best friends. Fabien, Francesco, Rossa, Simon, Tony and last but not the least Per. A special thank you to Per for being such a good friend, for taking time to talk about important things and for caring. Thanks for your support and thank you for all the good times, late nights, conferences and observations together. Finally the fab three, Rikard, Daniel and Dawid: it is so nice to still have you there after all these years!

To my parents Karin and Tore, you have always been there for me. And I am happy that you have supported me in pursuing my studies to higher and higher levels. To Stefan and Lena, thank you too for your support. I hope that I can be there for you when you need it. And finally: to Emma, it took some time for us to find each other. I am so happy together with you, and I am eager to see where the future takes us. Together is sufficient for me.

Daniel, Göteborg 2011

Contents

Preface

Calvin and Hobbes are standing outside gazing up on the starry night sky.

C — If people sat outside and looked at the stars each night, I'll bet they'd live a lot differently.
H — How so?
C — Well, when you look into infinity, you realize that there are more important things than what people do all day.
H — We spent our day looking under rocks in the creek.
C — I mean *other* people.

Bill Watterson

Looking up on the breathtaking night sky in a dark area, one can understand why it took astronomers such a long time to discover that most of the stars in the universe are located in other galaxies than our own. All the stars in our galaxy are blocking the view of the remaining Universe, and as late as hundred years ago it was believed that the Milky Way contained the entire Universe. Since then, our view of the Universe as a whole and of the galaxies that reside in it has changed dramatically, and the extragalactic nebulae have been given more and more focus by astronomers. Today's cosmological models predict many observable properties of our Universe. But many open questions in the subject of galaxy formation persist: *When did the first galaxies form? What are the progenitors of the massive submillimeter and radio galaxies that are detected at redshifts 2–5? Which is the evolutionary track for a star-forming galaxy? How does the growth of a supermassive black hole and onset of Active Galactic Nuclei (AGN) activity in the center of some galaxies occur? What happens with the massive high-redshift galaxies: do they end up as massive ellipticals in the center of galaxy clusters, as has been suggested?*

These are a few of the questions currently being researched. I will not even try to answer all of them in this thesis; but I will provide one small piece to the puzzle of galaxy formation.

About fifteen years ago a new window on our universe was opened up when the SCUBA instrument started observations on the James Clerk Maxwell Telescope (JCMT) on Mauna Kea, Hawaii. Prior to SCUBA, the IRAS satellite had detected infrared emission from low-redshift galaxies and shown that a small fraction of the local galaxies had very large infrared luminosities, which indicated the existence of large amounts of heated dust. Observations with the COBE satellite indicated a cosmic infrared signal arising from earlier times in the history of the Universe than the IRAS-detected galaxies. The SCUBA observations showed that the cosmic signal, when observed with an instrument sufficiently sensitive and with good spatial resolution, consisted of dusty, high-redshift galaxies. Since then, these submillimeter galaxies (submm galaxies, SMGs) have been thorougly studied. To understand the physical conditions in submm galaxies, multi-wavelength observations are necessary.

Which kind of observations are made to learn more about the high-redshift galaxies? Near-

infrared observations probe the old stellar population, and spectroscopy can detect atomic spectral lines from galaxies. If the dust is heated by a starburst - a "burst" of star-forming activity which is often causud by interaction with other galaxies - the mid-infrared spectrum shows strong emission lines from polycyclic aromatic hydrocarbons (PAHs), large carbon chain molecules known to form in stellar regions. At longer wavelengths we see the redshifted peak of the thermal dust emission, which peaks at $\sim$ 350 μm for submm galaxies. In the submm/mm part of the spectrum we can observe, in addition to continuum emission from dust, emission lines from several molecular species. Finally in the radio we can detect the synchrotron emission from electrons accelerated by supernova explosions. The radio flux and the far-infrared luminosity follow a surprisingly tight correlation, the FIR-radio correlation.

In this thesis, I present studies of submillimeter galaxies, as well as studies of clusters of galaxies and the temperature anisotropy that they induce on the cosmic microwave background temperature. The thesis is organized as follows. Chapter 1 is an introduction to the various methods and concepts that I have studied. First, I describe the submillimeter galaxies in Sect. 1.1. Section 1.2 gives a short introduction to cosmology, growth of structure and clusters of galaxies, while the the Sunyaev–Zeldovich effect is presented in section 1.3. The first chapter ends with a introduction to gravitational lensing (Sect. 1.4) and a description of the APEX telescope (Sect. 1.5). Chapter 2 includes the three main papers of the thesis, that are focused on studies of submm galaxies. The three sections has short descriptions of the papers I, II and III. Chapter 3 includes papers about Sunyaev–Zeldovich observations of clusters of galaxies. In chapter 4 I describe briefly the serendipitous detection of an ultra-bright submillimeter source and the follow-up program that we have initiated to detect counterparts at other wavelengths. Finally, the conclusions are found in chapter 5.

Thank you for reading this thesis. I hope that you will enjoy it.

Chapter 1

Introduction

Calvin and Hobbes are sitting at Calvin's desk. Hobbes is holding a piece of paper, looking puzzled.

C — I think we've got enough information now, don't you?
H — All we have is one "fact" that you made up.
C — That's plenty. By the time we add an introduction, a few illustrations, and a conclusion, it will look like a graduate thesis.

Bill Watterson

1.1 Submillimeter and infrared bright galaxies

The sensitivity of observations in the mid- and far-infrared part of the electromagnetic spectrum has been lagging behind that achieved in optical and radio observations for a long time. It was not until the 1970s that the first infrared bright galaxies were detected (Rieke & Lebofsky, 1979). The IRAS satellite, launched in 1983, discovered dust emission from normal spiral galaxies, as well as a high-luminosity tail of galaxies (e.g. Lagache et al., 2005). These Luminous InfraRed Galaxies (LIRGs) emit most of their energy in the infrared part of the spectrum, and their far-infrared luminosity, $L_{\rm FIR}$, is between $10^{11}\,L_\odot$ and $10^{12}\,L_\odot$. Similarly, the Ultra Luminous InfraRed Galaxies (ULIRGs) have $10^{12}\,L_\odot < L_{\rm FIR} < 10^{13}\,L_\odot$.

Submillimeter galaxies are a population of high-redshift dusty galaxies. All submm galaxies detected so far can be categorized as LIRGs or ULIRGs. They were discovered in the 1990s by the submillimeter and millimeter bolometer cameras SCUBA (on the JCMT telescope on Hawaii) and MAMBO (on the IRAM 30m telescope in Spain). The submm galaxies are the source of the extragalactic cosmic infrared background (CIB), a uniform and isotropic background radiation in the infrared band which was detected by the COBE satellite (e.g. Hauser et al., 1998). Due to the coarse resolution and insufficient sensitivity of COBE the sources giving rise to this background radiation could not be resolved.

1.1.1 Properties of the submillimeter galaxies

The ground-based telescopes provided angular resolutions far better than the COBE satellite. Observations with bolometer cameras thus resolved the infrared background into individual sources. Follow-up studies confirmed that the sources giving rise to the infrared background are high-redshift, dust-obscured galaxies. Today, several hundreds of submm galaxies have been detected in surveys with SCUBA (e.g. Serjeant et al., 2003; Coppin et al., 2006), MAMBO (e.g. Bertoldi

et al., 2007), AzTEC (e.g. Scott et al., 2008; Austermann et al., 2009) and LABOCA (e.g. Beelen et al., 2008; Weiß et al., 2009), paper I and II.

The Spectral Energy Distribution (SED) of dust in submillimeter galaxies can be described by a greybody spectrum in the infrared band that peaks at mid-infrared wavelengths. Dust heating by visible and UV photons causes the dust particles to radiate thermal emission. The dust is believed to be amorphous silicate grains and carbonaceous grains in sizes ranging from a few molecules to several hundreds of nanometers (Lagache et al., 2005). A greybody spectrum is a blackbody spectrum modified by an emissivity factor $\epsilon_\nu \propto \nu^\beta$, where β takes values between 1 and 2. The dust temperatures range between 20-200 K and variation can be due to differences in grain size or radiation fields (e.g. Blain et al., 2002). Such temperatures result in a spectrum that peaks at $\sim 100\,\mu$m. The large amounts of heated dust in submm galaxies give rise to large far-infrared luminosities and high star-formation rates (SFR). Submm galaxies show substantial extinction at visible wavelengths due to the large amounts of dust.

Because submillimeter galaxies are located at high redshifts the peak of the SED is redshifted towards the FIR wavelengths. Submm observations sample the SED where it is rising towards the peak in the mid-infrared. At the same time as the submm flux of these galaxies increases due to the redshifted thermal emission, the cosmological dimming factor lowers the flux by a similar magnitude. These two competing effects counteract each other and the resulting property of submm galaxies is an almost redshift-independent flux density at redshifts $z > 1$, for observations around 870 μm. This effect is illustrated in Fig. 1.1. The curves in that figure are calculated for a concordance cosmology, a dust temperature 38 K, and standard values for the dust emissivity index β and the mid-infrared spectral index α. Out of these parameters the redshift dependence of the SEDs is most sensitive to the value of the dust temperature, and less sensitive to the emissivity- and spectral indices (see eg. Blain et al., 2002, Fig. 5). Thus, submm surveys can detect galaxies out to very large redshifts, if they contain sufficient amounts of heated dust.

Examples of actual galaxy SEDs are shown in Fig. 1.2 for a ULIRG, a star-forming galaxy, a spiral and an elliptical galaxy. The difference between the ULIRG and the elliptical galaxy is striking. ULIRGs emit most of their power in the infrared, while the elliptical (which has low gas and dust contents) mostly emits in the visible. The bright spectral lines around 10 μm are caused by Polycyclic Aromatic Hydrocarbons (PAHs) (e.g Lagache et al., 2004). PAH features are also found around stars, HII regions and planetary nebulas and are tracers of star formation (Allamandola et al., 1989; Lagache et al., 2005).

1.1.2 Number counts of submillimeter galaxies

When studying a new population of astronomical sources it is interesting to deduce the number density of sources and how bright they are. Those properties can be summarized into the so-called number counts, which describe the number of sources per solid angle on the sky with a certain flux density. The number counts of submm galaxies have been derived in several surveys with good agreement (see the compilation in Paper I, or Coppin et al. 2006). The number counts rise toward low fluxes, meaning that there are more faint sources than bright ones. At these wavelengths the cosmic infrared background is thus dominated by a large number of faint sources – and not by a small number of bright sources. Therefore, observations of blank fields[1], which are biased towards finding bright sources, do not resolve a large portion of the infrared background. It is essential to complement such blank-field surveys (e.g. Weiß et al. 2008) by using gravitational lensing to

[1]A blank field is a part of the sky where there is no known large-scale structure that significantly boosts the brightness of background sources due to gravitational lensing.

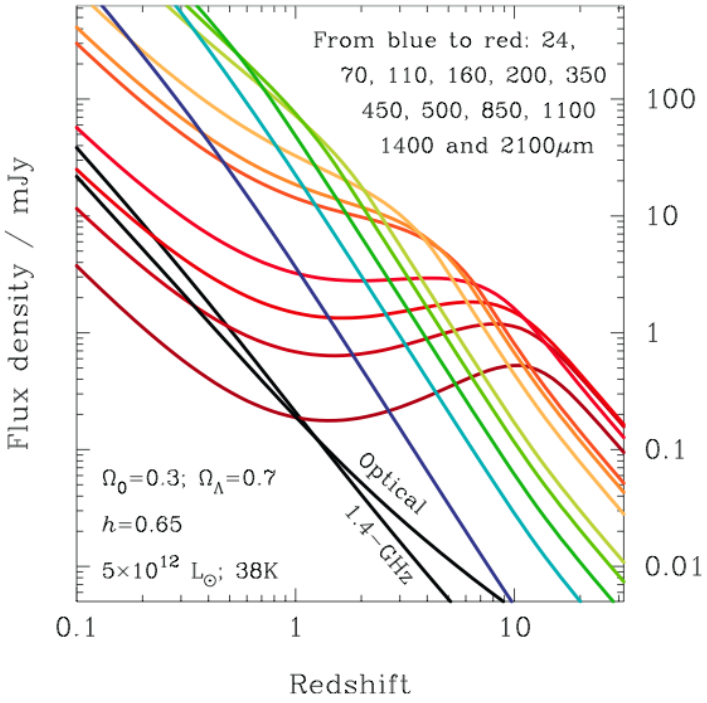

Figure 1.1: Flux density–redshift dependence for a submm galaxy with far-infrared luminosity $L_{\rm FIR} = 5 \times 10^{12}\,L_{\odot}$, taken from Blain et al. (2002). Each curve corresponds to one observational band, from 24 μm (blue) to 2100 μm (dark red). The steepness of the curves for the short wavelengths shows that observations sample mostly low-redshift galaxies. The 850 μm curve, in contrast, is flat between redshifts 1–10, meaning that galaxies with the same physical properties at redshift 1 and 10 should be almost equally bright, despite of their different distances.

probe the fainter source counts that are mainly responsible for the infrared background. That is the subject of the following section.

Gravitational lensing of submm galaxies

Several groups have used the gravitational magnification induced on background galaxies by massive galaxy clusters. Most of the information that we have today about the faint submm galaxy distribution is deduced from observations of galaxies lensed by galaxy clusters (e.g. Smail et al., 1997; Chapman et al., 2002; Knudsen et al., 2008, Paper I and Paper II). In the massive Bullet Cluster, which is studied in the three papers in this thesis, the magnification factor close to the center of mass is ~ 100 (Bradač et al., 2006). Such large magnification factors are rare and the Bullet Cluster provides a laboratory in which we can probe deep into the faint population of submm galaxies.

Because magnified galaxies often are the brightest, they provide good opportunities for follow-up observations at other wavelengths. The mapping speeds of submillimeter cameras have increased in recent years, so the probability of detecting such rare objects has increased. Swinbank et al. (2010) reported on the detection of the brightest submm galaxy (at 870 μm) so far. Due to the large magnification factor Swinbank et al. could pinpoint the location of the intense star formation in this galaxy to a handful of bright "knots" using the Submillimeter Array on Mauna Kea, Hawaii. Other detailed studies of submm galaxies include those of Ikarashi et al. (2010);

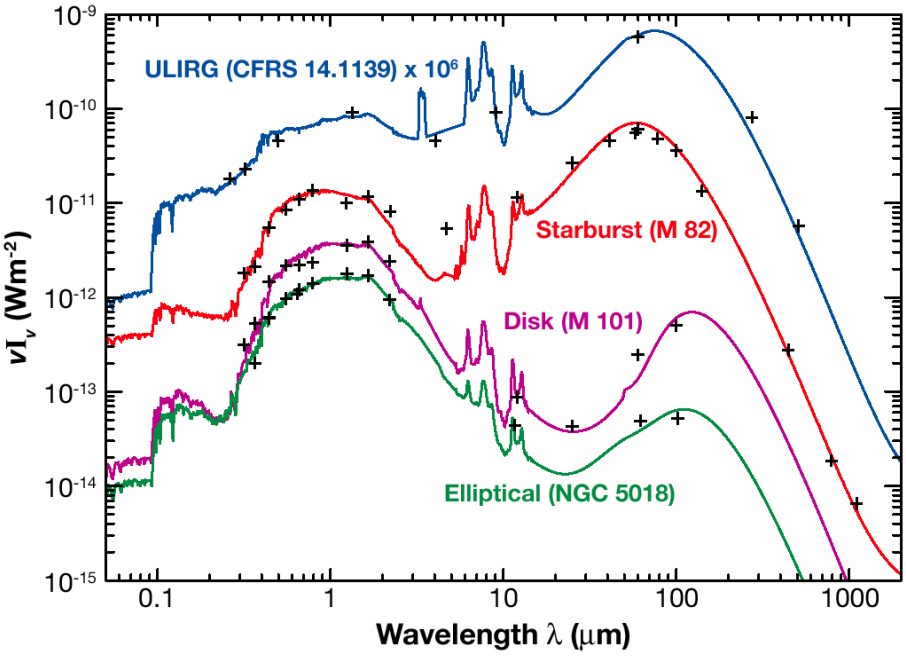

Figure 1.2: Spectral energy distributions for four different galaxy types. Figure adopted from Lagache, Puget, & Dole (2005).

Lestrade et al. (2010); Danielson et al. (2010) and Paper III.

The South Pole Telescope operates in the millimeter domain and studies the Cosmic Microwave Background radiation and its primary and secondary anisotropies. It has also detected many extremely bright, dusty galaxies (Vieira et al., 2010). Similarly, the Herschel Space Observatory has found a population of bright galaxies in the 500 μm band with the instrument SPIRE (Negrello et al., 2010) and has shown that at 500 μm a simple flux cut ($S_{500\,\mu\mathrm{m}} > 100$ mJy) sorts out all strongly lensed sources. Lima et al. (2010) and Hezaveh & Holder (2010) showed that the number of ultra-bright sources in the SPT field is consistent with the results of realistic simulations of lensing probabilities.

1.1.3 Clustering and confusion

All observations of nature are affected by noise. In astronomy the thermal noise in our receivers is reduced in longer observations. Noise induced on the signal by the earth's atmosphere does not integrate down in the same way, but can still be dealt with through proper modelling. Confusion noise, on the contrary, represents a fundamental limit in an observation with a specific telescope. The confusion noise is due to the faint, unresolved background population of galaxies. If there are more faint sources than bright ones[2], the sources that are too faint to be directly detected will act as a constant positive flux level in the observations. When this flux level has been reached it is no longer possible to improve an observation with a certain telescope and of a certain population of galaxies, because of the "sea" of faint sources (Condon, 1974).

The confusion limit S_{conf} can be estimated by using the rule-of-thumb that an image is "confused" when there is one source of flux density S_{conf} in 30 telescope beams (e.g. Hogg, 2001). To

[2]This is often the case in astronomy – and especially true for the population of submm galaxies, as was discussed in the previous section and in papers I and II.

simplify we use a single power-law ($N = N_0\, S^{\alpha}$) distribution for the number counts, where N_0 is a normalization and α the slope, although recent results (e.g. Paper II) show that a double power law is more appropriate. For a power law distribution the confusion level is $S_{\rm conf} = (30 N_0 \Omega_{\rm beam})^{1/\alpha}$ (Knudsen et al., 2008). For a LABOCA observation with the number counts determined by Barger et al. (1999) the confusion level is 2.5 mJy. This means that if sources are detected in a LABOCA map in an unlensed region with flux densities below 2.5 mJy, these detections cannot be trusted. It also means that more observations are not useful.

Gravitational lensing can raise faint sources above the confusion limit. For a magnification factor μ the flux densities of sources in the field will be μ times higher. One could think that the confusion level will rise with the same factor, but because the plane on the sky being imaged is intrinsically smaller because of the magnification, the number of sources per beam is actually less. Therefore, the confusion level in the lensed case is $\sqrt{1/\mu}$ times lower than in the blank-field case. This is why observations of gravitationally lensed submm galaxies can probe so deeply into the faint population.

Clustering in the observed population also induces confusion noise in observations. This effect was studied by Negrello et al. (2004) who found that surveys with poor spatial resolution will be more affected by confusion noise because the ratio of the "normal" Poisson confusion noise to the clustering confusion noise increases with higher spatial resolution. Thus, confusion noise due to clustering is not a major problem for ground-based submm observations with large antennas, but can be substantial for e.g. the Planck satellite. The existence of clustering in the submm galaxy population is mainly based on the fact that most submm galaxies detected so far have dark matter halos with inferred masses $M \sim 10^{13}\, M_{\odot}$, Negrello et al. (2004). These massive dark matter halos sample the highest density peaks of the dark matter distribution, and should therefore be strongly clustered. It is from these overdensities that the clusters of galaxies are believed to have formed. Several authors have claimed tentative detections of clustering of submm galaxies (e.g. Blain et al., 2004; Weiß et al., 2009; Maddox et al., 2010).

1.1.4 Redshift distribution

Chapman et al. (2005) presented the first survey of the redshift distribution of submm galaxies. Before deriving the redshift from optical spectroscopy, a precise position must be determined from deep radio continuum maps, which have a factor of ten higher angular resolution than the original submm maps. The median redshift of the galaxies in the sample of Chapman et al. (2005) is 2.2. Using a much larger catalog of sources detected with Herschel SPIRE, Amblard et al. (2010) showed that the redshift distribution peaks at $z \sim 2.2$, where the redshift was derived from photometric techniques. Aretxaga et al. (2007) presented a similar analysis for the sources found in the SCUBA SHADES survey, and found that 50% of the 120 sources detected were at redshifts $1.8 < z < 3.1$.

The Cosmic Infrared Background – star formation history of the universe

The instruments DIRBE (designed to measure a cosmic infrared background) and FIRAS (designed to measure the spectral shape of the CMB) on COBE found evidence of the CIB. Analysis of DIRBE data revealed an excess isotropic signal in the 140 and 240 μm bands (Hauser et al., 1998)[3]. The FIRAS detection (Puget et al., 1996; Fixsen et al., 1998) at wavelengths 2000–125 μm overlaps partly with the DIRBE detection. The results from the two instruments agree

[3]The requirement of isotropy is a necessary property of a cosmic signal. Excess signal from the solar system or our own galaxy is unlikely to be isotropic because of their geometries.

and can be described by a modified blackbody with a dust temperature of 18.2 K (Dwek et al., 1998).

What are the implications of this cosmic infrared background signal? The CIB contains information about the star formation history of the universe; where a major part is believed to be dust re-emission in the infrared of absorbed UV and optical photons. This background signal is the integrated effect from the surface of last scattering until today, i.e. from redshifts $z \sim 1100 - 0$. Therefore this cosmic signal is different from the CMB, which originates from the surface of last scattering and does not aggregate during its journey through the universe. Two types of physical processes can generate the energetic photons that are responsible for the dust heating; nuclear and gravitational forces (Dwek et al., 1998). Photons originating from nuclear forces are created in nucleosynthetic processes in stars, while the gravitational potential energy might come from brown dwarfs, gravitationally collapsing systems or accreting black holes. The submillimeter galaxies appear to have intense dust heating due to a period of intense star formation, and less likely due to accreting of matter around Active Galactic Nuclei (AGN).

1.2 Cosmology and clusters of galaxies

This section starts with a summary of the cosmological model, followed by a discussion of galaxy clusters and how they can be used to constrain the cosmological model.

1.2.1 The cosmological model

Our current understanding of the universe as a whole, the cosmological model, is remarkably simple. The theoretical foundation of the model is the theory of general relativity applied to an isotropic, homogeneous, expanding or contracting universe. A *metric* that meets those requirements is the Friedmann-Lemaître-Robertson-Walker metric, first reported by Friedmann in 1922. The solutions to the field equations for this metric, the Friedmann equations, describe the evolution of the universe within this metric. But to explain the contents of the universe, stars, galaxies and their distribution, appearance and properties, more physics is needed. The Friedmann model only describes the evolution of the universe as a whole.

Recent cosmological results imply that the universe is dominated by two exotic ingredients: *dark matter* and *dark energy*. Dark matter has been given its name because of its main feature; it does not radiate electromagnetic radiation. Its existence is inferred indirectly from observations such as the flat rotation curves or the velocity dispersion in galaxies compared to their mass deduced from their optical luminosity. Dark matter is more abundant than normal baryonic matter (see Table 1.1), and several searches for dark matter candidates are ongoing. Dark energy is even less understood than dark matter. It was discovered as an explanation to the apparent dimming of distant supernovae by two independent observations about a decade ago (Riess et al., 1998; Perlmutter et al., 1999), and its existence has been proven by several different cosmological observations. Dark energy has an equation of state with negative pressure, which acts to accelerate the expansion of the universe. In a universe without dark energy, the gravitational pull of the galaxies would eventually halt the expansion and reverse it, but today's cosmological model with dark energy included supports a forever expanding and accelerating universe.

The cosmic microwave background radiation (CMB) is a remarkably smooth signal that has a temperature of 2.7 K across the sky. It originates from the surface of last scattering, which occurred at redshift $z \sim 1100$, or a few hundred thousand years after the big bang. When the temperature of the universe decreased to 3000 K the photons did not ionize hydrogen atoms anymore, and the electrons and protons recombined into H atoms and made the universe transparent, so that the photons decoupled from the matter. These photons have since then travelled through the universe and are today seen as the 2.7 K CMB signal. The COBE satellite detected small variations of order $\Delta T/T \sim 10^{-5}$ in the CMB temperature. The variations, or anisotropies, are believed to be caused by gravitational reddening of CMB photon that climbed out of the small potential wells that existed in the universe at the surface of last scattering.

Observations of the CMB also support the existence of dark energy. The location of the acoustic peaks in the power spectrum of the CMB indicate that the universe is flat and the energy-density of the universe is dominated by dark energy (Komatsu et al., 2009). These observations indicate the existence of dark energy through the relation $\Omega_m + \Omega_\lambda = 1$, which states that the universe is flat and that the density of dark energy and dark matter add up to the critical density. The CMB measurements agree well with the supernovae results, although they have different dependence on cosmological parameters (see Fig. 1.3). A summary of the most recent results on cosmological parameter estimation from the WMAP satellite is presented in Table 1.1.

The observed distribution of matter in the universe (dark and baryonic) can be accounted for in the current cosmological model. The early universe was very homogenous, but structure started

Table 1.1: Values of the parameters of the cosmological model from the WMAP five year release (Komatsu et al., 2009), combined with Supernova Ia measurement and the Baryon Acoustic Oscillations method (Percival et al., 2007) which measures the power spectrum of galaxies. σ_8 is the mass variance in 8 Mpc/h spheres. H_0 is the Hubble constant. Ω_b is the fractional density of baryons with respect to the critical density. Ω_c is the density of cold dark matter and Ω_m is the total matter density. For $h = H_0/100 = 0.705$, $\Omega_m = 0.27$. t_0 is the age of the universe. Because the observations also show that the universe is flat, all types of energy must add up to the critical density, creating a universe dominated by dark energy (∼73%), while baryonic matter only constitutes ∼4% and dark matter ∼23%

σ_8	0.812 ± 0.026
H_0	70.5 ± 1.3 km s^{-1} Mpc^{-1}
Ω_b	0.0456 ± 0.0015
Ω_c	0.228 ± 0.013
$\Omega_m h^2$	$0.1358^{+0.0037}_{-0.0036}$
t_0	13.72 ± 0.12 Gyr

growing in the primordial small overdensities that were left after the big bang. These overdensities are also seen as anisotropies in the CMB temperature. There is a correlation between the CMB anisotropies and the large-scale distribution of matter in the universe today. So today's large-scale structure with galaxies, clusters of galaxies, voids and superclusters seem to have grown from initial perturbations in an otherwise smooth medium. The overdensities first expand together with the Hubble flow, but if their density is too high the expansion halts and turns around. This gravitational contraction is responsible for the formation of all structure in the universe

But how does structure grow? Do small "grains" collapse first and merge together with others to form larger and larger gravitationally bound structures? Or do large structures form first and then break up into smaller and smaller entities? The cold dark matter scenario (see e.g. Blumenthal et al., 1984) proposed that dark matter is cold (non-relativistic) at the time of decoupling. The *bottom–up* structure formation has proven to agree well with most cosmological observations, although it can still not explain the details of galaxy formation. The interplay between dark matter and visible (baryonic) matter and the hydrodynamic and thermodynamic forces complicates the picture of galaxy formation. The cosmological model with dark energy and cold dark matter is called ΛCDM.

1.2.2 Galaxy clusters

Galaxy clusters are used as sensitive probes in cosmology. Since structure forms bottom–up by merging of smaller substructures, larger structures form later in the evolution of the universe. Clusters of galaxies are currently the largest structures that are in virial equilibrium, although there is increasing evidence for mergin sub-clusters at high redshifts. Since the huge gravitational potential helps to retain most of the matter, galaxy clusters are almost closed systems and can be used as tracers of cosmological evolution. Galaxy clusters are extremely massive ($M \sim 10^{14} - 10^{15}\,M_\odot$) and a large fraction of their mass is in the form of dark matter, but they also have large amounts of baryonic matterd. The total mass gives rise to a deep gravitational potential in which the temperature of the baryonic gas becomes so high that the atoms are ionized. For gas in hydrostatic equilibrium with the cluster potential the temperature of the electrons in this plasma is of the order of kilo-electronvolts (keV), which corresponds to ∼100 million K . The galaxies that reside inside galaxy clusters have a complicated interplay with the intracluster medium (ICM).

Galaxy clusters can be detected across the entire electromagnetic spectrum from short to long wavelengths. In the X-ray regime the hot ionized intracluster gas radiates X-rays mainly due

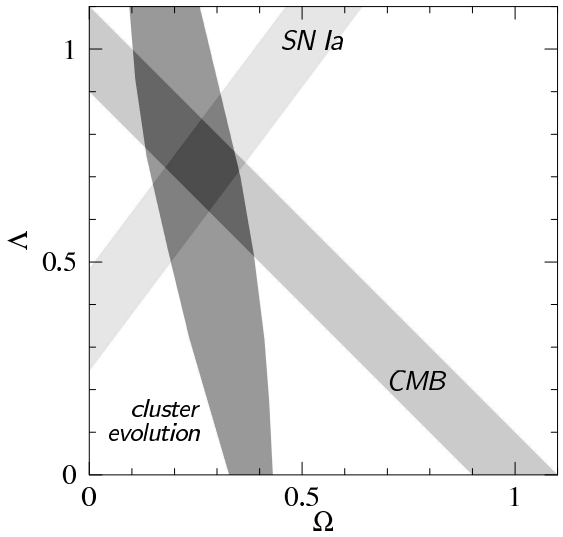

Figure 1.3: 68% confidence levels for dark matter and dark energy densities from supernova dimming, CMB and the evolution of the mass function of clusters of galaxies. Figure adopted from Vikhlinin et al. (2003).

to bremsstrahlung processes; in the optical window galaxy clusters are detected by observing spatially correlated reddened galaxies at a common redshift; and weak-lensing reconstructions using background galaxies can deduce the total mass of the cluster; in the millimeter and sub-millimeter bands the Sunyaev–Zeldovich effect is sensitive to the same gas as the X-ray, but is redshift-independent; and at longer radio wavelengths diffuse synchrotron halos are found in some merging clusters.

Every technique selects different galaxy clusters depending on which physical properties that it is sensitive to. The main cluster survey techniques are described below.

- *Optical observations* Identifying clusters of galaxies by observations of the individual members is possible because galaxies in clusters are redder than other galaxies. Galaxies in clusters are also spatially clustered on the sky. Optical cluster observations are biased towards lower redshift clusters with a brighter population of galaxies. Projection effects, like possible filamentary structure lie along the line-of-sight, may complicate the cluster identification but they can be quantified in simulations (Rosati et al., 2002).

- *X-ray observations*: Clusters emit X-rays mostly because of the radiation emitted when high-energy electrons in the ionized cluster plasma decelerate in electron-ion scatterings (free-free or bremsstrahlung radiation). X-ray observations are thus sensitive to massive clusters with high electron temperatures, and have a different selection function than optical observations, that are based on detection of the galaxies within the cluster. X-ray observations are also biased towards low-redshift galaxy clusters due to the cosmological dimming factor $\sim (1 + z)^{-3}$.

- *Sunyaev–Zeldovich observations*: The Sunyaev–Zeldovich effect arises also in high-temperature electron gas (ICM) as the X-rays, but the two types of observations have different selection functions. The SZ effect is redshift independent and observations are mass-limited, meaning that they will detect all clusters above a certain mass (e.g. Birkinshaw, 1999). The Planck satellite (for a review see e.g. The Planck Collaboration, 2006) launched in 2009 will perform

an all-sky survey and detect hundreds of clusters. The Sunyaev–Zeldovich effect is reviewed in the following section.

The clusters found in optical, X-ray and Sunyaev–Zeldovich surveys are thus different, owing to the different selection function of each technique. The selection function is a complicated function of several parameters; the most important being the redshift and the mass.

1.2.3 Cosmological tests with clusters of galaxies

Why do we study clusters of galaxies, and why is it important to know their masses and redshifts? Because clusters of galaxies are the largest virialized objects in the universe, their abundance, masses and redshift are governed by the cosmological model. A catalog of galaxy clusters can thus be used to constrain the cosmological model.

Cluster mass function

A useful test is the *mass function* which describes the number of clusters above a certain mass limit in a comoving volume element. This semianalytical approach (the Press-Schechter function; Press & Schechter 1974; Bond et al. 1991) combines the growth of linear perturbations with the spherical top hat collapse approach (Voit, 2005). When the density contrast $\Delta\rho/\rho$ exceeds a certain value (which has to be determined from simulations) these overdensities collapse and virialize. These semianalytical models are not rigorously derived and therefore should be seen as "fitting functions" to the results of cosmological simulations. Extending collapse to an elliptical geometry improves the correspondence with current N-body simulations (Sheth et al., 2001).

The mass function thus provides an attractive framework to compare a cluster catalog with theoretical structure formation, without having to resort to time-consuming N-body simulations. By sorting clusters in the catalog in mass and redshift bins, it is straightforward to make fits to the mass function. The confidence levels in Fig. 1.3 show the complementary nature of the different cosmological tests. The cluster mass function is most sensitive to the matter density, but together with CMB experiments it sets powerful constraints can be set on the dark energy density.

Gas mass fraction

Because clusters of galaxies are thought to be representative of the overall cosmic distribution of matter (the fraction of baryonic/dark matter), measurements of the gas mass fraction in galaxy clusters can constrain cosmological parameters. The gas mass fraction ($f_{\rm gas}$) in galaxy clusters can be inferred from deprojection of X-ray observations to find the radial temperature and density dependence (White & Fabian, 1995). The total baryonic content Ω_b of the universe can be determined from either CMB measurements or from big bang nucleosynthesis models and observations of deuterium in high-redshift systems (Rosati et al., 2002). The dark matter density is then simply $\Omega_m = \Omega_b/f_{\rm gas}$ (Fabian, 1991).

The $f_{\rm gas}$ test can be extended to probe the dark energy in the universe (Allen et al., 2008), by using the fact that the $f_{\rm gas}$ measurements depend on the assumed distances to the clusters. If the gas mass fraction is approximately constant with redshift, the gas mass fractions can be used to measure constrain the cosmological parameters through the angular diameter distance. Together with other methods these studies set constraints on the dark matter density, dark energy density and the dark energy equation of state.

1.3 The Sunyaev–Zeldovich effect

In the previous section the properties of clusters of galaxies and methods of their detections were discussed. Here I describe the Sunyaev–Zeldovich effect which is a technique that was discovered over 40 years ago, but only recently has reached maturity as a method for cluster studies.

In the late 1960s and early 1970s, R.A. Sunyaev & Y.B. Zeldovich laid the ground for what we today call the Sunyaev–Zeldovich (SZ) effect. The SZ effect is the distortion of the Cosmic Microwave Background radiation caused by the scattering process with hot electrons in galaxy clusters. The process can be described as an inverse Compton scattering. Since every scattered photons gains energy the blackbody spectrum of the CMB is shifted towards higher temperature, causing an increased intensity at high frequencies and a decreased intensity at low frequencies. The turning point (which is called the crossover frequency) is located around the frequency $\nu \simeq 217$ GHz. For common values of cluster parameters, the ratio of the SZ intensity to the CMB intensity is approximately 10^{-3}, indicating the magnitude of the SZ signal.

The magnitude of the SZ effect is independent of redshift, because it is only a distortion to the CMB photons, not an emission process. For a galaxy cluster with the same mass and electron temperature, the magnitude of the Sunyaev–Zeldovich signal is equally large at all redshifts. Using the SZ effect as a method of cluster detection thus has an advantage over other methods (e.g. X-ray observations) in which the magnitudes of objects depend on the luminosity distance (which diminishes with the inverse second power of the redshift) rendering high-redshift clusters hard to detect. The Sunyaev–Zeldovich signal does not give any information about the redshift of the galaxy cluster. The redshift can be determined in photometric or spectroscopic observations of cluster member galaxies in the optical, or by X-ray spectroscopy of atomic lines in the ICM.

The SZ effect depends on the CMB flux density, which is described by a Planck spectrum. The flux per solid angle and frequency interval is described by the formula

$$I = I_0 \frac{x^3}{e^x - 1} \quad \text{where} \quad x = \frac{h\nu}{kT}. \tag{1.1}$$

x is a non-dimensional frequency. ν is the frequency, h is Planck's constant, k is Boltzmann's constant, T is the CMB-temperature and $I_0 = 2(kT)^3/(hc)^2$. In most cosmological models the frequency and temperature of the CMB have the same dependence on cosmological redshift, and thus the dimensionless frequency is redshift-independent[4]. The distortion due to the SZ effect can be calculated using either the non-relativistic approximation, which is described in Sect. 1.3.1 or the more precise relativistic calculation, described in Sect. 1.3.2.

1.3.1 Non-relativistic SZE

The work of Zeldovich & Sunyaev (1969) and Sunyaev & Zeldovich (1970, 1972, 1980) describes the details of the SZ effect in the non-relativistic case[5]. Their calculations are based on the Kompaneets equation (Kompaneets, 1957) which is a diffusion approximation of the full scattering process of a incident photon spectrum on an electron gas.

The SZ effect transports photons from the low-frequency Rayleigh-Jeans side of the spectrum to the high frequency Wien side by an inverse Compton-scattering process. In the non-relativistic

[4] This is not true in all cosmologies and in principle large SZ surveys could help place constraints on the redshift dependence of the CMB temperature, e.g. Horellou et al. (2005)

[5] *Non-relativistic* means that the temperature of the electron gas is so low that relativistic corrections due to the velocities of the electrons are small. In rich galaxy clusters (which have masses $M \gtrsim 10^{15}\, M_\odot$) relativistic effects are not negligible. Since high-temperature galaxy clusters are the easiest to detect it is important to understand the key role that the relativistic effect plays.

regime the effect can be divided into two parts (see the reviews by Carlstrom et al., 2002; Birkinshaw, 1999);

- *The thermal effect.* Electrons of the intracluster gas are assumed to move in the rest frame of the cluster and to have an isotropic velocity distribution. Hence, there are equally many electrons with positive and negative velocities, and the scattered CMB-photons are isotropic. The velocity of the cluster with respect to the CMB-frame is neglected.

- *The kinetic effect* is essentially a Doppler effect. The *peculiar velocity* of the cluster causes an increase (decrease) of the SZ-signal when the line-of-sight motion of the cluster is toward (away from) us. We apply the convention of positive (negative) velocities for receding (approaching) clusters. The peculiar velocity is a term for velocity components of galaxy clusters that do not follow the general Hubble flow. In the study by Sheth & Diaferio (2001) a standard deviation of 414 km/s was found for the distribution of peculiar velocities in a ΛCDM cosmology, which illustrates the magnitude of the peculiar velocity.

Both the thermal and kinetic SZ effects are caused by scattering of photons by moving electrons. In the non-relativistic limit, we can disentangle the thermal and kinetic effects and superimpose them to get to the total SZ effect. The CMB distortion due to the combined SZ effect is

$$\frac{\Delta I_\nu}{I_0} = g(x)y - h(x)\frac{v}{c}\tau, \tag{1.2}$$

where v is the peculiar velocity, τ is the optical depth and y is the Compton parameter, which is the cluster parameter that determines the magnitude of the thermal SZ effect, defined as

$$y = \frac{k\sigma_T}{m_e c^2}\int n_e T_e \,\mathrm{d}l \tag{1.3}$$

where σ_T is the cross section for Thomson scattering, k is Boltzmann's constant, m_e the electron mass, c is the speed of light and n_e and T_e are the number density of electrons and the electron temperature. The optical depth is defined as $\tau = \int \sigma_T n_e dl$, which makes it possible to write the Compton parameter $y = kT_e/(m_e c^2)\tau$ for an isothermal electron gas. Finally, $g(x)$ and $h(x)$ are the line shapes of the thermal and kinetic effect:

$$\begin{cases} g(x) = h(x) \times [x/\tanh(x/2) - 4]\,, \\ h(x) = f(x) \times xe^x/(e^x - 1), \\ f(x) = x^3/(e^x - 1). \end{cases} \tag{1.4}$$

The frequency dependencies of the thermal and kinetic effects are thus different. Also, for realistic values of cluster parameters, the thermal effect is an order of magnitude larger than the kinetic effect. Therefore the superposition of the two effects (eq 1.2) is a good approximation. The thermal and kinetic SZ effects are plotted in Fig. 1.4 together with the CMB spectrum scaled down by a factor of 1000, indicating how small changes the Sunyaev–Zeldovich effect induces in the CMB temperature. The spectrum of the thermal SZ effect illustrates the photon-electron scattering process where low-frequency photons have acquired energy and there is an excess of photons at high-frequencies. Therefore observations at low frequencies will see a "hole in the sky", or a lower temperature than the CMB temperature, whereas higher-frequency observations will see an increased temperature. Multi-frequency observations of the SZ effect can be used to constrain the parameters (peculiar velocity, compton parameter, electron temperature).

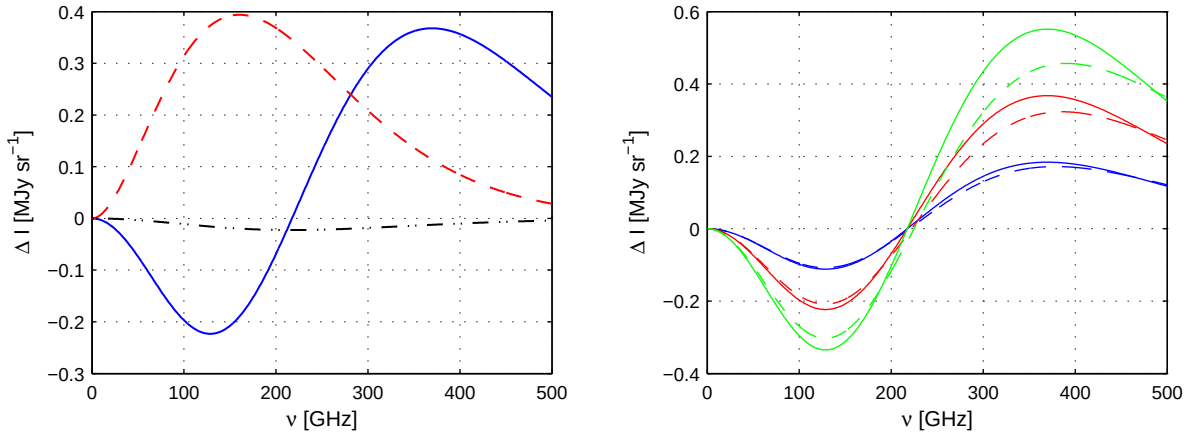

Figure 1.4: Left: *Blue solid line*: the thermal SZ spectrum. *Red dashed line*: CMB intensity (scaled down by a factor of 1000). *Black dash-dotted line*: kinetic SZ effect. All curves are calculated for an electron temperature $kT_e = 10\,\mathrm{keV}$, optical depth $\tau = 0.01$ and peculiar velocity $v = +500\,\mathrm{km\,s^{-1}}$. **Right**: Solid lines show the thermal SZ signature for a cluster with $\tau = 0.01$, no peculiar velocity and the electron temperatures 5,10 and 15 keV, in blue, red and green color respectively. The dashed lines are calculated for the same parameters but instead using the relativistic formulation of the SZ effect (using the series expansions of Itoh et al. 1998).

The thermal SZ-curve passes through zero at a frequency of 217 GHz, or dimensionless frequency $x = 3.83$. Since the thermal SZ effect vanishes around this frequency this has been suggested as a possibility to detect the kinetic SZ-effect from galaxy clusters. The kinetic Sunyaev–Zeldovich signal is much smaller than the thermal effect (see Fig. 1.4), and the effect of confusion of background sources at 220 GHz further complicates detection of the kinetic SZ signal. In the relativistic treatment of the SZ effect the crossover frequency changes with electron temperature.

The SZ- and the X-ray signal from the cluster both depend on combinations of the products of the line-of sight averaged electron temperature (T_e) and density (n_e). The SZ-signal is proportional to the electron "pressure" $\int_l T_e(r)\, n_e(r)\, dl$, while for the X-ray signal $\int_l \sqrt{T_e(r)}\, n_e(r)^2\, dl$. The two measurements thus probe the ICM electron gas in two ways and can be used to disentangle its temperature and density.

1.3.2 Relativistic SZE

The formalism derived by Sunyaev & Zeldovich was based on the Kompaneets equation, which is only valid in the non-relativistic regime. The electron temperature of galaxy clusters can be as high as 15 keV. Plasmas at such high temperatures have a relativistic velocity distribution. Since the Kompaneets equation is a diffusion approximation, each CMB photon is assumed to be scattered at least once by electrons. The optical depth in clusters is low ($\tau \simeq 0.01$), so not all photons are scattered even once (Rephaeli, 1995). The nonrelativistic formalism thus over-estimates the magnitude of the SZ effect.

Attempts to solve the full kinetic equation for a distribution of photons scattered by a relativistic distribution of electrons have been made by e.g. Wright (1979). Rephaeli (1995) and Rephaeli & Yankovitch (1997) have derived the full relativistic corrections to the SZE. They assume that the photons obey a blackbody spectrum, and that the electrons are described by a relativistic Maxwellian distribution. The full relativistic calculation includes the possibility that the number of scatterings per photon is variable. The probability distribution for the number of scatterings is

approximated by keeping only the first two terms; representing one or zero scatterings per photon. This approximation is valid because of the low optical depth in galaxy clusters.

The formulas for the relativistic SZ effect will not be presented here. The interested reader is referred to Rephaeli & Yankovitch (1997). Challinor & Lasenby (1998) derived a generalized version of the Kompaneets equation, valid for a relativistic electron distribution. They provide analytic expansions up to the third order in the electron temperature, and claim that the formula is valid to excellent approximation for $kT_e \leq 15$ keV. Itoh et al. (1998) used a similar approach and achieved power series expansions of higher order than those of Challinor & Lasenby. The results of Itoh et al. are in excellent agreement with those of Rephaeli & Yankovitch, although their derivations were made using different approaches. The power series expansions of Itoh et al. require substantially less computational time than the triple-integrals of Rephaeli & Yankovitch.

It is interesting to examine the differences between the relativistic and the non-relativistic SZ-formalisms. In the right-hand panel of Fig. 1.4 these two effects are compared for three values of the electron temperatures representative for actual clusters of galaxies. Fig. 1.4 shows that the difference between the relativistic and non-relativistic curves is greatest at high frequencies and high electron temperatures. Another difference is that the relativistic SZE has a temperature-dependent crossover frequency. The crossover frequency increases with increasing electron temperature (Sazonov & Sunyaev, 1998).

1.3.3 Sunyaev–Zeldovich effect observations

In recent years there has been a steady increase in the number of SZ experiments at telescopes across the world, and in the last three years the number of publications from these experiments has exploded. There are several reasons for this. The receivers that employ bolometric techniques (the bolometer cameras) have become so sensitive that they not only detect the faint Sunyaev–Zeldovich signal from galaxy clusters, but also make maps of it. Many experiments are today placed at observing sites where the atmosphere is stable and the water vapour content is low (Schwan et al., 2003; Carlstrom et al., 2009), which further improves the detection of the SZ signal. Heterodyne techniques have been improved and the number of telescopes in interferometers such as the Sunyaev–Zeldovich array (SZA, Muchovej et al. 2007) has increased, giving better angular resolution, image fidelity and sensitivity than before. Using small antennas mounted on a hexapod mount, the AMIBA experiment find clusters via interferometric observations (Ho et al., 2009). In this section I will summarize recent results from SZ observations of clusters of galaxies, discuss briefly their implications and make an outlook towards future results and experiments.

The APEX-SZ bolometer camera on the APEX telescope has been used extensively in the last few years to map the SZ decrement at 150 GHz in about 50 clusters covering a large redshift range (Halverson et al. 2009; Nord et al. 2009; Basu et al. 2010; Bender et al. in prep; Horellou, Johansson et al. in prep). I have been working in the APEX-SZ collaboration since 2008, and a summary of three papers where I am a coauthor is found in Chapter 3.2. The instrument was dismounted in December 2010.

The largest SZ experiments in operation are the *South Pole Telescope* (SPT), the *Atacama Cosmology Telescope* (ACT) and the *Planck Observatory*. These telescopes will produce catalogs of hundreds of galaxy clusters each, detected in the SZ decrement or increment. SPT (Carlstrom et al., 2009) and ACT (Hincks et al., 2009) observe from the ground and the telescope dishes are ~ 10 m which gives spatial resolutions of the order of one arcminute at 2 mm wavelength. Both experiments benefit from dry observing sites in the Chilean Andes (ACT) and the south pole (SPT). Both experiments operate at several wavelengths, a necessity when one wants to model the SZ effect carefully. *Planck*, on the other hand, is a satellite launched in 2009 that observes

from the second Lagrangian point (L2) of the Earth-Sun system. It has nine frequency bands between 30 and 860 GHz, which will be useful when modelling the Galactic foreground emission. The beam is Gaussian with $FWHM \sim 33'$ at 30 GHz and $\sim 4'$ at 860 GHz (Planck Collaboration, 2011b). The spatial resolution is thus slightly worse than that of ground-based experiments. This becomes important when observing clusters of galaxies, that have angular size of a few to tens of arcminutes. Many clusters will be resolved by ACT and SPT, while for *Planck* they will appear almost point-like. This makes *Planck* a perfect instrument to build large catalogs of clusters of galaxies, and study their statistical properties, and use them to constrain cosmology. The ground-based instruments are also suited for studies of the physics of the ICM.

Recent results from the SPT, ACT and *Planck* instruments show that blind SZ surveys detect massive galaxy clusters. Vanderlinde et al. (2010) reported the detection of 21 clusters with the South Pole Telescope. Out of the 21, three are previously known Abell clusters, while the remaining objects are new SZ detections. Marriage et al. (2010) presented the first Sunyaev–Zeldovich survey from the ACT instrument. They found 21 clusters, out of which ten are new detections. The first results from *Planck* were recently made public. The early Sunyaev–Zeldovich cluster catalog (Planck Collaboration et al., 2011) includes 169 galaxy clusters, and where 20 are new detections. The continuation of the mission will allow Planck to detect less SZ luminous clusters and build an even larger catalog that can be used to constrain the cosmological model.

Sunyaev–Zeldovich observations of high-redshift galaxy clusters

That the observed CMB temperature decrement/increment does not depend upon the redshift of the galaxy cluster is one of the most important properties of the SZ method. It would make it possible to observe clusters out to very high redshifts, as long as the integrated pseudo-pressure $\propto \int n_e T_e \, dl$ is high enough. The redshift independence makes the SZ method complementary to other cluster-finding methods. Today the X-ray and Optical/infrared methods also find clusters at high redshifts (Brodwin et al., 2010b; Stanford et al., 2005; Fassbender et al., 2010).

Before using the SZ method to find high redshift clusters, it is important to observe known X-ray or optically detected clusters with SZ experiments. Such a study was recently published by Culverhouse et al. (2010), who used the Sunyaev–Zeldovich Array in California to study high-z galaxy clusters detected in the optical or X-ray. Three out of twelwe clusters were detected, and those with significant SZ signals were those having large gas masses as derived from the X-ray measurements. The nondetection of all optically selected high-z clusters in Culverhouse et al. (2010) is perhaps not very unexpected; the optical selection does not require large amounts of intra-cluster gas (as the X-ray detections do). On the contrary the SZ signal from a gas-poor cluster would give a very low Sunyaev–Zeldovich signal.

The first cluster initially detected at $z \geq 1$ redshift range via its SZ signal is SPT-CL J0546-5345, a massive $M = 8.0 \pm 1.0 \times 10^{14} \, M_{\odot}$ system at $z = 1.067$ (Brodwin et al., 2010a). It is the system with highest dynamical mass detected at $z > 1$. It was detected in the large SPT survey, and first reported in Staniszewski et al. (2009). Follow-up optical and infrared imaging, as well as spectroscopy of potential cluster members resulted in the determination of the redshift. Chandra observations determined the electron temperature $T_X = 7.5^{+1.7}_{-1.1}$ keV. The discovery of this Sunyaev–Zeldovich detected cluster shows the potential of large SZ surveys to detect massive galaxy clusters at all redshifts.

1.4 Gravitational lensing

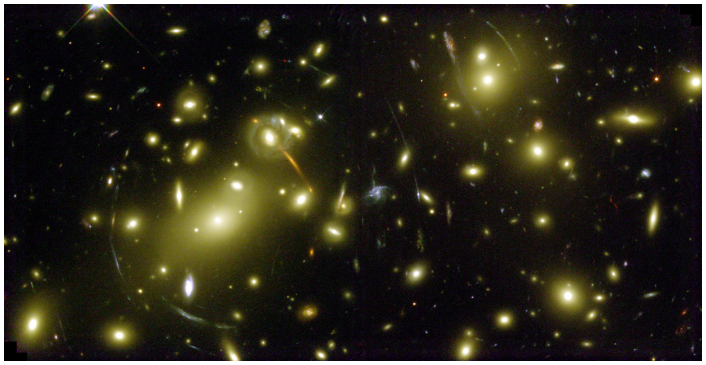

Figure 1.5: Hubble Space Telescope color image of the galaxy cluster Abell 2218. Several arcs curved around the cluster center are seen in the image. They are images of background galaxies, gravitationally magnified and bent by the mass of the galaxy cluster. *Image credit*: NASA.

Here I present a short introduction to the theory and application of gravitational lensing in astronomy. Several books and reviews have been written over the years; for this text the main reference is Schneider et al. (2006). Other reviews include Schneider et al. (1992); Petters et al. (2001); Narayan & Bartelmann (1996); Blandford & Narayan (1992). Interesting features of gravitational lensing include Einstein rings, giant arcs in clusters of galaxies, microlensing, weak lensing, time delays. It is a very rich field and the technique has applications on scales ranging from those within our own galaxy (microlensing) to the entire universe (weak lensing observations of the large scale matter distribution).

In Paper I and II in this thesis, we use the gravitational lensing effect that massive clusters of galaxies induce on the background field galaxy population. We use mass models of the galaxy clusters and calculate magnification values for the positions of detected submm galaxies. This section is a summary of the theory behind the calculations and a discussion of a few interesting properties of gravitational lensing.

Bending of light by a gravitational potential was discussed already almost 300 years ago (see the interesting discussion about the history of gravitational lensing in Schneider et al. 2006) and Einstein (1911) showed before his theory of general relativity, that the incoming light upon a body of mass M with impact parameter ξ would be deflected by an angle

$$\alpha = \frac{2GM}{c^2\xi} \tag{1.5}$$

where G is Newton's constant and c is the speed of light, using the equivalence principle. Equivalent results had been derived earlier. This simple formula tells us that a light ray propagating through the gravitational field of a heavenly body (such as the sun) should be displaced. Inserting the mass of the sun and the values of the constants Eq. (1.5) is

$$\alpha = 0.9'' \times \left(\frac{M}{M_\odot}\right)\left(\frac{\xi}{R_\odot}\right)^{-1} \tag{1.6}$$

The apparent positions of stars behind the sun should thus be displaced by one arcsecond. In a calculation within the framework of General Relativity, it was found that the constant in Eq. (1.5) is twice as large. I now investigate the theory of gravitational lensing in more detail.

1.4.1 The lens equation

It is beyond the scope of this thesis to perform a full proof of the derivation of the lens equation from the field equations of general relativity. Instead, I start by discussing how a light ray is lensed by a general mass distribution. Generally, the hypothetical plane going through the source, which is perpendicular to the line of sight between us and the source, is called the *source plane* (see Fig. 1.6). Analogously, we define the *lens plane* or *image plane* as the plane passing through the lens. This is the plane where the lensed image of the source will appear to lie.

By representing the mass distribution of the lens as a sum of point masses, and assuming that the deflection of light is small, the deflection angle α can be written

$$\hat{\boldsymbol{\alpha}}(\boldsymbol{\xi}) = \frac{4G}{c^2} \int \Sigma(\boldsymbol{\xi}') \frac{\boldsymbol{\xi} - \boldsymbol{\xi}'}{|\boldsymbol{\xi} - \boldsymbol{\xi}'|^2} \, d^2\boldsymbol{\xi}' \tag{1.7}$$

where ξ is the coordinates in the lens plane (see Fig. 1.6) and Σ is the projected two-dimensional surface mass density. This equation holds as long as the deflection of the incoming light is small on the scale where the mass distribution changes significantly (Schneider et al., 2006).

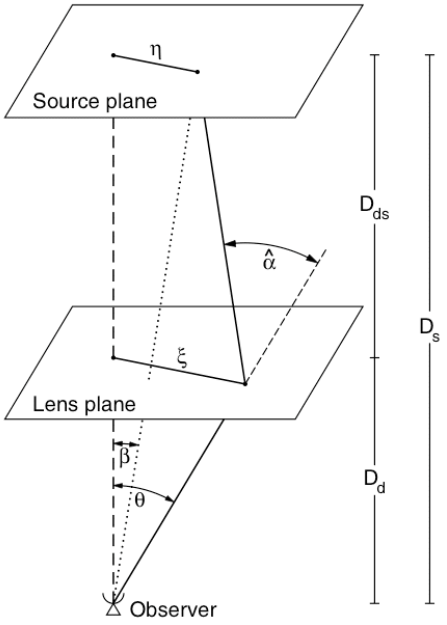

Figure 1.6: Sketch of the setup in a gravitational lens system. The symbols are described in the text. *Figure from Schneider et al. (2006).*

We can use the setup in Fig. 1.6 to relate the apparent coordinate of the source ($\boldsymbol{\xi}$) in the lens plane to its real position (η) in the source plane. Both these vectors are measured with respect to the imaginary line that is perpendicular to the source and lens plane. If we instead turn to the angular coordinates $\boldsymbol{\beta}$ and $\boldsymbol{\theta}$, the distances shown in Fig. 1.6 are eliminated from the equations, and the resulting relation becomes simpler

$$\boldsymbol{\beta} = \boldsymbol{\theta} - \frac{D_{ds}}{D_s} \hat{\boldsymbol{\alpha}}(D_d \boldsymbol{\theta}) \equiv \boldsymbol{\theta} - \boldsymbol{\alpha}(\boldsymbol{\theta}) \tag{1.8}$$

where the distances D are defined in Fig. 1.6 and $\alpha(\boldsymbol{\theta})$ is called the *scaled deflection angle*. This equation is called the *lens equation* and it relates the deflection angle to the intrinsic position of

the source and the position of the image. Rewriting Eq. 1.7 in terms of the scaled deflection angle, we have

$$\alpha(\boldsymbol{\theta}) = \frac{1}{\pi} \int \kappa(\boldsymbol{\theta}') \frac{\boldsymbol{\theta} - \boldsymbol{\theta}'}{|\boldsymbol{\theta} - \boldsymbol{\theta}'|^2} \, d^2\boldsymbol{\theta}' \tag{1.9}$$

where κ is the *convergence*

$$\kappa(\boldsymbol{\theta}) = \frac{\Sigma(D_d\boldsymbol{\theta})}{\Sigma_{cr}}, \quad \Sigma_{cr} = \frac{c^2}{4\pi G} \frac{D_s}{D_d D_{ds}} \tag{1.10}$$

and Σ_{cr} is the critical mass density. The value of κ determines whether there will be several images of the lensed source. If a mass distribution has $\kappa \geq 1$, or equivalently $\Sigma(\boldsymbol{\theta}) > \Sigma_{cr}$ at some $\boldsymbol{\theta}$, there is no longer a unique β for that $\boldsymbol{\theta}$, and there will be several images of the source. Thus, determining the position in the source plane for a corresponding image position in the lens plane is straightforward, but the opposite is much harder.

1.4.2 Gravitational magnification

Equation 1.8 relates the intrinsic position in the source plane to its apparent position in the image plane. But lensing does not only change the position of the source. As is evident in the arcs in the field of Abell 2218 (see Figure 1.5), gravitational lensing also magnifies and distorts the background sources.

Two properties of the gravitational lens, the *convergence* and the *complex shear* determine the magnification and distortion of the images. To see how the shear and convergence influence the gravitational lensing, we first define the *deflection potential*

$$\psi(\boldsymbol{\theta}) = \frac{1}{\pi} \int \kappa(\boldsymbol{\theta}') \, \ln|\boldsymbol{\theta} - \boldsymbol{\theta}'| \, d^2\theta' \tag{1.11}$$

which is related to the deflection angle $\boldsymbol{\alpha}$ through $\boldsymbol{\alpha} = \nabla\psi$, from the vector identity $\nabla \ln|\boldsymbol{\theta}| = \boldsymbol{\theta}/|\boldsymbol{\theta}|^2$. Furthermore, using that $\nabla^2 \ln|\boldsymbol{\theta}| = 2\pi\delta_D(\boldsymbol{\theta})$, where δ_D is the Dirac delta function, one can show that the following relation

$$\nabla^2\psi = 2\kappa \tag{1.12}$$

can be derived from Eq. 1.11. This is the two-dimensional equivalent of the Poisson equation. The convergence κ was defined in Eq. 1.10, and the shear is a complex number $\gamma \equiv \gamma_1 + i\gamma_2 = |\gamma|e^{2i\phi}$, related to the deflection potential through $\gamma_1 = 1/2(\psi_{11} - \psi_{22})$ and $\gamma_2 = \psi_{12}$.

To see how the convergence and shear explicitly determine the magnification and distortion of images we start by noting that gravitational lensing preserves surface brightness, because no photons are emitted or absorbed in the gravitational deflection, and by the Liouville theorem, this means that surface brightness must be preserved. If I is the surface brightness in the image plane and $I^{(\mathrm{s})}(\boldsymbol{\beta})$ is the surface brightness distribution in the source plane, these must be equal.

$$I(\boldsymbol{\theta}) = I^{(\mathrm{s})}(\boldsymbol{\beta}(\boldsymbol{\theta})) \tag{1.13}$$

If the background source is much smaller than the angular scale on which the lens properties change, this equation can be linearized locally[6]. The lens equation relates $\boldsymbol{\beta}$ to $\boldsymbol{\theta}$, and Taylor expanding it to first order around the point $\boldsymbol{\beta}_0$ gives

$$I(\boldsymbol{\theta}) = I^{(\mathrm{s})} \left[\boldsymbol{\beta}_0 + \mathcal{A}(\boldsymbol{\theta}_0) \cdot (\boldsymbol{\theta} - \boldsymbol{\theta}_0)\right] \tag{1.14}$$

[6]This is the case e.g. for a submm galaxy behind a galaxy cluster.

where $\mathcal{A}$ is the Jacobian matrix which is related to the shear and convergence by the following:

$$\mathcal{A}(\boldsymbol{\theta}) = \frac{\partial \boldsymbol{\beta}}{\partial \boldsymbol{\theta}} = \left(\delta_{ij} - \frac{\partial^2 \psi(\boldsymbol{\theta})}{\partial \theta_i \, \partial \theta_j} \right) = \begin{pmatrix} 1 - \kappa - \gamma_1 & -\gamma_2 \\ -\gamma_2 & 1 - \kappa + \gamma_1 \end{pmatrix}. \tag{1.15}$$

The inverse of the Jacobian is the magnification tensor $M(\boldsymbol{\theta}) = \mathcal{A}^{-1}$. If the source is small (so that Eq. 1.14 is valid) the magnification μ is related to the magnification tensor

$$\mu = \det M = \frac{1}{\det \mathcal{A}} = \frac{1}{(1-\kappa)^2 - |\gamma|^2}. \tag{1.16}$$

If the area of the source is magnified by a factor μ it means that the observed flux density is increased by the same factor. The magnification factor is independent of the frequency of the radiation.

Caustics and critical lines

The magnification factor of an image μ can mathematically be infinite if $\det \mathcal{A} = 0$, according to Eq. 1.16. This infinite magnification is found along lines where the (locally linearized) determinant of the Jacobian tends to zero. These lines of infinite magnification in the image plane are called *critical lines*, while the curves which they are mapped onto in the source plane are called *caustics*. The critical lines are smooth in the image plane, while the caustics in the source plane can have cusps, and are not generally smooth. In the case of the submm observations that are discussed in Paper I and Paper II we are mostly interested in the total magnification factor that boosts the flux of a source. When we determine the position of an observed source (in the image plane) we can calculate the magnification factor from the determinant of the Jacobian $\mathcal{A}$, using relations for the convergence and shear of the mass distribution.

The bright submillimeter galaxy behind the Bullet Cluster lies close to a caustic line. This source was discussed both in Paper I, Paper II and Paper III, and has also been the subject of several other studies (Bradač et al., 2006; Wilson et al., 2008; Gonzalez et al., 2009, 2010). It has been shown that the LABOCA source consists of two images of the same background galaxy. The two images can be detected in Spitzer IRAC infrared images of the region.

1.4.3 Weak gravitational lensing

Contrary to the arcs in images of the centers of clusters of galaxies, or the double images that are detected for example in the bright source in the Bullet Cluster, in weak lensing the effect of the lensing cannot be seen directly in the images, but must be inferred by statistical techniques. Weak lensing studies of galaxy clusters has become an important technique to measure their mass distribution. Compared to other techniques, like X-ray, SZ or optical measurements, which measure either only the hot gas or the stellar components, the lensing depends on the total mass of the system observed, both the dark and luminous matter.

To derive the mass of a galaxy cluster, one needs to measure the ellipticities of many galaxies behind the galaxy cluster. The small distortions of each of the background galaxies induced by the mass distribution of the galaxy cluster are then averaged, and the averaged signal (the *reduced shear*, related to the shear discussed in the previous section) is used to infer the mass distribution of the lens.

There are several matters complicating this simple description. First, the intrinsic ellipticities of the background galaxies are not known. How can this effect be corrected for? By making the

assumption that the *intrinsic* ellipticities of the galaxies is random[7] an estimate of the reduced shear can be made. The expectation value of the total ellipticity is then directly related to the reduced shear (see Schneider et al. 2006, Weak lensing, Section 2). Each image thus gives an unbiased, but noisy, estimate of the local shear. To beat down the noise, measurements of many galaxies have to be made, since the noise scales as $\sigma_e = \sqrt{\langle \epsilon^{(s)} \epsilon^{(s)*} \rangle}/N$, where ϵ are the intrinsic source ellipticities, N is the number of galaxies images used in the average, and the star denotes the complex conjugate. Another technical complication is that the Point-Spread Function (PSF) function of the telescope must be known with high accuracy to correct for the distortion of galaxy images from the optics.

Which types of object can be detected with weak lensing measurements? Following the discussions in Schneider et al. (2006); Bartelmann & Schneider (2001), the signal to noise in the weak lensing measurement of matter distributed according to a Single Isothermal Sphere SIS profile, within an annulus with $\theta_{\rm in} \leq \theta \leq \theta_{\rm out}$ can be approximated as

$$S/N = 8.4 \times \left(\frac{n}{30\,\mathrm{arcmin}^{-2}}\right)^{1/2} \left(\frac{\sigma_\epsilon}{0.3}\right)^{-1} \left(\frac{\sigma_v}{600\,\mathrm{km\,s}^{-1}}\right)^{2} \left(\frac{\ln\left[\theta_{\rm out}/\theta_{\rm in}\right]}{\ln 10}\right)^{1/2} \left(\frac{D_{ds}}{D_s}\right). \qquad (1.17)$$

By discussing each term in this equation we can understand the limitations of weak lensing measurements. n is the number density of galaxies that can be used for the lensing study. In an optical image of a galaxy cluster the galaxies belonging to the cluster (and thus the lens itself) must be masked, or otherwise they would distort the lensing result. σ_ϵ is the dispersion of intrinsic ellipticities, σ_v is the velocity dispersion of the mass model within the aperture, and D_{ds} and D_s are the angular diameter distances from the source to the image plane, and from us to the source plane respectively (see Fig. 1.6).

Equation (1.17) tells us many interesting properties of the applicability of the weak lensing techniques. The signal-to-noise increases weakly with the number density of galaxies while it depends more strongly on the velocity dispersion within the mass distribution. The last term in equation (1.17), the fraction of distances, shows that for a given background source population the lensing signal decreases when the lens is placed further away. Hence, individual galaxies with typical velocity dispersions $\sigma_v \leq 200\,\mathrm{km\,s}^{-1}$ are very hard to detect via gravitational lensing, because their masses do not induce enough shear into the lensing signal.

[7]This appears to be a valid assumption, as the homogeneity and isotropy of the universe makes a preferred ellipticity unlikely.

1.5 The APEX telescope

The APEX Telescope (Atacama Pathfinder EXperiment)[8] is described by Güsten et al. (2006). It is located in northern Chile at an altitude of 5100 meters. The dry weather at this site makes it one of the best places in the world for sub-mm observations. Its main scientific drivers are the study of warm and cold dust in the Milky Way and in distant galaxies, observations of high frequency spectral lines from forming and dying stars and planetary systems. The excellent atmospheric transmission at this site makes it possible to perform observations at higher frequencies than ever before.

For the research presented in this thesis, I have used the three bolometer cameras LABOCA operating at 870 μm(Siringo et al., 2009), SABOCA operating at 350 μm (Siringo et al., 2010) and APEX-SZ operating at 2 mm (Dobbs et al., 2006; Schwan et al., 2003). Properties of the bolometer cameras are summarized in Table 1.2. Two pictures of APEX are shown in Figure 1.7.

Table 1.2: Parameters of the bolometer array cameras on the APEX telescope.

	LABOCA	SABOCA	APEX-SZ
frequency/wavelength	345 GHz/0.87 mm	860 GHz/350 μm	150 GHz/2 mm
Bandwidth	60 GHz	120 GHz	30 GHz
Angular resolution	19.5″	7.5″	60″
Number of bolometers	295	37	300
Field of view	11.4′	1.5′	22′
Sensitivity	75 mJy $s^{1/2}$	200 mJy $s^{1/2}$	24 mJy $s^{1/2}$

Figure 1.7: The APEX telescope at day and night.

[8]APEX is a collaboration between Max Planck Institut für Radioastronomie (MPIfR) (50%), Onsala Space Observatory (23%), and the European Southern Observatory (27%). `www.apex-telescope.org`

Chapter 2

Papers on submillimeter galaxies lensed by galaxy clusters

2.1 Introduction to Paper I

In Paper I we analyzed submm maps of the Bullet Cluster (at $z \sim 0.3$) obtained with the LABOCA receiver on the APEX telescope. The aims of the observations were initially two-fold; we wanted to map the Sunyaev–Zeldovich increment from the hot intra-cluster gas while searching for background submm galaxies, gravitationally lensed by the cluster's potential. Paper I describes the latter, while the SZ signal in the Bullet Cluster will be discussed in a future paper (Sigurdarson et al, *in prep*; see also my licentiate thesis Johansson 2009).

One of the main findings of Paper I is the discovery of an extremely bright submm galaxy ($S_{870\,\mu\mathrm{m}} \sim 50$ mJy), which had already been detected in near-infrared Spitzer images (Gonzalez et al., 2009) and in millimeter observations with the AzTEC bolometer camera mounted on the Atacama Submillimeter Telescope Experiment (ASTE) (Wilson et al., 2008). The position of the source was predicted in the strong-lensing reconstruction of the Bullet Cluster by Bradač et al. (2006) and subsequently identified in Spitzer IRAC and MIPS images by Gonzalez et al. (2009), who showed that two infrared galaxies are images of the same background galaxy. These images, denoted A and B by Gonzalez et al. (2009), are separated by $8''$ on the sky. Such a strong gravitational lensing event can occur close to a critical line of the gravitational lens.

In addition to the bright submm galaxy, we found 16 other submm sources. We calculated cumulative number counts for the field, and found, using a mass model of the gravitational lensing effect, that the counts were consistent with the results from previous surveys (see Sect. 5.3 and Fig. 10 in Paper I).

We also investigated the connection between the LABOCA sources and possible infrared counterparts detected with the Spitzer satellite's detectors IRAC (Fazio et al., 2004) and MIPS (Rieke et al., 2004). The spatial resolution of the Spitzer instruments is better than that of LABOCA, so it is possible to find several Spitzer sources within one LABOCA beam. We identified nine LABOCA sources with Spitzer counterparts. For the other eight sources the position determined from the LABOCA map was not sufficiently accurate to single out the counterpart from the many Spitzer sources within the LABOCA beam.

We chose to study the Bullet Cluster because it is one of the most massive galaxy clusters. Since it is a merging cluster a range of interesting questions about the state of the intracluster gas and its distribution compared to the dark matter can be investigated. The high mass increases

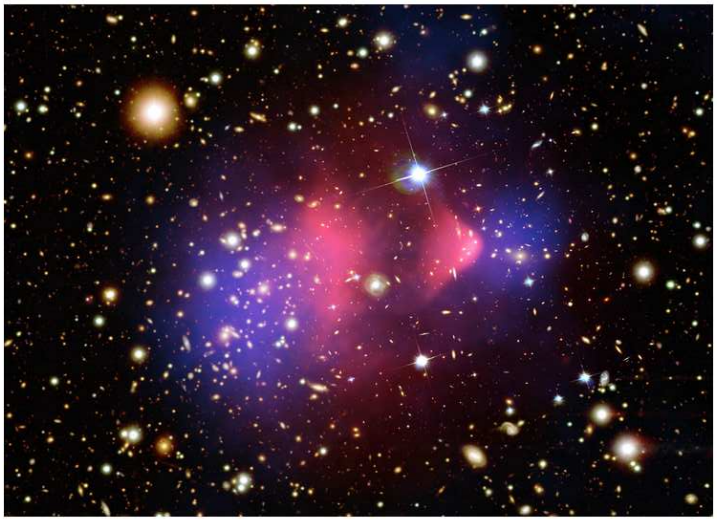

Figure 2.1: Color-composite image of the Bullet Cluster overlaid on an optical image. The pink color represents the X-ray luminosity, and the blue color the projected mass density obtained from weak lensing analysis. The shift between the collisional gas component (pink) and the collisionless dark matter (blue) is evident. The size of the image is $7.5' \times 5.4'$. *Image credit*: X-ray: NASA/CXC/CfA/M.Markevitch et al.; Optical: NASA/STScI; Magellan/U.Arizona/D.Clowe et al.; Lensing Map: NASA/STScI; ESO WFI; Magellan/U.Arizona/D.Clowe et al.

the chances of having large areas of high gravitational magnification. In the following section I present a summary of the many interesting properties of the Bullet Cluster.

The Bullet Cluster

The Bullet Cluster (1E 0657–56) (see Fig. 2.1) is one of the hottest and most X-ray luminous clusters known to date. It was discovered as an extended X-ray source by the *Einstein* observatory (Tucker et al., 1995) and subsequently identified as a rich cluster of galaxies at the redshift of 0.296 (Tucker et al., 1998). The cluster's average temperature is $14.8^{+1.7}_{-1.2}$ keV but large spatial variations are seen (Markevitch et al. 2002, 2005). The cluster hosts a luminous radio halo (Liang et al., 2000) and displays a large amount of substructure. Barrena et al. (2002) made spectroscopic measurements of the cluster member galaxies and found a subcluster of low velocity dispersion in the eastern part of the main cluster. *Chandra* X-ray observations revealed a prominent bow shock propagating ahead of a bullet-like gas cloud with a Mach number of 2–3, which corresponds to a velocity of 3000–4000 $\mathrm{km\,s^{-1}}$ relative to the main cluster (Markevitch et al., 2002).

Interestingly, the position of the subcluster of galaxies found by Barrena et al. (2002) differs from that of the gaseous bullet observed by *Chandra*. The gas lags behind the galaxies, which coincide with the peak of the projected total mass inferred from a weak lensing analysis (Clowe, Gonzalez, & Markevitch, 2004). This observed offset has been used as an argument in favor of the collisionless nature of dark matter; the collisional gas lags behind the dark matter due to ram pressure stripping (Clowe et al., 2006). Bradač et al. (2006) combined strong and weak lensing mass reconstruction to produce a high-resolution, absolutely calibrated mass map. They estimated a mass $M_{\mathrm{cluster}}(< 250\,\mathrm{kpc}) \simeq 2.8 \times 10^{14}\,\mathrm{M}_{\odot}$ for the central region of the main cluster and $M_{\mathrm{sub}}(< 250\,\mathrm{kpc}) \simeq 2.3 \times 10^{14}\,\mathrm{M}_{\odot}$ for the subcluster.

Several experiments have detected the Sunyaev–Zeldovich increment and decrement from the Bullet Cluster. Andreani et al. (1999) used a double channel photometer on the SEST telescope to observe the Bullet Cluster and detected the SZ decrement at 150 GHz and the increment at 250 GHz. Gomez et al. (2004) imaged the Bullet Cluster with the bolometer array ACBAR on the Viper telescope at the South pole. The maps have an angular resolution of ~ 4.5 arcmin and show extended emission. Both the decrement at 150 GHz and the increment at 275 GHz were detected, and the 220 GHz map is consistent with the absence of signal, as expected for the thermal SZ effect around the cross-over frequency. Halverson et al. (2009) detected the decrement at 150 GHz of the cluster with the APEX-SZ bolometer camera and made the first $1'$ resolution map. Zemcov et al. (2010) recently detected the SZ increment at 350 and 500 μm in deep Herschel SPIRE-maps.

We became interested in the Bullet Cluster system when reading the results of Hayashi & White (2006), who used the *Millennium Run*, a large cosmological N-body simulation with 2160^3 dark matter particles in a $(500\,\mathrm{Mpc}/h)^3$ cube evolving from redshift $z = 127$ (Springel et al., 2005), to search for structures similar to the Bullet Cluster where a subcluster moves through a massive cluster at supersonic speed. They found that about one out of 100 subclusters in massive haloes have such a high speed, although this result is very sensitive to the exact value of the velocity. They concluded that the speed of the subcluster, although high, is compatible with a ΛCDM cosmology. Later studies by Farrar & Rosen (2007), that included revised shock results from additional Chandra observations of the Bullet Cluster indicated that the velocity of the dark matter subcluster was too high (4700 km/s) to be accounted for in a ΛCDM cosmology (as indicated in the fit by Hayashi & White 2006). These new results made the authors propose a new type of long-range interaction that could account for the high velocity of the subcluster. More recent simulations by Springel & Farrar (2007) showed that the velocity is actually lower (2700 km/s) and that the previous authors had used an erroneous interpretation when calculating the relative velocity.

Paper I

Submillimeter galaxies behind the Bullet Cluster (1E 0657–56)

Daniel Johansson, C. Horellou, M. Sommer, K. Basu, F. Bertoldi, M. Birkinshaw
K. Lancaster, O. Lopez-Cruz, H. Quintana

A&A, 2010, 514, A77

2.2 Introduction to Paper II

In Paper II we extended the target sample in to Paper I with four additional clusters. The clusters in the sample were initially chosen for their expected large SZ signal, but because the magnitude of the Sunyaev–Zeldovich signal scales with the total mass of the system, SZ-bright targets are also likely to be good gravitational lenses. Properties of the cluster sample are summarized in Table 1 in Paper II. Three of the clusters (1E 0657–56, Abell 2744 and AC 114) reside at a redshift of $z \simeq 0.3$, while Abell 2163 is at $z \sim 0.2$ and MS 1054-03 is at $z \sim 0.8$. For a given mass, which redshift range is the most preferable in terms of area of high magnification? Figure 5 of Paper II shows the area with a certain magnification or higher, as a function of the magnification. From this figure, and from more general considerations we can draw some conclusions about the lensing efficiency.

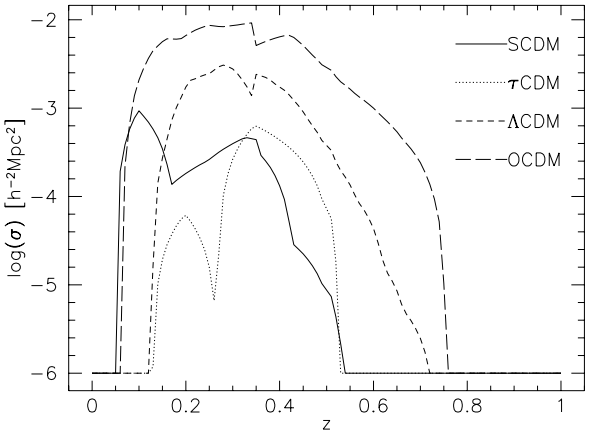

Figure 2.2: Lensing cross sections as a function of redshift for four cosmological models (Figure from Bartelmann et al. 1998). For the currently favored, ΛCDM model (corresponding to the line with short dashes) the cross-section peaks at redshift $z \sim 0.3$, showing that the best lensing performance is achieved for clusters around this redshift.

1. A cluster with given mass, and thus a given size (we assume that the clusters do not evolve significantly with redshift), will have a smaller angular extent at large redshifts. In a massive, but low-redshift cluster like Abell 2163, the large angular extent results in a low projected mass density. Abell 2163 is the least efficient lens in the sample. In MS 1054-03, which has a small angular extent because of its large redshift, the total magnified area in the image plane is smaller than that in the three clusters at $z \sim 0.3$.

2. The lensing power of a cluster depends on the distances between the us and the lens plane (D_d), us and the source plane (D_s) as well as the distance between the lens plane and the source plane (D_{ds}). The dependence can be seen in the last term in Eq. (1.17); the signal-to-noise ratio is proportional to D_{ds}/D_s. In the lensing situation discussed in Paper I and Paper II only D_{ds} varies for the different clusters. For a high-redshift cluster, the numerator decreases and the lens becomes less effective because the optical configuration is less favorable. This effect has been quantified by the works of Meneghetti et al. (2003) and Bartelmann et al. (1998) who calculated the lensing *cross-section*[1] for gravitational arcs in clusters. Although we do not look for arcs in our study (the coarse resolution of the submm

[1]The cross section is proportional to the probability of a strong lensing event to occur.

instruments would make that impossible) we can use the results to indicate the best redshifts of gravitational lensing by clusters. In Fig. 2.2 we show the lensing cross sections for four cosmological models and it is clear that the lensing configuration is the best around redshifts $z \sim 0.3$, especially for the ΛCDM model. That figure is taken from Bartelmann et al. (1998), who used N-body simulations. Similar curves for the cross section were derived by Meneghetti et al. (2003), using a semianalytical model.

3. Bradač et al. (2009) studied the use of the Bullet Cluster as a cosmic telescope, and found that its redshift $z \sim 0.3$ is preferable for lensing. They also discuss how the sizes of the cluster members influence the mass reconstruction of a cluster. The member galaxies of a cluster at low redshift appear larger and may shadow the background population.

Examining the final source list of Paper II (Table 3) the number of sources in the Bullet Cluster field constitutes almost half the number of total sources. This has several reasons. First, the Bullet Cluster data are the deepest, with 25 hours observing time. The Bullet Cluster is also the most efficient lens. The fewest sources are found in the Abell 2163 map which is to be expected, as it is the least efficient lens and the most shallow map.

In the following section we discuss the other topic of Paper II: stacking analysis.

Introduction to stacking analysis

We use the gravitational lensing provided by clusters of galaxies to probe to deeper flux levels in our observations. In the survey described in Paper II we find one source with an intrinsic flux density below the mJy level. Contrary to gravitational magnification, where a fortunate optical configuration is needed, stacking could in principle be made on any submm map . It provides a *statistical* method to detect sources below the threshold for source extraction in the map.

Stacking in map space involves adding together data in a map at positions that are determined from maps at another observing wavelength. The stacking is done in the map with a coarser spatial resolution on positions of sources taken from a map with higher spatial resolution. Submm/mm continuum maps like those coming from LABOCA, SCUBA, ACT, SPT, MAMBO or Herschel, with spatial resolutions between a few tens of arcseconds to an arcminute, are suitable for stacking. The stacking catalog commonly consists of sources from an (near) infrared observation.

Stacking provides a way of extracting more information from a map than what the eye can see. It is common to search for correlations between different classes of galaxies and the stacked signal in a submm/mm map. Most high-z galaxies detected in the infrared are too faint in the submm to be directly detected because of their infrared SEDs. We will now discuss the stacking results in Paper II.

Examples of stacking in Paper II

In Paper II we present the results from the stacking analysis in our LABOCA maps on positions of sources detected in Spitzer MIPS 24 μm maps. The main results (which can be found in Section 5) are summarized here.

- In each of the four clusters with MIPS coverage we make $> 5\sigma$ stacking detections, when excluding significant sources in the LABOCA maps.
- The noise levels of the stacked maps follow Gaussian statistics, and scale down as $\propto 1/\sqrt{N}$ where N is the number of submaps extracted.

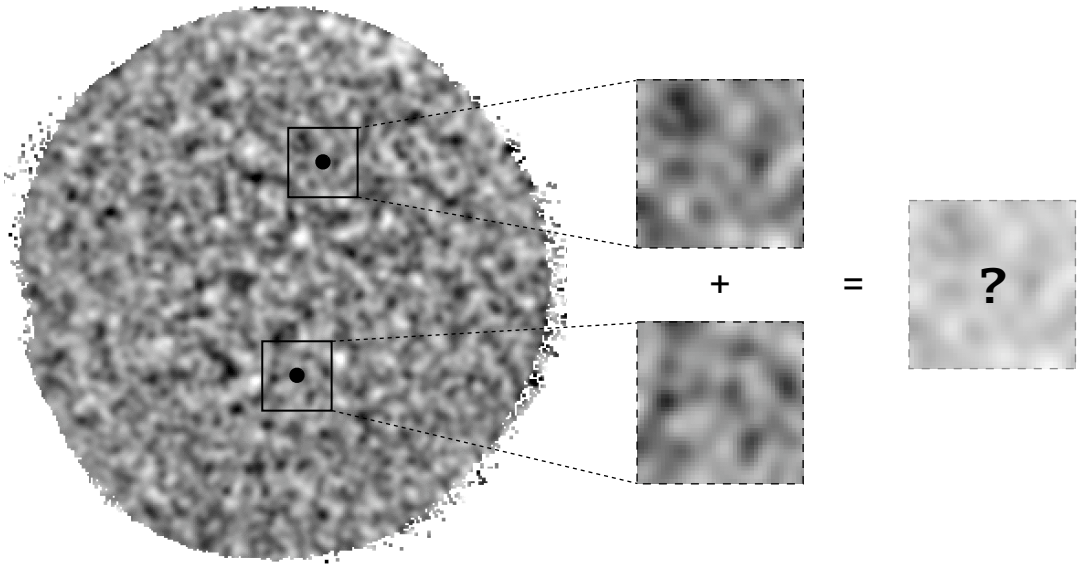

Figure 2.3: Illustration of the stacking process. The two dots correspond to the positions of two MIPS sources. The squares illustrate the extraction of submaps and the final stacking to reduce the noise level in the initial map.

- When averaging the stacked signal over the four cluster fields, and taking into account the gravitational magnification of each position, we find a demagnified 870 μm signal of ~ 0.4 mJy, at 14.5σ significance.
- We show that at low 24 μm flux densities the stacked 870 μm signal increases linearly with the MIPS flux, followed by a flattening at $S_{24\,\mu\mathrm{m}} > 300\,\mu$Jy.

It is important to remember that stacking techniques measures only average quantities of the source populations. To determine *which* sources contribute to the stacking results we would need a thorough characterization of the sources in the MIPS catalog. Such a characterization can be made by color-cuts like BzK and DRG (Distant Red Galaxies). BzK galaxies are selected based on their optical and near-infrared detections through a color cut from their B (central wavelength $\sim$0.45 μm), z ($\sim 0.9\,\mu$m) and K (~ 2.2 μm) band magnitudes. Daddi et al. (2004) showed that the color cut $BzK \equiv (z-K)_{\mathrm{AB}} - (B-z)_{AB} > -0.2$ selects star-forming galaxies at $z \geq 1.4$, while imposing $Bzk < 0.2$ and $(z-K)_{\mathrm{AB}} > 2.5$ selects passively evolving galaxies at similar redshifts. The BzK color cut thus sorts out high-redshift star-forming galaxies from optical and near-infrared surveys. DRGs are selected by the near-infrared color criterion $J-K > 2.3$ (central wavelengths J $\sim$1.2μm and $K \sim 2.2\mu$m). DRGs are generally very red high-z galaxies with old stellar populations and obscured by dust. In a survey of SMGs at submm wavelengths, it is likely that the SMGs are also categorized as DRGs.

Here, I show some explanatory figures together with a description of the stacking process. In Fig. 2.3 a rough sketch of the stacking process is presented. The difference in the actual stacking process is that (1) the number of sources needed to integrate down the noise must be many more than two; (2) the stacking is an addition weighted by the local weight map; (3) the significant

sources in the submm maps are initially subtracted from the maps. Three figures drawn from an actual stacking process are shown in Fig. 2.4. Here, we stacked on the 552 MIPS positions in the field of MS 1054-03. From the data we show (1) the LABOCA map with the positions of the MIPS sources overlaid; (2) the noise level as a function of the cumulative number of submaps; (3) the stacked maps comprised of different number of submaps.

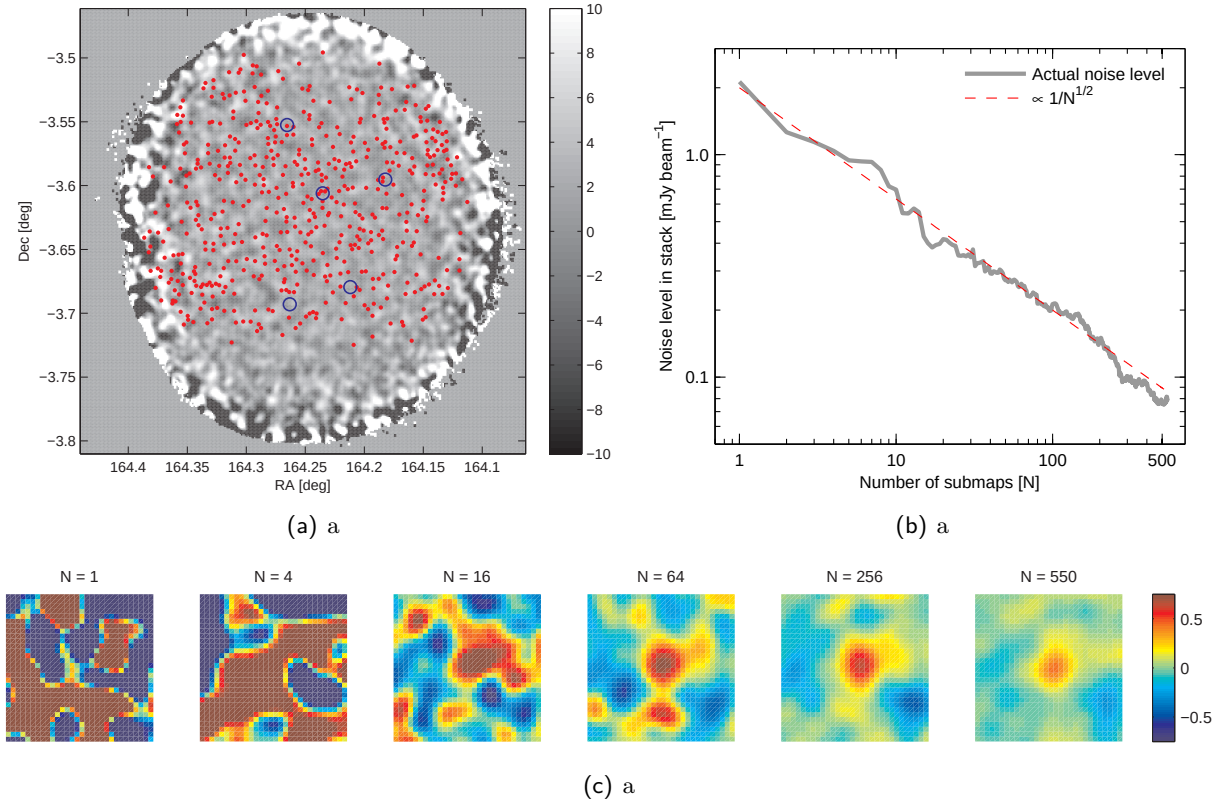

(a) a (b) a (c) a

Figure 2.4: Stacking in MS 1054-03. In this example we used the MIPS 24 μm catalog in MS 1054-03 which consists of 552 positions. All significant LABOCA sources were masked in the map. (a) LABOCA map of MS 1054-03, overlaid with red points marking the positions of the MIPS 24 μm sources, and blue circles corresponding to the significant LABOCA detections (which have been subtracted from the map). (b) Noise level as a function of the number of submaps used in the stacking, where we measured the noise level in consecutive iterations of the stacking process. As illustrated in the figure, the noise level scales as expected as $1/\sqrt{N}$ where N is the number of submaps. The noise level was calculated while excluding the central 27″.5, corresponding to the FWHM of the LABOCA beam. (c) Stacked images with N submaps. The factor between the number of submaps in a map compared to the next is four, which was chosen so that if the noise is Gaussian distributed, the noise level in one of the maps should be two times lower than that to the left (except for the last map). The size of each map is $2' \times 2'$.

Previous stacking results

Many studies have presented stacking results in submm/mm maps with positions drawn from near-infrared maps. Daddi et al. (2005) discussed stacking on MIPS 24 μm detected BzK-galaxies in SCUBA maps of the Great Observatories Origins Deep Survey (GOODS, Giavalisco et al. 2004). Using the positions of 97 BzK galaxies with detected 24 μm counterparts, they stacked the SCUBA 850 μm map and found a signal of 1.0 ± 0.2 mJy, corresponding to a far-infrared

luminosity $L_{\rm IR} \sim 1.0 \times 10^{12}\,L_\odot$ and a star formation rate SFR $\sim 170\,M_\odot\,{\rm yr}^{-1}$. Knudsen et al. (2005) did a similar stacking analysis on positions corresponding to Distant Red Galaxies (DRGs). They found a total stacked 850 μm signal of 1.2 ± 0.2 mJy for 30 DRG positions.

The previous studies used optical or infrared detection to stack on submillimeter maps. Stacking techniques have also been used at infrared wavelengths (e.g. Dole et al., 2006). They used $\sim$ 19000 positions of Spitzer MIPS 24 μm sources in three deep fields to stack the 70 and 160 μm MIPS maps of the same fields. Together with the total stacked flux densities at 70 and 160 μm they also provide the fluxes as a function of 24 μm flux density.

Paper II

A LABOCA survey of submillimeter galaxies behind galaxy clusters

Daniel Johansson, H. Sigurdarson, C. Horellou

A&A, 2011, 527, A117

2.3 Introduction to Paper III

Calvin and Hobbes have found a lot of trash in the woods. Calvin, wearing a jungle-style hat, investigates the items together with Hobbes.

C — Gosh, look at all the spectra that we discovered.
C — Let's glue them together so we can see how they fit. Then you can draw a reconstruction of the actual molecule.
C — After that, we'll write up our findings and get them published in a scientific journal.
C — Then we'll win the Nobel prize, get rich and go on talk shows.
H — What about babes? When do we get those?

Bill Watterson

(Thanks to the Oka group webpages at University of Chigaco for bringing this comic to my attention)

In Paper I and Paper II we used LABOCA to find and count submm-bright galaxies. Those studies provided us with a sample of 37 significantly detected sources. However, the continuum measurement in the submm wavelength range does not provide any information about the redshift of the galaxies. To understand better the physical conditions in submm galaxies we decided to make follow-up observations of the brightest galaxy in our sample: the submm source behind the Bullet Cluster (SMM J065837.6-555705, hereafter SMM J0658). Because of its high magnification factor ($\mu_{\rm AB} = 80 - 115$) it is also the source with the lowest intrinsic flux density ($S_{870\,\mu{\rm m}} \sim 0.5$ mJy).

Previous observations of SMM J0658 include continuum detections in the mm, submm and FIR part of the spectrum (Wilson et al., 2008; Gonzalez et al., 2009; Rex et al., 2009; Johansson et al., 2010) and Paper D and E. Before a spectroscopic redshift was found, the measured continuum flux densities of SMM J0658 constrained its redshift to the range $2.5 < z < 3.1$, and a shape of the spectral energy distribution consistent with a dust-enshrouded system, where the dust is heated by high-energy photons from newborn stars.

Gonzalez et al. (2010) spatially resolved a faint arc in WFC3 images at 1.6 μm between the Spitzer images of the galaxy. With its coarser angular resolution, Spitzer does not resolve the arc but the emission is concentrated into two lobes (Gonzalez et al., 2010). A spectroscopic redshift was measured ($z \sim 2.79$) in Spitzer observations with the Infrared Spectrograph (IRS) instrument. The receiver was tuned to observe in the wavelength range between 20 and 35 μm, where the PAH lines of a $z \sim 2.8$ galaxy were expected. The spectrum shows significant detections of the PAH lines emitted at 6.2, 7.7, 8.6 μm in the rest frame of the galaxy. It also shows detections of rotational lines of H_2. H_2 is the main molecular constituent of the interstellar medium, but its lack of a permanent electrical dipole moment make dipole transitions, like those in CO, impossible. The H_2 lines observed in SMM J0658 ($\nu = 0 - 0$ S(4) and $\nu = 0 - 0$ S(5)[2]) originate from quadrupole rotational transitions, and arise in areas of warm molecular gas. Using the line flux ratios of the S(4) and S(5) lines Gonzalez et al. (2010) could estimate the temperature of the gas ($T = 375^{+68}_{-85}$ K) and a gas mass for the warm gas of $M_{\rm H_2} = 2.2^{+17}_{-0.8} \times 10^8\,(\mu_{AB}/100)^{-1}\,M_\odot$.

Gonzalez et al. (2009, 2010) considered the AGN contribution in SMM J0658. They found that the 24 μm emission and the 1.6 μm stellar emission have similar magnification ratios between image A and B, evidence for that they are cospatial within the galaxy. An AGN however, would not be distributed in the same way as the stars, and then the flux ratios would be different. Thus it

[2]The H_2 transitions are generally ro-vibrational, meaning that both the rotational and vibrational quantum numbers change. In this case, $\nu = 0 - 0$ shows that the transition is between vibrational states with the same quantum number (0), while S(4) tells us that the rotational quantum number J changes from $J_{\rm upper} = 6$ to $J_{\rm lower} = 4$.

appears that the production of energetic photons heating the dust in SMM J0658 is dominated by starburst activity, with a possible contribution by an AGN.

At this point a study of the cold molecular gas in SMM J0658 was missing. We therefore initiated a follow-up program. To complement existing observations we used:

- APEX/SABOCA: we used the 37 element bolometer array SABOCA operating at 350 μm to image the dust emission in SMM J0658.
- ATCA: we observed SMM J0658 in the 3 mm and 7 mm observing bands of the six-element interferometer ATCA, into which two molecular rotation transitions of carbon monoxide are redshifted.

The results of these observations are presented in Paper III, and summarized here.

1. Both transitions CO(1–0) and CO(3–2) were detected. To improve the signal-to-noise ratio in the spectra we combined the emission toward the infrared images A and B of SMM J0658.
2. The spectra indicate a redshift $z = 2.7795 \pm 0.0005$ from both lines. This is lower than the redshift determined from PAH lines by Gonzalez et al. (2010) ($z = 2.791 \pm 0.007$). We believe that measuring the redshift from CO lines should be more accurate as the emission lines are narrower than the PAH lines.
3. The spatial distribution of the CO-emitting gas was investigated. We found larger offsets between the gas and the infrared emission of image B than that of image A. We speculate that this may be due to differential gravitational magnification across the galaxy.
4. We detected continuum emission from an elliptical galaxy within the Bullet Cluster in the 7 mm data. Together with previous centimeter wave observations and near-infrared HST observations we used the position of this galaxy to show that the astrometry in the 7 mm data is better than $1''$. Since the source has a negative spectral index, its flux density at 3 mm is significantly lower; it also falls near the edge of the primary beam at 3 mm, and therefore we did not detect it those data.
5. The SABOCA imaging yielded a 3.6σ detection of SMM J0658. The flux density is consistent with previous Herschel SPIRE measurements within error bars. The SABOCA map shows an elongated structure, but does not resolve the two images A and B of SMM J0658.

Paper III

Molecular gas and dust in a highly magnified galaxy at $z \sim 2.8$

Daniel Johansson et al.

To be submitted to A&A.

2.4 Papers D and E

Papers D and E present observations of the Bullet Cluster taken by the Herschel Space Observatory (Pilbratt et al., 2010). We complemented the Herschel data with LABOCA photometry of all the Herschel sources in the field. Although Herschel can measure accurately the shape of the spectral energy distribution of the submm galaxies with its five observing bands provided by the photometers *PACS* and *SPIRE* (Poglitsch et al., 2010; Griffin et al., 2010), the inclusion of the submm/mm observations sets tighter constraints on the SED models. Two papers were written to discuss the Herschel sources, and their results are summarized here.

Paper D

The far-infrared/submillimeter properties of galaxies located behind the Bullet cluster

In Rex et al. (2010, Paper D) we present SPIRE and PACS maps of the Bullet Cluster field, with the aim to probe deeper than the Herschel confusion limit[3]. Sources were extracted from deep Spitzer MIPS 24 μm maps and used as position priors for the Herschel sources, in order to minimize the effect of flux boosting on the Herschel photometry.

PACS and SPIRE (operating at central wavelengths 100, 160, 250, 350 & 500 μm) are also sensitive to the FIR emission from galaxies within the Bullet Cluster, contrary to LABOCA.[4] Redshift information is important in order to distinguish the background field galaxies from those within the cluster. Rawle et al. (2010) presented spectroscopic redshifts to galaxies within the Bullet Cluster field, and showed that there is a second concentration of galaxies with a mean redshift of 0.35, behind the Bullet Cluster. With this information, cluster galaxies could be excluded from the analysis in paper D, and a sample of Herschel detected high-redshift galaxies could be assembled. This sample consists of 15 galaxies.

The remainder of paper D investigates what the Herschel SED can tell us about the physical state in the galaxies. One of the major findings is that when using a family of SED templates derived from local galaxies (Rieke et al., 2009), we could show that the high-z galaxies in general are cooler, and that the starburst is occurring on larger spatial scales than in local galaxies. The Rieke et al. templates provide good fits to the measured Herschel SEDs, but the total far-infrared luminosity of the templates is higher than for the measured SEDs. There appears to be a difference between local ULIRGs and the high-z Herschel detected galaxies. As a consequence, using relations calibrated from observations of local galaxies for the high-z universe would overpredict the star-formation rates by a factor of 10.

[3]The angular resolution of the Herschel satellite combined with the high density of dusty sources in the SPIRE and PACS bands, makes the confusion noise in the Herschel maps more severe than in the LABOCA maps presented in this thesis.

[4]The SED dust peak ($\lambda_0 \simeq 70\,\mu$m) of galaxies at $z \approx 0.3$ is redshifted directly into the PACS bands

Paper E

Improving the identification of high-z Herschel sources with position priors and optical/NIR and FIR/mm photometric redshifts

In this paper (Pérez-González et al., 2010, paper E), which is a companion paper to Paper D, we present a method for deblending Herschel source with Spitzer MIPS 24 μm source positions as priors. We also present photometric redshift determinations for Herschel sources, and found that the near-infrared photo-z methods and the submm/mm methods agree to good precision.

Furthermore, paper E discusses two Herschel sources in detail. One is the counterpart of a gravitational arc initially detected in VLT/FORS imaging (Mehlert et al., 2001), at a redshift $z = 3.24$. This source was not included in the catalog presented in Johansson et al. (2010), however there appears to be a flux overdensity at this position in the LABOCA map. We used SED fitting to find a photometric redshift estimate $z = 3.24$ (coinciding with the previously determined spectroscopic redshift from Mehlert et al. 2001). The second source is LABOCA Source #10 in Paper I, or SMM J065845.6-555848. It has a moderate submm flux of $S_{870\,\mu\mathrm{m}}$∼5.5 mJy, but in paper E it is categorized as a Hyper-LIRG (having $L_{\mathrm{FIR}} > 10^{13}\,L_{\odot}$) because of its high dust temperature. However, the gravitational magnification factor $\mu \sim 1.35$ (Paper II), which was not included in this study makes this galaxy a ULIRG.

Chapter 3

Papers on Sunyaev–Zeldovich observations

3.1 The APEX-SZ project

The APEX-SZ receiver (also referred to sometimes as ASZCA – APEX Sunyaev–Zeldovich CAmera), is a broadband continuum bolometer receiver that was mounted in the Cassegrain cabin of the APEX telescope. It recorded scientific data from August 2007 during seven observing runs until it was dismounted from the APEX telescope in December 2010. It is designed for the detection of galaxy clusters through their Sunyaev–Zeldovich decrement at a frequency of 150 GHz (corresponding to a wavelength of 2 mm), where the decrement is close to its deepest point (see Fig. 1.4). Technical aspects of APEX-SZ are described by Schwan et al. (2003), Dobbs et al. (2006) and Schwan et al. (2010). A summary of technical parameters of the receiver can be found in Section 1.5.

APEX-SZ consists of 320 bolometer receivers on six hexagonal wedges. It operates at a frequency of 150 GHz with the bandwidth of ∼20 GHz (Halverson et al., 2009). The broad band is useful in order to maximize the signal-to-noise in the measurement. Waves with higher and lower frequencies than the band are filtered out by conical feedhorns, one for each bolometer. The resolution of APEX-SZ is one arcminute, the size of typical galaxy clusters in a survey (Battye & Weller, 2005). APEX-SZ has mostly been used for pointed observations of known galaxy clusters with previous detections in the X-ray, optical or SZ.

The bolometer camera is undersampled on the sky because of the size of the feed horns that direct the photons onto the bolometers. To fully sample the sky the telescope is scanning in a circular drift scan pattern in horizontal coordinates. Drift scans are performed on positions specified is azimuth and in elevation, while the sources drift through the scanning field. This results in a large coverage that appears extended along the right ascension axis as shown in Fig. 3.1. Figs. 3.2, kindly provided by M. Sommer, shows examples of APEX-SZ detections of the Sunyaev–Zeldovich decrement from nine galaxy clusters.

The APEX-SZ project is run by an international collaboration of scientists in several universities and countries (UC Berkeley – USA, University of Colorado – USA, Mc Gill University – Canada, MPIfR Bonn & Bonn University – Germany, MPE Munich – Germany, Chalmers/Onsala – Sweden, ESO).

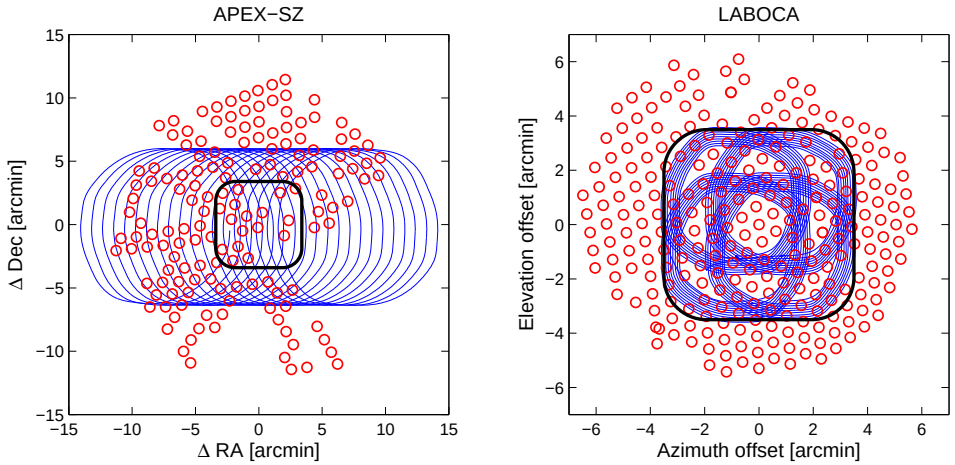

Figure 3.1: *Left*: Scanning pattern during an APEX-SZ observation (blue lines) and imprint of the functioning bolometers (red circles). This figure illustrates the extent of the scanning pattern compared to the field-of-view of the bolometer camera. *Right*: The same for our LABOCA observations. The rounded rectangles shown in both panels has the same angular size.

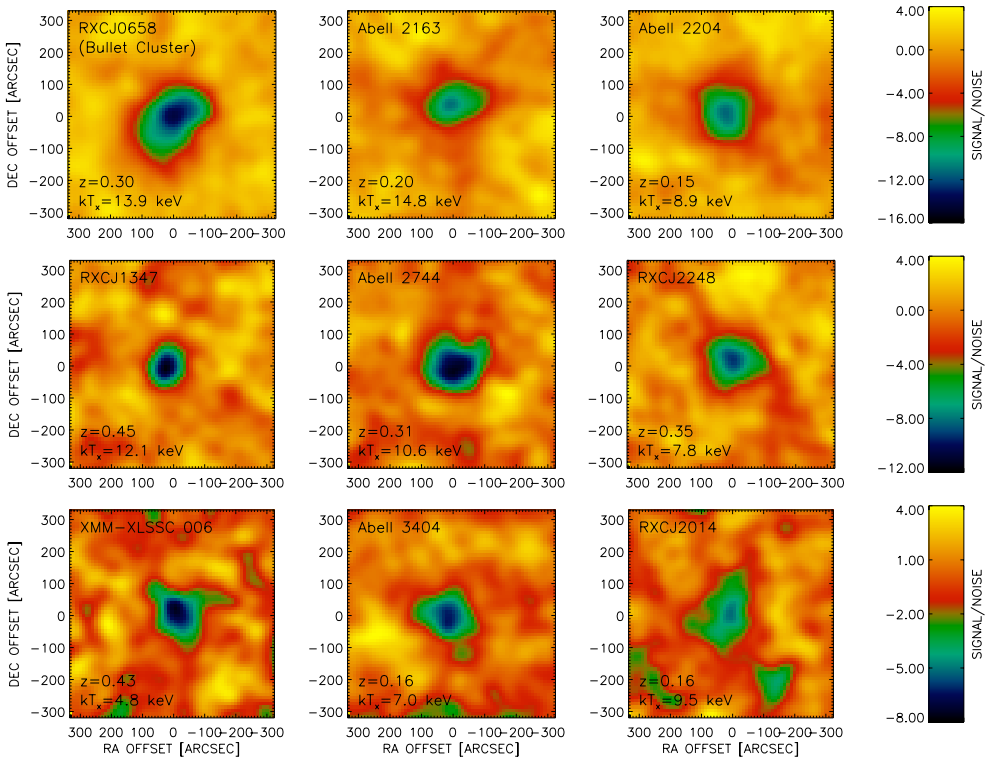

Figure 3.2: Signal-to-noise maps of nine galaxy clusters significantly detected with APEX-SZ. Figure taken from Nord (2009).

3.2 Papers A - C

Papers A, B and C are based on data taken with the APEX-SZ experiment. I participated in all the six observing runs for the project at the APEX telescope in Chile between 2008 and 2010. I have also attended weekly telephone meetings where the entire collaboration has discussed various matters, from the planning of the observations to the content of the papers A–C.

Paper A

Multi-frequency imaging of the galaxy cluster Abell 2163 using the Sunyaev-Zel'dovich effect

The study by Nord et al. (2009, paper A) is focused on observations of the merging galaxy cluster Abell 2163, a massive system (weak lensing-derived mass $M = (1.6\pm0.2)\times10^{15}\,M_{\odot}$, Radovich et al. 2008) at $z \approx 0.2$. Its angular extent is $15'$. Recovering the extended profile of Abell 2163 with the APEX-SZ and LABOCA instruments is complicated because the size of the cluster is larger or similar to that of the fields-of-view of the bolometer cameras.

In paper A we used two different methods to find the "true" distribution of gas in Abell 2163. The reduction pipeline transfer function was used in both of these approaches. The first method was a direct application of the *clean* algorithm used in radio interferometry processing, to deconvolve the transfer function from the image. The second approach is to fit an elliptical β-model, convolved with the point-source transfer function, to the raw Sunyaev–Zeldovich map. Both methods yield similar resulting cluster profiles. The downside to the first method is that a high-significance SZ-detection is needed for the deconvolution to work. Its advantage is that it results in a deconvolved SZ map, in contrast to the second method that yields only parameter values of a theoretical profile.

We also performed one of the first non-parameteric fits to the electron gas of the intracluster medium, combining the APEX-SZ data with data from the XMM-Newton observations of Abell 2163. Using the Abel inversion technique (Silk & White, 1978), the radial dependence of electron temperature and density can be determined. This was the first time that such an analysis was performed with actual cluster data, as previous studies were merely simulations. The method also allows for relaxing the assumption of isothermality that is explicit in model fits of the isothermal β-profile. The resulting radial temperature and electron profiles are consistent with those derived from X-ray surface brightness data combined with X-ray spectra. They extend radially towards the virial radius of the cluster, where they indicate, with low significance, a drop in temperature.

Finally, we constrained the SZ spectrum of Abell 2163 using the SZ data from APEX-SZ and LABOCA combined with data from OVRO/BIMA (LaRoque et al., 2002) and SUZIE (Holzapfel et al., 1997) and showed that tighter constraints can be imposed on the central comptonization parameter and peculiar velocity with addition of the APEX measurements.

Paper B

Constraints on the High-ℓ Power Spectrum of Millimeter-Wave Anisotropies from APEX-SZ

The study by Reichardt et al. (2009b, paper B) presented an investigation of millimeter-wave fluctuations on different angular scales, as measured with the APEX-SZ instrument. CMB anisotropies were already observed by the COBE and WMAP satellites, but due to their limited spatial resolution, they measure only the larger angular scales (corresponding to small angular multipoles ℓ) CMB power spectrum. Ground-based experiments have been used to constrain the higher multipoles (corresponding mainly to secondary CMB anisotropies and high-redshift

dusty galaxies). Such studies were performed with the Cosmic Background Imager (CBI) (Sievers et al., 2009) and the Berkeley Illinois Maryland Association (BIMA) interferometer (Dawson et al., 2006), both operating at 30 GHz. BIMA and CBI both found excess signal at angular multipoles that are believed to the dominated by secondary CMB anisotropies (e.g. the SZ effect from galaxy clusters not directly detected in the maps). At these frequencies the main source of confusion is radio sources associated with the galaxy clusters. At 2 mm wavelength (150 GHz) the ACBAR experiment (Reichardt et al., 2009a) made another detection of excess power, mainly contaminated by the unresolved "sea" of high-redshift, dusty star-forming galaxies. Finally, the BOLOCAM bolometer camera mounted on the Caltech Submillimeter Observatory (CSO) published another study of the high-ℓ power spectrum, where a constraint on the matter density variance $\sigma_8 < 1.57$ could be imposed at 90% significance (Sayers et al., 2009)

Paper B improved upon the ACBAR results with a deeper map obtained with the more sensitive APEX-SZ receiver (noise level 12 $\mu\mathrm{K_{CMB}}$). The paper presented APEX-SZ observations of a subset (0.8 deg^2) of the XMM-LSS field (Pierre et al., 2004). Two galaxy clusters were directly detected in the map, as well as 27 point sources, believed to be a mix of synchotron and dust-spectrum sources. When the clusters and the point sources have been masked out from the map, the power spectrum shows an excess signal at multipoles $l = [3000, 1000]$ corresponding to angular scales of 1/2–2 arcminutes. This signal is thought to be due to the Poisson distributed point-source distribution and the SZ-effect from undetected clusters. Through simultaneous fitting of the the dusty point source distribution and a model of the SZ-power spectrum, an upper limit on the matter variance could be imposed ($\sigma_8 < 1.18$) at 95% confidence. This is not a tight constraint compared with other methods, but with deeper data this result could be improved.

Paper C

Non-parametric modeling of the intra-cluster gas using APEX-SZ bolometer imaging data

In Paper C Basu et al. (2010) continued along the lines of the work by Paper A with another study of a hot galaxy cluster. Abell 2204, at $z \sim 0.15$, has an angular size of $\sim 12'$ and a mass of $M_{200} = 7.1 \times 10^{14}\, M_\odot$ (derived from weak-lensing observations, Corless et al. 2009), and is, contrary to Abell 2163, in a relaxed state. APEX-SZ detected the cluster with a peak significance of 8.5σ at a noise level of 44 $\mu\mathrm{K_{CMB}}$. Together with the APEX-SZ radial profile, the X-ray profile from XMM-Newton was used to obtain the non-parametric radial profile. The temperature profile, binned to only two radial values, shows a clear drop towards the outskirts. This was the first time such a result was obtained from an SZ map of a galaxy cluster. The central gas mass fraction was found to be lower than what is obtained from X-ray methods alone. The entropy profiles derived for Abell 2204 and Abell 2163 (from paper A) were compared, and it was shown that the central entropy for Abell 2163 is significantly larger than that for Abell 2204. This was interpreted as a sign of relaxation of the two clusters; since Abell 2204 is more relaxed it has a lower central entropy value.

Chapter 4

An unidentified bright submillimeter source

4.1 Motivation

In recent years, observations with ground-based bolometric cameras with large fields-of view and increased mapping speeds (LABOCA, SPT, AzTEC, ACT) have led to the discovery a population of extremely bright extragalactic submm galaxies. From space, a similar class of sources have been detected with the Herschel Space Observatory. It has already been shown that many of these bright submm galaxies are gravitationally lensed by a foreground galaxy or galaxy cluster (e.g. Paper I and Paper II, Wilson et al. 2008; Swinbank et al. 2010; Negrello et al. 2010).

We have re-analyzed all data from the LABOCA large program *Dust at low and high redshifts* (PI: René Liseau). The main aim of the program was to observe stars with an infrared excess (see Nilsson et al, 2009, 2010) and to search for submm galaxies in the field. The study of the LABOCA maps is ongoing, but we have detected one spectacular submm source with a flux density of 45 ± 6 mJy in the map centered on the star HD216435 (see Fig. 4.2). Because the noise level increases rapidly towards the edge, we applied for director's time with LABOCA in point-source photometry mode to confirm the detection. This improves the possibility to remove sky noise from the data, and is four to five times faster than the mapping mode. The observations were done in August 2010; they confirmed the existence of the source, and a flux density of 53 ± 5 mJy.[1]

4.2 Spectral energy distribution and counterparts

We have performed an extensive search in the archives for overlapping data, but we have not found any clear counterpart to the source. The central star in the map, HD216435, has been observed in all Spitzer bands, but the field is not large enough to cover the bright submm source. We have found overlapping 2MASS and DSS2 data and checked the IRAS and AKARI all-sky catalogs, as well as SUMSS. The observed field lies away from the Galactic plane (at Galactic latitude $b \approx -58°$), making it less likely that the source is of galactic origin. Having confirmed the initial LABOCA detection, we have started a follow-up program, where we already have proposed more APEX observations.

It is likely that the intense submm emission derives from a dusty, high-redshift submm galaxy, but without photometric measurements at other wavelengths we must speculate about the origin

[1] We are currently investigating the cause of the $\sim 20\%$ difference between the two flux density measurements (calibration, intrinsic variability, details in the data reduction). In any case, the two observations confirm the existence of an extremely bright point source of ~ 50 mJy.

of the high submm flux. We present in Fig. 4.1 a plausible scenario where we have used an SED of Arp 220, a nearby ULIRG (Ultra Luminous InfraRed Galaxy), from the near-infrared to the radio. We show the SED of Arp 220, and three versions of it, which are redshifted to $z = 1, 2, 3$ and scaled to fit the LABOCA flux. Together with the SEDs we show upper limits or sensitivities from various surveys[2]. We can draw some interesting conclusions from the non-detection in these observations. While the IRAS and AKARI upper limits do not set any interesting constraints on the SED, SUMSS would detect an Arp 220–type source with the high submm flux, if it were at a redshift $z < 1.5$ showing that an even higher redshift is plausible. Finally, a source at $z \lesssim 2.0$ should be detected in the 2MASS Ks-band. Thus, it appears plausible, given the shape of the SED, that the submm source lies at $z > 2$. Since the median redshift of known submm galaxies is $< z >= 2.2$ (Chapman et al, 2005), this estimate strenghtens the idea that the source is a dust-enshrouded, star-forming submm galaxy. The argument relies on the adopted SED model with its uncertainties.

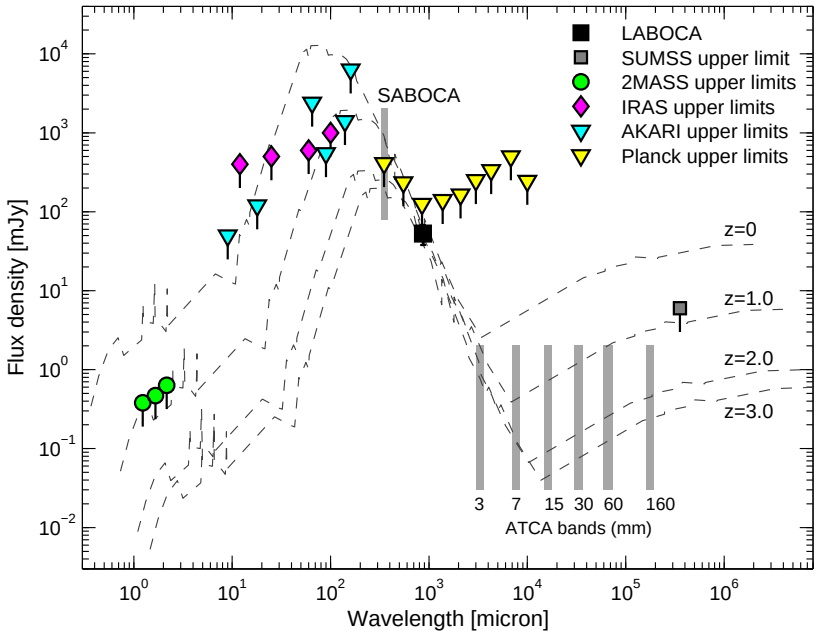

Figure 4.1: Photometric LABOCA flux measurement of the unidentified submm source, together with the observed spectral energy distribution of Arp 220, the archetypal ULIRG, obtained from archival data. We plot Arp 220's SED, and three redshifted versions. All the SEDs are scaled to fit the LABOCA data point. The vertical shaded region indicates the passband of SABOCA and ATCA. Filled symbols show the upper limits from different all-sky surveys (see text).

With the non-detections, we can rule out other types of objects. Local galaxies would be detected by IRAS or AKARI, and they are also not point-like. High-redshift radio galaxies (HzRGs, e.g. De Breuck et al, 2003) are another class of high-redshift, submm-bright objects, but they are ruled out by the non-detection at 843 MHz. A similar argument can be made about submm bright QSOs.

[2]We have investigated the appropriate all-sky surveys for counterparts. In the following surveys that search led to non-detections. The Sydney University Molonglo Sky Survey (SUMSS) is a 843 MHz radio survey of the southern skies (Bock et al., 1999). The 5σ sensitivity for point sources is $\sim$ 6 mJy. Limits of the Infrared Astronomical Satellite (IRAS) come from the IRAS point source catalog (Beichman et al., 1988). AKARI upper limits from Onaka & Salama (2009) while the 2MASS upper limits are from Skrutskie et al. (2006). Finally, the recently presented Planck sensitivities (Planck Collaboration, 2011a) from the first year of observations were also included.

We have also investigated visually the environment in the vicinity of the submm source. We show in Fig. 4.3 postage stamp images of Galex near-UV and DSS2 RGB images. Overlaid are also 2MASS-detected sources as white boxes, while the submm source itself is shown in black contours. The images show that the source has no counterpart in either GALEX or 2MASS. The DSS2 image shows a tentative detection in the center of the LABOCA contours, but the DSS2 image is affected by clear visual artefacts originating from the nearby star HD216435. Judging from the SED examples (Fig 4.1) an optical counterpart is very improbable. The flux density decreases very rapidly towards the optical wavelengths for the adopted SED of Arp 220.

4.3 Proposed observations

Follow-up observations are needed to characterize the submm-bright source. The nondetection in the all-sky surveys shows that deep, targeted observations are required. The SED models show that the observations with the most discriminative power would be either in the infrared or the radio part of the spectrum. We have thus started a follow-up campaign, and two proposals have already been written. They are summarized here.

- *APEX-SABOCA* – The SABOCA bolometer array at APEX operates at 350μm. Its pass-band is illustrated in Fig. 4.1. From that figure we see that SABOCA observations sample the dust peak of the spectral energy distribution, if the source is a high-z submm galaxy. This proposal has been granted 2.3 hours of observations which will take place in the summer of 2011.

- *ATCA* – we proposed to observe the radio emission from the submm source with the Australia Telescope Compact Array. For this proposal, we concentrated on the ATCA bands with the longest wavelengths. In the 3 mm and 7 mm ATCA bands it is very hard to estimate the predicted flux of the galaxy, and the best estimates gave very long required integration times. Thus, we decided to use first the four cm bands where the shape of the SED is such that the flux probably rises (this is generally the case for synchotron emission). In the proposal it was estimated that one ATCA track (12 hours of observations) would suffice to detect the source in the four cm bands. *Unfortunately observing time was not granted for this proposal. An updated proposal will be sent, since a detection in the radio bands of the source is necessary to characterize it.*

- *Z-Spec* – we want to use the Z-spec instrument to search for redshifted molecular or atomic emission lines from the bright galaxy. The Z-spec receiver has a bandwidth large enough so that several CO transitions of a high-z galaxy fall within the bandpass.

In Fig. 4.1 we have indicated the central wavelengths of the ATCA receivers on top of the four SEDs. As discussed above, the non-detections in the various surveys indicated in the figure points towards that the source is situated at $z \geq 2$. Focusing on the $z = 2$ and $z = 3$ SEDs, the expected flux densities at the ATCA wavelengths are in all cases (except for the 3 mm band) below the mJy level. It will be interesting to pursue this project further in order to understand what this bright submm source really is.

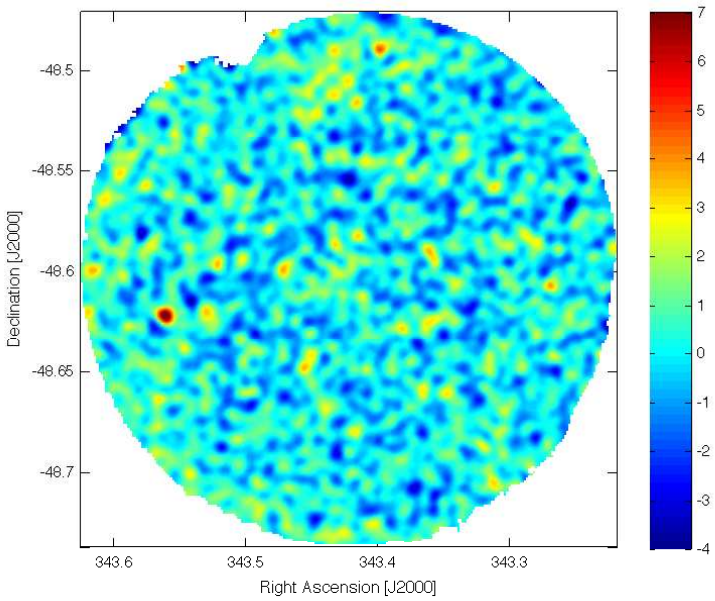

Figure 4.2: Signal-to-noise LABOCA map of the HD216435-field. The angular resolution of this map is $\sim$ 27 arcsec. The central star is not detected. The serendipitously detected submm source is visible as a dark red spot on the left-hand side of this image. It has a signal-to-noise ratio of $\sim$ 8 and a flux density of $\sim$ 50 mJy.

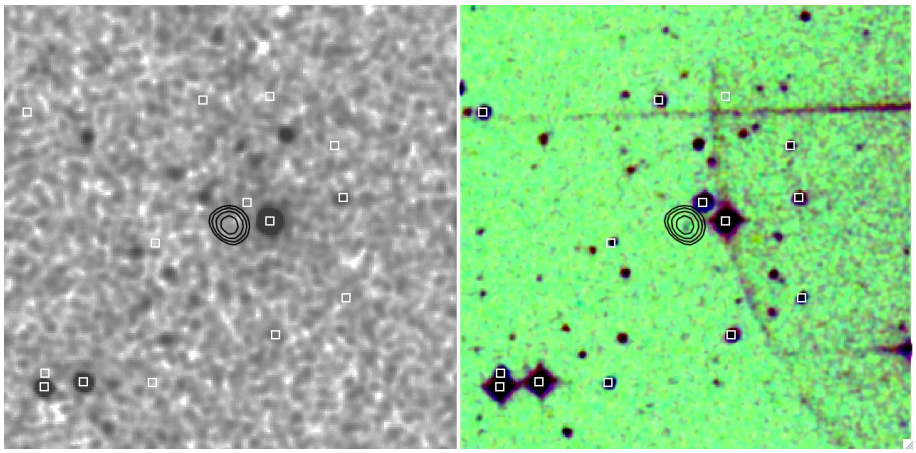

Figure 4.3: *Left*: Galex near-UV image of the vicinity of the submm source. *Right*: DSS2 RGB image created from the blue (B), red (G), and near-infrared (R) DSS2 images. In both images, the 4,5,6,7 σ LABOCA countours are plotted in black. The white boxes represent positions of 2MASS sources. The images show a region of $7' \times 7'$.

Chapter 5

Conclusions

The main content of my work during these five years has been to understand observations, data processing and interpretation of submillimeter data on galaxy clusters. Here I summarize the main conclusions drawn from the work presented in this thesis.

- I used the LABOCA bolometer camera on the APEX telescope to search for high-redshift submm galaxies behind galaxy clusters. In total, 37 such sources were detected, an addition to the growing number of known submm galaxies.
- One of the sources, SMM J0658, is comprised of two images of the same background galaxy and is one of the galaxies with the largest magnification factor (~ 100) discovered so far.
- Taking into account the gravitational lensing effect that the observed galaxy clusters induce on the population of background galaxies we could: (1) calculate the intrinsic source flux densities. (2) derive number counts, both the effect of the flux boosting due to magnification as well as how the area in the source plane varies across the lens. This led to number counts at some of the deepest flux density levels achieved so far in submm surveys. The results are consistent with those of previous studies.
- In Paper I and Paper II we studied the correlation between the submm maps and infrared Spitzer IRAC and MIPS maps. We identified counterparts to the submm sources detected in Paper I and we used the stacking method in Paper II to probe deeper than both the statistical noise in our maps as well as the confusion noise. Stacking uncovered a significant signal (14.5σ) in the 870 μm stacked map at the positions of MIPS 24 μm sources in four of the observed galaxy cluster fields. The flux density of the stacked signal is an order of magnitude lower than the formal flux limit for source extraction in the original maps.
- Paper III focuses on the brightest submm galaxy in our sample, SMM J0658. We detected the CO(1–0) and CO(3–2) rotational transitions in the $z \sim 2.8$ galaxy, and refined the spectroscopic redshift. The ratio between the brightness temperatures of CO(3–2) and CO(1–0) is ~ 0.56 which is close to the values found in other star-forming galaxies, but higher than those in more quiescent galaxies.
- We observed SMM J0658 with the SABOCA bolometer camera operating at 350 μm. The resulting map is consistent with earlier observations with the Herschel Space Observatory instrument SPIRE (at the same wavelength). The 3.6σ detection shows a slight elongation between the infrared Spitzer images A and B positions of SMM J0658.

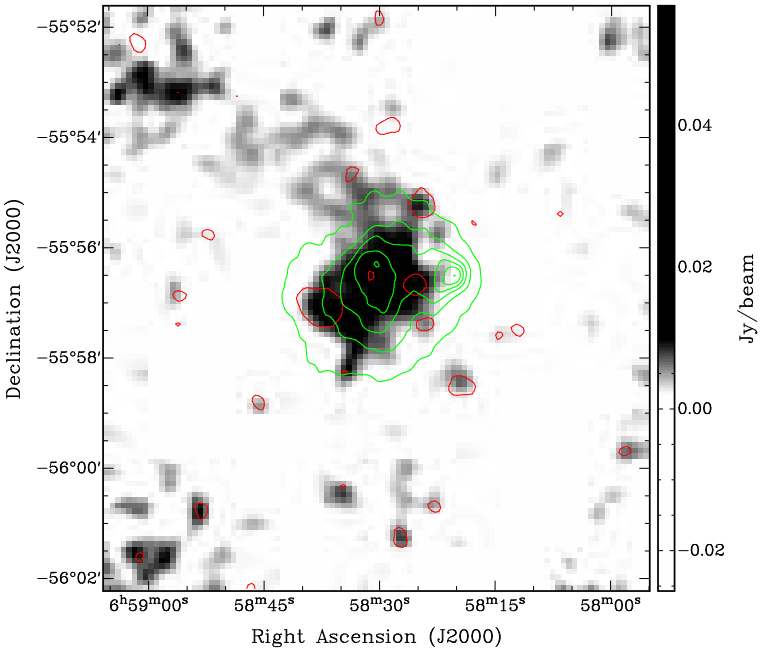

Figure 5.1: LABOCA map of the Bullet Cluster showing the detection of the Sunyaev–Zeldovich effect. The green contours show the X-ray map from the XMM-Newton satellite, and the red contours the LABOCA point sources.

- We used the APEX-SZ camera on the APEX telescope to observe a sample of about fifty galaxy clusters at 2 mm wavelength, where the amplitude of the Sunyaev–Zeldovich decrement is close to its maximum. We have been able to show that the APEX-SZ can detect and map massive galaxy clusters, and that pointed Sunyaev–Zeldovich observations are useful to study the physics of the intra-cluster medium.

Joint observations of the Sunyaev–Zeldovich effect and submm galaxies

I have presented the observations of the submillimeter galaxies and those of the Sunyaev - Zeldovich effect as two distinct projects in this thesis. There are, however, many situations when the two types of observations must be studied together. One of the main complications with observations of the SZ increment and decrement, is bright point sources that affect the SZ flux determination. At low frequencies radio emission from galaxies within the observed galaxy cluster is not unusual. At these frequencies the SZ effect gives rise to a negative flux density (a "hole in the sky"), when viewed in contrast to the 2.7 K background. A radio source can then "fill" the hole created by the cluster. If the radio sources can be identified in another observation (either by an interferometer with better spatial resolution, or at even longer wavelengths, which requires extrapolation by an unknown spectral index) the radio source can in principle be subtracted, but this is a complicated technique.

For the SZ increment things are slightly different. Here, Sunyaev–Zeldovich observations are mostly affected by lensed submm galaxies, such as the ones studied in the three papers in this thesis. In the 2 mm band where APEX-SZ operates, even the brightest submm galaxy in our survey does not influence the SZ measurement. At 870 μm, however, the flux density of the bright submm galaxy SMM J0658 behind the Bullet Cluster is of the same order as the total flux density of the Sunyaev–Zeldovich signal from the cluster itself. Initially, our LABOCA observations of the

Bullet Cluster were done with the aim to detect the SZ increment from the hot cluster gas, but the data reduction process is complicated by the many bright galaxies within the field. We can make a map filtered for detection of point sources, and use it to subtract the brightest point-like sources. Using this approach, I could make the Sunyaev–Zeldovich map of the Bullet Cluster presented in Figure 5.1. Finding the optimal filter set for these data is still work in progress, and will be presented by Sigurdarson et al, in prep.

As mentioned in Section 1.3.3, high-z galaxy clusters detected in the optical or X-ray appear to be harder to detect with SZ experiments than expected. One of the reasons for this may be that star-forming galaxies *within* the galaxy clusters are filling the SZ decrement. One example is the cluster XMMU J1230.3+1339 at $z = 0.975$ (Fassbender et al., 2011), that has eluded detection with APEX-SZ despite 50 hours of observing time. To find out whether a dust emission from a star-forming galaxy within the cluster is the cause of the non-detection, we have used LABOCA and MAMBO2 on the IRAM 30 m telescope (operating at 1.2 mm) to observe XMMU J1230.3+1339. The results of these observations have not been fully analyzed yet, but confirm a positive signal towards the center of the cluster.

These are just a few examples where the SZ and submm galaxy observations either complement each other, or where one confuses the other. Studying the population of star-forming galaxies in high-z galaxy clusters must be done to understand the SZ observations. This becomes even more important in the *Planck* observations, as it has a substantially larger beam and confusion with cluster sources can be more severe.

An outlook

Within six months, it is expected that the Atacama Large Millimeter Array (ALMA) will begin scientific observations. With its unprecedented sensitivity and angular resolution, it will likely lead to a revolution in the study of high-redshift galaxies. Observations like the ones presented in Paper III in this thesis will be possible for normal, un-lensed galaxies at high redshifts, although the magnified galaxies will still be interesting because they will provide the possibility to study the chemistry in the inter-stellar medium, as other lines than CO will be bright enough to be detected. ALMA can also be used to observe the Sunyaev–Zeldovich effect in galaxy clusters since it will have both an array with very short spacings as well as several single-dish telescopes that will provide sensitivity to emission on large scales. It will be very interesting to see what imprint ALMA will make on extragalactic astronomy.

Bibliography

Allamandola, L. J., Tielens, A. G. G. M., & Barker, J. R. 1989, ApJs, 71, 733

Allen, S. W., Rapetti, D. A., Schmidt, R. W., Ebeling, H., Morris, R. G., & Fabian, A. C. 2008, MNRAS, 383, 879

Amblard, A., Cooray, A., Serra, P., Temi, P., Barton, E., Negrello, M., Auld, R., Baes, M., Baldry, I. K., Bamford, S., Blain, A., Bock, J., Bonfield, D., Burgarella, D., Buttiglione, S., Cameron, E., Cava, A., Clements, D., Croom, S., Dariush, A., de Zotti, G., Driver, S., Dunlop, J., Dunne, L., Dye, S., Eales, S., Frayer, D., Fritz, J., Gardner, J. P., Gonzalez-Nuevo, J., Herranz, D., Hill, D., Hopkins, A., Hughes, D. H., Ibar, E., Ivison, R. J., Jarvis, M., Jones, D. H., Kelvin, L., Lagache, G., Leeuw, L., Liske, J., Lopez-Caniego, M., Loveday, J., Maddox, S., Michałowski, M., Norberg, P., Parkinson, H., Peacock, J. A., Pearson, C., Pascale, E., Pohlen, M., Popescu, C., Prescott, M., Robotham, A., Rigby, E., Rodighiero, G., Samui, S., Sansom, A., Scott, D., Serjeant, S., Sharp, R., Sibthorpe, B., Smith, D. J. B., Thompson, M. A., Tuffs, R., Valtchanov, I., van Kampen, E., van der Werf, P., Verma, A., Vieira, J., & Vlahakis, C. 2010, A&A, 518, L9+

Andreani, P., Böhringer, H., dall'Oglio, G., Martinis, L., Shaver, P., Lemke, R., Nyman, L.-Å., Booth, R., Pizzo, L., Whyborn, N., Tanaka, Y., & Liang, H. 1999, ApJ, 513, 23

Aretxaga, I., Hughes, D. H., Coppin, K., Mortier, A. M. J., Wagg, J., Dunlop, J. S., Chapin, E. L., Eales, S. A., Gaztañaga, E., Halpern, M., Ivison, R. J., van Kampen, E., Scott, D., Serjeant, S., Smail, I., Babbedge, T., Benson, A. J., Chapman, S., Clements, D. L., Dunne, L., Dye, S., Farrah, D., Jarvis, M. J., Mann, R. G., Pope, A., Priddey, R., Rawlings, S., Seigar, M., Silva, L., Simpson, C., & Vaccari, M. 2007, MNRAS, 379, 1571

Austermann, J. E., Dunlop, J. S., Perera, T. A., Scott, K. S., Wilson, G. W., Aretxaga, I., Hughes, D. H., Almaini, O., Chapin, E. L., Chapman, S. C., Cirasuolo, M., Clements, D. L., Coppin, K. E. K., Dunne, L., Dye, S., Eales, S. A., Egami, E., Farrah, D., Ferrusca, D., Flynn, S., Haig, D., Halpern, M., Ibar, E., Ivison, R. J., van Kampen, E., Kang, Y., Kim, S., Lacey, C., Lowenthal, J. D., Mauskopf, P. D., McLure, R. J., Mortier, A. M. J., Negrello, M., Oliver, S., Peacock, J. A., Pope, A., Rawlings, S., Rieke, G., Roseboom, I., Rowan-Robinson, M., Scott, D., Serjeant, S., Smail, I., Swinbank, A. M., Stevens, J. A., Velazquez, M., Wagg, J., & Yun, M. S. 2009, ArXiv e-prints

Barger, A. J., Cowie, L. L., & Sanders, D. B. 1999, ApJ, 518, L5

Barrena, R., Biviano, A., Ramella, M., Falco, E. E., & Seitz, S. 2002, A&A, 386, 816

Bartelmann, M., Huss, A., Colberg, J. M., Jenkins, A., & Pearce, F. R. 1998, A&A, 330, 1

Bartelmann, M. & Schneider, P. 2001, Phys. Rep., 340, 291

Basu, K., Zhang, Y., Sommer, M. W., Bender, A. N., Bertoldi, F., Dobbs, M., Eckmiller, H., Halverson, N. W., Holzapfel, W. L., Horellou, C., Jaritz, V., Johansson, D., Johnson, B., Kennedy, J., Kneissl, R., Lanting, T., Lee, A. T., Mehl, J., Menten, K. M., Navarrete, F. P., Pacaud, F., Reichardt, C. L., Reiprich, T. H., Richards, P. L., Schwan, D., & Westbrook, B. 2010, A&A, 519, A29+

Battye, R. A. & Weller, J. 2005, MNRAS, 362, 171

Beelen, A., Omont, A., Bavouzet, N., Kovács, A., Lagache, G., De Breuck, C., Weiss, A., Menten, K. M., Colbert, J. W., Dole, H., Siringo, G., & Kreysa, E. 2008, A&A, 485, 645

Beichman, C. A., Neugebauer, G., Habing, H. J., Clegg, P. E., & Chester, T. J., eds. 1988, Infrared astronomical satellite (IRAS) catalogs and atlases. Volume 1: Explanatory supplement, ed. C. A. Beichman, G. Neugebauer, H. J. Habing, P. E. Clegg, & T. J. Chester, Vol. 1

Bertoldi, F., Carilli, C., Aravena, M., Schinnerer, E., Voss, H., Smolcic, V., Jahnke, K., Scoville, N., Blain, A., Menten, K. M., Lutz, D., Brusa, M., Taniguchi, Y., Capak, P., Mobasher, B., Lilly, S., Thompson, D., Aussel, H., Kreysa, E., Hasinger, G., Aguirre, J., Schlaerth, J., & Koekemoer, A. 2007, ApJs, 172, 132

Birkinshaw, M. 1999, Phys. Rep., 310, 97

Blain, A. W., Chapman, S. C., Smail, I., & Ivison, R. 2004, ApJ, 611, 725

Blain, A. W., Smail, I., Ivison, R. J., Kneib, J.-P., & Frayer, D. T. 2002, Phys. Rep., 369, 111

Blandford, R. D. & Narayan, R. 1992, ARA&A, 30, 311

Blumenthal, G. R., Faber, S. M., Primack, J. R., & Rees, M. J. 1984, Nature, 311, 517

Bock, D. C.-J., Large, M. I., & Sadler, E. M. 1999, ApJ, 117, 1578

Bond, J. R., Cole, S., Efstathiou, G., & Kaiser, N. 1991, ApJ, 379, 440

Bradač, M., Clowe, D., Gonzalez, A. H., Marshall, P., Forman, W., Jones, C., Markevitch, M., Randall, S., Schrabback, T., & Zaritsky, D. 2006, ApJ, 652, 937

Bradač, M., Treu, T., Applegate, D., Gonzalez, A. H., Clowe, D., Forman, W., Jones, C., Marshall, P., Schneider, P., & Zaritsky, D. 2009, ApJ, 706, 1201

Brodwin, M., Ruel, J., Ade, P. A. R., Aird, K. A., Andersson, K., Ashby, M. L. N., Bautz, M., Bazin, G., Benson, B. A., Bleem, L. E., Carlstrom, J. E., Chang, C. L., Crawford, T. M., Crites, A. T., de Haan, T., Desai, S., Dobbs, M. A., Dudley, J. P., Fazio, G. G., Foley, R. J., Forman, W. R., Garmire, G., George, E. M., Gladders, M. D., Gonzalez, A. H., Halverson, N. W., High, F. W., Holder, G. P., Holzapfel, W. L., Hrubes, J. D., Jones, C., Joy, M., Keisler, R., Knox, L., Lee, A. T., Leitch, E. M., Lueker, M., Marrone, D. P., McMahon, J. J., Mehl, J., Meyer, S. S., Mohr, J. J., Montroy, T. E., Murray, S. S., Padin, S., Plagge, T., Pryke, C., Reichardt, C. L., Rest, A., Ruhl, J. E., Schaffer, K. K., Shaw, L., Shirokoff, E., Song, J., Spieler, H. G., Stalder, B., Stanford, S. A., Staniszewski, Z., Stark, A. A., Stubbs, C. W., Vanderlinde, K., Vieira, J. D., Vikhlinin, A., Williamson, R., Yang, Y., Zahn, O., & Zenteno, A. 2010a, ApJ, 721, 90

Brodwin, M., Stern, D., Vikhlinin, A., Stanford, S. A., Gonzalez, A. H., Eisenhardt, P. R., Ashby, M. L. N., Bautz, M., Dey, A., Forman, W. R., Gettings, D., Hickox, R. C., Jannuzi, B. T., Jones, C., Mancone, C., Miller, E. D., Moustakas, L. A., Ruel, J., Snyder, G., & Zeimann, G. 2010b, ArXiv e-prints

Carlstrom, J. E., Ade, P. A. R., Aird, K. A., Benson, B. A., Bleem, L. E., Busetti, S., Chang, C. L., Chauvin, E., Cho, H., Crawford, T. M., Crites, A. T., Dobbs, M. A., Halverson, N. W., Heimsath, S., Holzapfel, W. L., Hrubes, J. D., Joy, M., Keisler, R., Lanting, T. M., Lee, A. T., Leitch, E. M., Leong, J., Lu, W., Lueker, M., McMahon, J. J., Mehl, J., Meyer, S. S., Mohr, J. J., Montroy, T. E., Padin, S., Plagge, T., Pryke, C., Ruhl, J. E., Schaffer, K. K., Schwan, D., Shirokoff, E., Spieler, H. G., Staniszewski, Z., Stark, A. A., & Vieira, K. V. J. D. 2009, ArXiv e-prints

Carlstrom, J. E., Holder, G. P., & Reese, E. D. 2002, ARA&A, 40, 643

Challinor, A. & Lasenby, A. 1998, ApJ, 499, 1

Chapman, S. C., Blain, A. W., Smail, I., & Ivison, R. J. 2005, ApJ, 622, 772

Chapman, S. C., Scott, D., Borys, C., & Fahlman, G. G. 2002, MNRAS, 330, 92

Clowe, D., Bradač, M., Gonzalez, A. H., Markevitch, M., Randall, S. W., Jones, C., & Zaritsky, D. 2006, ApJ, 648, L109

Clowe, D., Gonzalez, A., & Markevitch, M. 2004, ApJ, 604, 596

Condon, J. J. 1974, ApJ, 188, 279

Coppin, K., Chapin, E. L., Mortier, A. M. J., Scott, S. E., Borys, C., Dunlop, J. S., Halpern, M., Hughes, D. H., Pope, A., Scott, D., Serjeant, S., Wagg, J., Alexander, D. M., Almaini, O., Aretxaga, I., Babbedge, T., Best, P. N., Blain, A., Chapman, S., Clements, D. L., Crawford, M., Dunne, L., Eales, S. A., Edge, A. C., Farrah, D., Gaztañaga, E., Gear, W. K., Granato, G. L., Greve, T. R., Fox, M., Ivison, R. J., Jarvis, M. J., Jenness, T., Lacey, C., Lepage, K., Mann, R. G., Marsden, G., Martinez-Sansigre, A., Oliver, S., Page, M. J., Peacock, J. A., Pearson, C. P., Percival, W. J., Priddey, R. S., Rawlings, S., Rowan-Robinson, M., Savage, R. S., Seigar, M., Sekiguchi, K., Silva, L., Simpson, C., Smail, I., Stevens, J. A., Takagi, T., Vaccari, M., van Kampen, E., & Willott, C. J. 2006, MNRAS, 372, 1621

Corless, V. L., King, L. J., & Clowe, D. 2009, MNRAS, 393, 1235

Culverhouse, T. L., Bonamente, M., Bulbul, E., Carlstrom, J. E., Gralla, M. B., Greer, C., Hasler, N., Hawkins, D., Hennessy, R., Jetha, N. N., Joy, M., Lamb, J. W., Leitch, E. M., Marrone, D. P., Miller, A., Mroczkowski, T., Muchovej, S., Pryke, C., Sharp, M., Woody, D., Andreon, S., Maughan, B., & Stanford, S. A. 2010, ApJ, 723, L78

Daddi, E., Cimatti, A., Renzini, A., Fontana, A., Mignoli, M., Pozzetti, L., Tozzi, P., & Zamorani, G. 2004, ApJ, 617, 746

Daddi, E., Dickinson, M., Chary, R., Pope, A., Morrison, G., Alexander, D. M., Bauer, F. E., Brandt, W. N., Giavalisco, M., Ferguson, H., Lee, K., Lehmer, B. D., Papovich, C., & Renzini, A. 2005, ApJ, 631, L13

Danielson, A. L. R., Swinbank, A. M., Smail, I., Cox, P., Edge, A. C., Weiss, A., Harris, A. I., Baker, A. J., De Breuck, C., Geach, J. E., Ivison, R. J., Krips, M., Lundgren, A., Longmore, S., Neri, R., & Flaquer, B. O. 2010, MNRAS, 1565

Dawson, K. S., Holzapfel, W. L., Carlstrom, J. E., Joy, M., & LaRoque, S. J. 2006, ApJ, 647, 13

Dobbs, M., Halverson, N. W., Ade, P. A. R., Basu, K., Beelen, A., Bertoldi, F., Cohalan, C., Cho, H. M., Güsten, R., Holzapfel, W. L., Kermish, Z., Kneissl, R., Kovács, A., Kreysa, E., Lanting, T. M., Lee, A. T., Lueker, M., Mehl, J., Menten, K. M., Muders, D., Nord, M., Plagge, T., Richards, P. L., Schilke, P., Schwan, D., Spieler, H., Weiss, A., & White, M. 2006, New Astronomy Review, 50, 960

Dole, H., Lagache, G., Puget, J., Caputi, K. I., Fernández-Conde, N., Le Floc'h, E., Papovich, C., Pérez-González, P. G., Rieke, G. H., & Blaylock, M. 2006, A&A, 451, 417

Dwek, E., Arendt, R. G., Hauser, M. G., Fixsen, D., Kelsall, T., Leisawitz, D., Pei, Y. C., Wright, E. L., Mather, J. C., Moseley, S. H., Odegard, N., Shafer, R., Silverberg, R. F., & Weiland, J. L. 1998, ApJ, 508, 106

Einstein, A. 1911, Annalen der Physik, 340, 898

Fabian, A. C. 1991, MNRAS, 253, 29P

Farrar, G. R. & Rosen, R. A. 2007, Physical Review Letters, 98, 171302

Fassbender, R., Böhringer, H., Santos, J. S., Pratt, G. W., Suhada, R., Kohnert, J., Lerchster, M., Rovilos, M., Pierini, D., Chon, G., Schwope, A. D., Lamer, G., Mühlegger, M., Rosati, P., Quintana, H., Nastasi, A., de Hoon, A., Seitz, S., & Mohr, J. J. 2010, ArXiv e-prints

Fassbender, R., Böhringer, H., Santos, J. S., Pratt, G. W., Šuhada, R., Kohnert, J., Lerchster, M., Rovilos, E., Pierini, D., Chon, G., Schwope, A. D., Lamer, G., Mühlegger, M., Rosati, P., Quintana, H., Nastasi, A., de Hoon, A., Seitz, S., & Mohr, J. J. 2011, A&A, 527, A78+

Fazio, G. G., Hora, J. L., Allen, L. E., Ashby, M. L. N., Barmby, P., Deutsch, L. K., Huang, J.-S., Kleiner, S., Marengo, M., Megeath, S. T., Melnick, G. J., Pahre, M. A., Patten, B. M., Polizotti, J., Smith, H. A., Taylor, R. S., Wang, Z., Willner, S. P., Hoffmann, W. F., Pipher, J. L., Forrest, W. J., McMurty, C. W., McCreight, C. R., McKelvey, M. E., McMurray, R. E., Koch, D. G., Moseley, S. H., Arendt, R. G., Mentzell, J. E., Marx, C. T., Losch, P., Mayman, P., Eichhorn, W., Krebs, D., Jhabvala, M., Gezari, D. Y., Fixsen, D. J., Flores, J., Shakoorzadeh, K., Jungo, R., Hakun, C., Workman, L., Karpati, G., Kichak, R., Whitley, R., Mann, S., Tollestrup, E. V., Eisenhardt, P., Stern, D., Gorjian, V., Bhattacharya, B., Carey, S., Nelson, B. O., Glaccum, W. J., Lacy, M., Lowrance, P. J., Laine, S., Reach, W. T., Stauffer, J. A., Surace, J. A., Wilson, G., Wright, E. L., Hoffman, A., Domingo, G., & Cohen, M. 2004, ApJs, 154, 10

Fixsen, D. J., Dwek, E., Mather, J. C., Bennett, C. L., & Shafer, R. A. 1998, ApJ, 508, 123

Giavalisco, M., Ferguson, H. C., Koekemoer, A. M., Dickinson, M., Alexander, D. M., Bauer, F. E., Bergeron, J., Biagetti, C., Brandt, W. N., Casertano, S., Cesarsky, C., Chatzichristou, E., Conselice, C., Cristiani, S., Da Costa, L., Dahlen, T., de Mello, D., Eisenhardt, P., Erben, T., Fall, S. M., Fassnacht, C., Fosbury, R., Fruchter, A., Gardner, J. P., Grogin, N., Hook, R. N., Hornschemeier, A. E., Idzi, R., Jogee, S., Kretchmer, C., Laidler, V., Lee, K. S., Livio, M., Lucas, R., Madau, P., Mobasher, B., Moustakas, L. A., Nonino, M., Padovani, P., Papovich, C., Park, Y., Ravindranath, S., Renzini, A., Richardson, M., Riess, A., Rosati, P., Schirmer, M., Schreier, E., Somerville, R. S., Spinrad, H., Stern, D., Stiavelli, M., Strolger, L., Urry, C. M., Vandame, B., Williams, R., & Wolf, C. 2004, ApJ, 600, L93

Gomez, P., Romer, A. K., Peterson, J. B., Chase, W., Runyan, M., Holzapfel, W., Kuo, C. L., Newcomb, M., Ruhl, J., Goldstein, J., & Lange, A. 2004, in AIP Conf. Proc. 703: Plasmas in the Laboratory and in the Universe: New Insights and New Challenges, ed. G. Bertin, D. Farina, & R. Pozzoli, 361–366

Gonzalez, A. H., Clowe, D., Bradač, M., Zaritsky, D., Jones, C., & Markevitch, M. 2009, ApJ, 691, 525

Gonzalez, A. H., Papovich, C., Bradač, M., & Jones, C. 2010, ApJ, 720, 245

Griffin, M. J., Abergel, A., Abreu, A., Ade, P. A. R., André, P., Augueres, J., Babbedge, T., Bae, Y., Baillie, T., Baluteau, J., Barlow, M. J., Bendo, G., Benielli, D., Bock, J. J., Bonhomme, P., Brisbin, D., Brockley-Blatt, C., Caldwell, M., Cara, C., Castro-Rodriguez, N., Cerulli, R., Chanial, P., Chen, S., Clark, E., Clements, D. L., Clerc, L., Coker, J., Communal, D., Conversi, L., Cox, P., Crumb, D., Cunningham, C., Daly, F., Davis, G. R., de Antoni, P., Delderfield, J., Devin, N., di Giorgio, A., Didschuns, I., Dohlen, K., Donati, M., Dowell, A., Dowell, C. D., Duband, L., Dumaye, L., Emery, R. J., Ferlet, M., Ferrand, D., Fontignie, J., Fox, M., Franceschini, A., Frerking, M., Fulton, T., Garcia, J., Gastaud, R., Gear, W. K., Glenn, J., Goizel, A., Griffin, D. K., Grundy, T., Guest, S., Guillemet, L., Hargrave, P. C., Harwit, M., Hastings, P., Hatziminaoglou, E., Herman, M., Hinde, B., Hristov, V., Huang, M., Imhof, P., Isaak, K. J., Israelsson, U., Ivison, R. J., Jennings, D., Kiernan, B., King, K. J., Lange, A. E., Latter, W., Laurent, G., Laurent, P., Leeks, S. J., Lellouch, E., Levenson, L., Li, B., Li, J., Lilienthal, J., Lim, T., Liu, S. J., Lu, N., Madden, S., Mainetti, G., Marliani, P., McKay, D., Mercier, K., Molinari, S., Morris, H., Moseley, H., Mulder, J., Mur, M., Naylor, D. A., Nguyen, H., O'Halloran, B., Oliver, S., Olofsson, G., Olofsson, H., Orfei, R., Page, M. J., Pain, I., Panuzzo, P., Papageorgiou, A., Parks, G., Parr-Burman, P., Pearce, A., Pearson, C., Pérez-Fournon, I., Pinsard, F., Pisano, G., Podosek, J., Pohlen, M., Polehampton, E. T., Pouliquen, D., Rigopoulou, D., Rizzo, D., Roseboom, I. G., Roussel, H., Rowan-Robinson, M., Rownd, B., Saraceno, P., Sauvage, M., Savage, R., Savini, G., Sawyer, E., Scharmberg, C., Schmitt, D., Schneider, N., Schulz, B., Schwartz, A., Shafer, R., Shupe, D. L., Sibthorpe, B., Sidher, S., Smith, A., Smith, A. J., Smith, D., Spencer, L., Stobie, B., Sudiwala, R., Sukhatme, K., Surace, C., Stevens, J. A., Swinyard, B. M., Trichas, M., Tourette, T., Triou, H., Tseng, S., Tucker, C., Turner, A., Vaccari, M., Valtchanov, I., Vigroux, L., Virique, E., Voellmer, G., Walker, H., Ward, R., Waskett, T., Weilert, M., Wesson, R., White, G. J., Whitehouse, N., Wilson, C. D., Winter, B., Woodcraft, A. L., Wright, G. S., Xu, C. K., Zavagno, A., Zemcov, M., Zhang, L., & Zonca, E. 2010, A&A, 518, L3+

Güsten, R., Nyman, L. Å., Schilke, P., Menten, K., Cesarsky, C., & Booth, R. 2006, A&A, 454, L13

Halverson, N. W., Lanting, T., Ade, P. A. R., Basu, K., Bender, A. N., Benson, B. A., Bertoldi, F., Cho, H., Chon, G., Clarke, J., Dobbs, M., Ferrusca, D., Güsten, R., Holzapfel, W. L., Kovács, A., Kennedy, J., Kermish, Z., Kneissl, R., Lee, A. T., Lueker, M., Mehl, J., Menten, K. M., Muders, D., Nord, M., Pacaud, F., Plagge, T., Reichardt, C., Richards, P. L., Schaaf, R., Schilke, P., Schuller, F., Schwan, D., Spieler, H., Tucker, C., Weiss, A., & Zahn, O. 2009, ApJ, 701, 42

Hauser, M. G., Arendt, R. G., Kelsall, T., Dwek, E., Odegard, N., Weiland, J. L., Freudenreich, H. T., Reach, W. T., Silverberg, R. F., Moseley, S. H., Pei, Y. C., Lubin, P., Mather, J. C., Shafer, R. A., Smoot, G. F., Weiss, R., Wilkinson, D. T., & Wright, E. L. 1998, ApJ, 508, 25

Hayashi, E. & White, S. D. M. 2006, MNRAS, 370, L38

Hezaveh, Y. D. & Holder, G. P. 2010, ArXiv e-prints

Hincks, A. D., Acquaviva, V., Ade, P., Aguirre, P., Amiri, M., Appel, J. W., Barrientos, L. F., Battistelli, E. S., Bond, J. R., Brown, B., Burger, B., Chervenak, J., Das, S., Devlin, M. J., Dicker, S., Doriese, W. B., Dunkley, J., Dünner, R., Essinger-Hileman, T., Fisher, R. P., Fowler, J. W., Hajian, A., Halpern, M., Hasselfield, M., Hernández-Monteagudo, C., Hilton, G. C., Hilton, M., Hlozek, R., Huffenberger, K., Hughes, D., Hughes, J. P., Infante, L., Irwin, K. D., Jimenez, R., Juin, J. B., Kaul, M., Klein, J., Kosowsky, A., Lau, J. M., Limon, M., Lin, Y., Lupton, R. H., Marriage, T., Marsden, D., Martocci, K., Mauskopf, P., Menanteau, F., Moodley, K., Moseley, H., Netterfield, C. B., Niemack, M. D., Nolta, M. R., Page, L. A., Parker, L., Partridge, B., Quintana, H., Reid, B., Sehgal, N., Sievers, J., Spergel, D. N., Staggs, S. T., Stryzak, O., Swetz, D., Switzer, E., Thornton, R., Trac, H., Tucker, C., Verde, L., Warne, R., Wilson, G., Wollack, E., & Zhao, Y. 2009, ArXiv e-prints

Ho, P. T. P., Altamirano, P., Chang, C., Chang, S., Chang, S., Chen, C., Chen, K., Chen, M., Han, C., Ho, W. M., Huang,

Y., Hwang, Y., Ibañez-Romano, F., Jiang, H., Koch, P. M., Kubo, D. Y., Li, C., Lim, J., Lin, K., Liu, G., Lo, K., Ma, C., Martin, R. N., Martin-Cocher, P., Molnar, S. M., Ng, K., Nishioka, H., O'Connell, K. E., Oshiro, P., Patt, F., Raffin, P., Umetsu, K., Wei, T., Wu, J., Chiueh, T., Chiueh, T., Chu, T., Huang, C., Hwang, W. Y. P., Liao, Y., Lien, C., Wang, F., Wang, H., Wei, R., Yang, C., Kesteven, M., Kingsley, J., Sinclair, M. M., Wilson, W., Birkinshaw, M., Liang, H., Lancaster, K., Park, C., Pen, U., & Peterson, J. B. 2009, ApJ, 694, 1610

Hogg, D. W. 2001, ApJ, 121, 1207

Holzapfel, W. L., Ade, P. A. R., Church, S. E., Mauskopf, P. D., Rephaeli, Y., Wilbanks, T. M., & Lange, A. E. 1997, ApJ, 481, 35

Horellou, C., Nord, M., Johansson, D., & Lévy, A. 2005, A&A, 441, 435

Ikarashi, S., Kohno, K., Aguirre, J. E., Aretxaga, I., Arumugam, V., Austermann, J. E., Bock, J. J., Bradford, C. M., Cirasuolo, M., Earle, L., Ezawa, H., Furusawa, H., Furusawa, J., Glenn, J., Hatsukade, B., Hughes, D. H., Iono, D., Ivison, R. J., Johnson, S., Kamenetzky, J., Kawabe, R., Lupu, R., Maloney, P., Matsuhara, H., Mauskopf, P. D., Motohara, K., Murphy, E. J., Nakajima, K., Nakanishi, K., Naylor, B. J., Nguyen, H. T., Perera, T. A., Scott, K. S., Shimasaku, K., Takagi, T., Takata, T., Tamura, Y., Tanaka, K., Tsukagoshi, T., Wilner, D. J., Wilson, G. W., Yun, M. S., & Zmuidzinas, J. 2010, ArXiv e-prints

Itoh, N., Kohyama, Y., & Nozawa, S. 1998, ApJ, 502, 7

Johansson, D. 2009, Licentiate thesis, Chalmers University of Technology

Johansson, D., Horellou, C., Sommer, M. W., Basu, K., Bertoldi, F., Birkinshaw, M., Lancaster, K., Lopez-Cruz, O., & Quintana, H. 2010, A&A, 514, A77+

Knudsen, K. K., van der Werf, P., Franx, M., Förster Schreiber, N. M., van Dokkum, P. G., Illingworth, G. D., Labbé, I., Moorwood, A., Rix, H., & Rudnick, G. 2005, ApJ, 632, L9

Knudsen, K. K., van der Werf, P. P., & Kneib, J.-P. 2008, MNRAS, 384, 1611

Komatsu, E., Dunkley, J., Nolta, M. R., Bennett, C. L., Gold, B., Hinshaw, G., Jarosik, N., Larson, D., Limon, M., Page, L., Spergel, D. N., Halpern, M., Hill, R. S., Kogut, A., Meyer, S. S., Tucker, G. S., Weiland, J. L., Wollack, E., & Wright, E. L. 2009, ApJs, 180, 330

Kompaneets, A. 1957, Sov. Phys. JETP, 4, p. 730.

Lagache, G., Dole, H., Puget, J., Pérez-González, P. G., Le Floc'h, E., Rieke, G. H., Papovich, C., Egami, E., Alonso-Herrero, A., Engelbracht, C. W., Gordon, K. D., Misselt, K. A., & Morrison, J. E. 2004, ApJs, 154, 112

Lagache, G., Puget, J.-L., & Dole, H. 2005, ARA&A, 43, 727

LaRoque, S. J., Carlstrom, J. E., Reese, E. D., Holder, G. P., Holzapfel, W. L., Joy, M., & Grego, L. 2002, ArXiv Astrophysics e-prints

Lestrade, J., Combes, F., Salomé, P., Omont, A., Bertoldi, F., André, P., & Schneider, N. 2010, A&A, 522, L4+

Liang, H., Hunstead, R. W., Birkinshaw, M., & Andreani, P. 2000, ApJ, 544, 686

Lima, M., Jain, B., & Devlin, M. 2010, MNRAS, 406, 2352

Maddox, S. J., Dunne, L., Rigby, E., Eales, S., Cooray, A., Scott, D., Peacock, J. A., Negrello, M., Smith, D. J. B., Benford, D., Amblard, A., Auld, R., Baes, M., Bonfield, D., Burgarella, D., Buttiglione, S., Cava, A., Clements, D., Dariush, A., de Zotti, G., Dye, S., Frayer, D., Fritz, J., Gonzalez-Nuevo, J., Herranz, D., Ibar, E., Ivison, R., Jarvis, M. J., Lagache, G., Leeuw, L., Lopez-Caniego, M., Pascale, E., Pohlen, M., Rodighiero, G., Samui, S., Serjeant, S., Temi, P., Thompson, M., & Verma, A. 2010, A&A, 518, L11+

Markevitch, M., Gonzalez, A. H., David, L., Vikhlinin, A., Murray, S., Forman, W., Jones, C., & Tucker, W. 2002, ApJ, 567, L27

Markevitch, M., Govoni, F., Brunetti, G., & Jerius, D. 2005, ApJ, 627, 733

Marriage, T. A., Acquaviva, V., Ade, P. A. R., Aguirre, P., Amiri, M., Appel, J. W., Barrientos, L. F., Battistelli, E. S., Bond, J. R., Brown, B., Burger, B., Chervenak, J., Das, S., Devlin, M. J., Dicker, S. R., Doriese, W. B., Dunkley, J., Dunner, R., Essinger-Hileman, T., Fisher, R. P., Fowler, J. W., Hajian, A., Halpern, M., Hasselfield, M., Hern'andez-Monteagudo, C., Hilton, G. C., Hilton, M., Hincks, A. D., Hlozek, R., Huffenberger, K. M., Hughes, D. H., Hughes, J. P., Infante, L., Irwin, K. D., Juin, J. B., Kaul, M., Klein, J., Kosowsky, A., Lau, J. M., Limon, M., Lin, Y., Lupton, R. H., Marsden, D., Martocci, K., Mauskopf, P., Menanteau, F., Moodley, K., Moseley, H., Netterfield, C. B., Niemack, M. D., Nolta, M. R., Page, L. A., Parker, L., Partridge, B., Quintana, H., Reese, E. D., Reid, B., Sehgal, N., Sherwin, B. D., Sievers, J., Spergel, D. N., Staggs, S. T., Swetz, D. S., Switzer, E. R., Thornton, R., Trac, H., Tucker, C., Warne, R., Wilson, G., Wollack, E., & Zhao, Y. 2010, ArXiv e-prints

Mehlert, D., Seitz, S., Saglia, R. P., Appenzeller, I., Bender, R., Fricke, K. J., Hoffmann, T. L., Hopp, U., Kudritzki, R., & Pauldrach, A. W. A. 2001, A&A, 379, 96

Meneghetti, M., Bartelmann, M., & Moscardini, L. 2003, MNRAS, 340, 105

Muchovej, S., Mroczkowski, T., Carlstrom, J. E., Cartwright, J., Greer, C., Hennessy, R., Loh, M., Pryke, C., Reddall, B., Runyan, M., Sharp, M., Hawkins, D., Lamb, J. W., Woody, D., Joy, M., Leitch, E. M., & Miller, A. D. 2007, ApJ, 663, 708

Narayan, R. & Bartelmann, M. 1996, ArXiv Astrophysics e-prints

Negrello, M., Hopwood, R., De Zotti, G., Cooray, A., Verma, A., Bock, J., Frayer, D. T., Gurwell, M. A., Omont, A., Neri, R., Dannerbauer, H., Leeuw, L. L., Barton, E., Cooke, J., Kim, S., da Cunha, E., Rodighiero, G., Cox, P., Bonfield, D. G.,

Jarvis, M. J., Serjeant, S., Ivison, R. J., Dye, S., Aretxaga, I., Hughes, D. H., Ibar, E., Bertoldi, F., Valtchanov, I., Eales, S., Dunne, L., Driver, S. P., Auld, R., Buttiglione, S., Cava, A., Grady, C. A., Clements, D. L., Dariush, A., Fritz, J., Hill, D., Hornbeck, J. B., Kelvin, L., Lagache, G., Lopez-Caniego, M., Gonzalez-Nuevo, J., Maddox, S., Pascale, E., Pohlen, M., Rigby, E. E., Robotham, A., Simpson, C., Smith, D. J. B., Temi, P., Thompson, M. A., Woodgate, B. E., York, D. G., Aguirre, J. E., Beelen, A., Blain, A., Baker, A. J., Birkinshaw, M., Blundell, R., Bradford, C. M., Burgarella, D., Danese, L., Dunlop, J. S., Fleuren, S., Glenn, J., Harris, A. I., Kamenetzky, J., Lupu, R. E., Maddalena, R. J., Madore, B. F., Maloney, P. R., Matsuhara, H., Michaowski, M. J., Murphy, E. J., Naylor, B. J., Nguyen, H., Popescu, C., Rawlings, S., Rigopoulou, D., Scott, D., Scott, K. S., Seibert, M., Smail, I., Tuffs, R. J., Vieira, J. D., van der Werf, P. P., & Zmuidzinas, J. 2010, Science, 330, 800

Negrello, M., Magliocchetti, M., Moscardini, L., De Zotti, G., Granato, G. L., & Silva, L. 2004, MNRAS, 352, 493

Nord, M. 2009, PhD thesis, University of Bonn

Nord, M., Basu, K., Pacaud, F., Ade, P. A. R., Bender, A. N., Benson, B. A., Bertoldi, F., Cho, H., Chon, G., Clarke, J., Dobbs, M., Ferrusca, D., Halverson, N. W., Holzapfel, W. L., Horellou, C., Johansson, D., Kennedy, J., Kermish, Z., Kneissl, R., Lanting, T., Lee, A. T., Lueker, M., Mehl, J., Menten, K. M., Plagge, T., Reichardt, C. L., Richards, P. L., Schaaf, R., Schwan, D., Spieler, H., Tucker, C., Weiss, A., & Zahn, O. 2009, A&A, 506, 623

Onaka, T. & Salama, A. 2009, Experimental Astronomy, 27, 9

Percival, W. J., Cole, S., Eisenstein, D. J., Nichol, R. C., Peacock, J. A., Pope, A. C., & Szalay, A. S. 2007, MNRAS, 381, 1053

Pérez-González, P. G., Egami, E., Rex, M., Rawle, T. D., Kneib, J., Richard, J., Johansson, D., Altieri, B., Blain, A. W., Bock, J. J., Boone, F., Bridge, C. R., Chung, S. M., Clément, B., Clowe, D., Combes, F., Cuby, J., Dessauges-Zavadsky, M., Dowell, C. D., Espino-Briones, N., Fadda, D., Fiedler, A. K., Gonzalez, A., Horellou, C., Ilbert, O., Ivison, R. J., Jauzac, M., Lutz, D., Pelló, R., Pereira, M. J., Rieke, G. H., Rodighiero, G., Schaerer, D., Smith, G. P., Valtchanov, I., Walth, G. L., van der Werf, P., Werner, M. W., & Zemcov, M. 2010, A&A, 518, L15+

Perlmutter, S., Aldering, G., Goldhaber, G., Knop, R. A., Nugent, P., Castro, P. G., Deustua, S., Fabbro, S., Goobar, A., Groom, D. E., Hook, I. M., Kim, A. G., Kim, M. Y., Lee, J. C., Nunes, N. J., Pain, R., Pennypacker, C. R., Quimby, R., Lidman, C., Ellis, R. S., Irwin, M., McMahon, R. G., Ruiz-Lapuente, P., Walton, N., Schaefer, B., Boyle, B. J., Filippenko, A. V., Matheson, T., Fruchter, A. S., Panagia, N., Newberg, H. J. M., Couch, W. J., & The Supernova Cosmology Project. 1999, ApJ, 517, 565

Petters, A. O., Levine, H., & Wambsganss, J. 2001, Singularity theory and gravitational lensing, ed. Petters, A. O., Levine, H., & Wambsganss, J.

Pierre, M., Valtchanov, I., Altieri, B., Andreon, S., Bolzonella, M., Bremer, M., Disseau, L., Dos Santos, S., Gandhi, P., Jean, C., Pacaud, F., Read, A., Refregier, A., Willis, J., Adami, C., Alloin, D., Birkinshaw, M., Chiappetti, L., Cohen, A., Detal, A., Duc, P., Gosset, E., Hjorth, J., Jones, L., Le Fèvre, O., Lonsdale, C., Maccagni, D., Mazure, A., McBreen, B., McCracken, H., Mellier, Y., Ponman, T., Quintana, H., Rottgering, H., Smette, A., Surdej, J., Starck, J., Vigroux, L., & White, S. 2004, JCAP, 9, 11

Pilbratt, G. L., Riedinger, J. R., Passvogel, T., Crone, G., Doyle, D., Gageur, U., Heras, A. M., Jewell, C., Metcalfe, L., Ott, S., & Schmidt, M. 2010, A&A, 518, L1+

Planck Collaboration. 2011a, ArXiv e-prints

—. 2011b, ArXiv e-prints

Planck Collaboration, Ade, P. A. R., Aghanim, N., Arnaud, M., Ashdown, M., Aumont, J., Baccigalupi, C., Balbi, A., Banday, A. J., Barreiro, R. B., & et al. 2011, ArXiv e-prints

Poglitsch, A., Waelkens, C., Geis, N., Feuchtgruber, H., Vandenbussche, B., Rodriguez, L., Krause, O., Renotte, E., van Hoof, C., Saraceno, P., Cepa, J., Kerschbaum, F., Agnèse, P., Ali, B., Altieri, B., Andreani, P., Augueres, J., Balog, Z., Barl, L., Bauer, O. H., Belbachir, N., Benedettini, M., Billot, N., Boulade, O., Bischof, H., Blommaert, J., Callut, E., Cara, C., Cerulli, R., Cesarsky, D., Contursi, A., Creten, Y., De Meester, W., Doublier, V., Doumayrou, E., Duband, L., Exter, K., Genzel, R., Gillis, J., Grözinger, U., Henning, T., Herreros, J., Huygen, R., Inguscio, M., Jakob, G., Jamar, C., Jean, C., de Jong, J., Katterloher, R., Kiss, C., Klaas, U., Lemke, D., Lutz, D., Madden, S., Marquet, B., Martignac, J., Mazy, A., Merken, P., Montfort, F., Morbidelli, L., Müller, T., Nielbock, M., Okumura, K., Orfei, R., Ottensamer, R., Pezzuto, S., Popesso, P., Putzeys, J., Regibo, S., Reveret, V., Royer, P., Sauvage, M., Schreiber, J., Stegmaier, J., Schmitt, D., Schubert, J., Sturm, E., Thiel, M., Tofani, G., Vavrek, R., Wetzstein, M., Wieprecht, E., & Wiezorrek, E. 2010, A&A, 518, L2+

Press, W. H. & Schechter, P. 1974, ApJ, 187, 425

Puget, J.-L., Abergel, A., Bernard, J.-P., Boulanger, F., Burton, W. B., Desert, F.-X., & Hartmann, D. 1996, A&A, 308, L5+

Radovich, M., Puddu, E., Romano, A., Grado, A., & Getman, F. 2008, A&A, 487, 55

Rawle, T. D., Chung, S. M., Fadda, D., Rex, M., Egami, E., Pérez-González, P. G., Altieri, B., Blain, A. W., Bridge, C. R., Fiedler, A. K., Gonzalez, A. H., Pereira, M. J., Richard, J., Smail, I., Valtchanov, I., Zemcov, M., Appleton, P. N., Bock, J. J., Boone, F., Clement, B., Combes, F., Dowell, C. D., Dessauges-Zavadsky, M., Ilbert, O., Ivison, R. J., Jauzac, M., Kneib, J., Lutz, D., Pelló, R., Rieke, G. H., Rodighiero, G., Schaerer, D., Smith, G. P., Walth, G. L., van der Werf, P., & Werner, M. W. 2010, A&A, 518, L14+

Reichardt, C. L., Ade, P. A. R., Bock, J. J., Bond, J. R., Brevik, J. A., Contaldi, C. R., Daub, M. D., Dempsey, J. T., Goldstein, J. H., Holzapfel, W. L., Kuo, C. L., Lange, A. E., Lueker, M., Newcomb, M., Peterson, J. B., Ruhl, J., Runyan, M. C., & Staniszewski, Z. 2009a, ApJ, 694, 1200

Reichardt, C. L., Zahn, O., Ade, P. A. R., Basu, K., Bender, A. N., Bertoldi, F., Cho, H.-M., Chon, G., Dobbs, M., Ferrusca, D., Halverson, N. W., Holzapfel, W. L., Horellou, C., Johansson, D., Johnson, B. R., Kennedy, J., Kneissl, R., Lanting, T., Lee, A. T., Lueker, M., Mehl, J., Menten, K. M., Nord, M., Pacaud, F., Richards, P. L., Schaaf, R., Schwan, D., Spieler, H., Weiss, A., & Westbrook, B. 2009b, ApJ, 701, 1958

Rephaeli, Y. 1995, ApJ, 445, 33

Rephaeli, Y. & Yankovitch, D. 1997, ApJ, 481, L55+

Rex, M., Ade, P. A. R., Aretxaga, I., Bock, J. J., Chapin, E. L., Devlin, M. J., Dicker, S. R., Griffin, M., Gundersen, J. O., Halpern, M., Hargrave, P. C., Hughes, D. H., Klein, J., Marsden, G., Martin, P. G., Mauskopf, P., Montaña, A., Netterfield, C. B., Olmi, L., Pascale, E., Patanchon, G., Scott, D., Semisch, C., Thomas, N., Truch, M. D. P., Tucker, C., Tucker, G. S., Viero, M. P., & Wiebe, D. V. 2009, ApJ, 703, 348

Rex, M., Rawle, T. D., Egami, E., Pérez-González, P. G., Zemcov, M., Aretxaga, I., Chung, S. M., Fadda, D., Gonzalez, A. H., Hughes, D. H., Horellou, C., Johansson, D., Kneib, J., Richard, J., Altieri, B., Fiedler, A. K., Pereira, M. J., Rieke, G. H., Smail, I., Valtchanov, I., Blain, A. W., Bock, J. J., Boone, F., Bridge, C. R., Clement, B., Combes, F., Dowell, C. D., Dessauges-Zavadsky, M., Ilbert, O., Ivison, R. J., Jauzac, M., Lutz, D., Omont, A., Pelló, R., Rodighiero, G., Schaerer, D., Smith, G. P., Walth, G. L., van der Werf, P., Werner, M. W., Austermann, J. E., Ezawa, H., Kawabe, R., Kohno, K., Perera, T. A., Scott, K. S., Wilson, G. W., & Yun, M. S. 2010, A&A, 518, L13+

Rieke, G. H., Alonso-Herrero, A., Weiner, B. J., Pérez-González, P. G., Blaylock, M., Donley, J. L., & Marcillac, D. 2009, ApJ, 692, 556

Rieke, G. H. & Lebofsky, M. J. 1979, ARA&A, 17, 477

Rieke, G. H., Young, E. T., Engelbracht, C. W., Kelly, D. M., Low, F. J., Haller, E. E., Beeman, J. W., Gordon, K. D., Stansberry, J. A., Misselt, K. A., Cadien, J., Morrison, J. E., Rivlis, G., Latter, W. B., Noriega-Crespo, A., Padgett, D. L., Stapelfeldt, K. R., Hines, D. C., Egami, E., Muzerolle, J., Alonso-Herrero, A., Blaylock, M., Dole, H., Hinz, J. L., Le Floc'h, E., Papovich, C., Pérez-González, P. G., Smith, P. S., Su, K. Y. L., Bennett, L., Frayer, D. T., Henderson, D., Lu, N., Masci, F., Pesenson, M., Rebull, L., Rho, J., Keene, J., Stolovy, S., Wachter, S., Wheaton, W., Werner, M. W., & Richards, P. L. 2004, ApJs, 154, 25

Riess, A. G., Filippenko, A. V., Challis, P., Clocchiatti, A., Diercks, A., Garnavich, P. M., Gilliland, R. L., Hogan, C. J., Jha, S., Kirshner, R. P., Leibundgut, B., Phillips, M. M., Reiss, D., Schmidt, B. P., Schommer, R. A., Smith, R. C., Spyromilio, J., Stubbs, C., Suntzeff, N. B., & Tonry, J. 1998, ApJ, 116, 1009

Rosati, P., Borgani, S., & Norman, C. 2002, ARA&A, 40, 539

Sayers, J., Golwala, S. R., Rossinot, P., Ade, P. A. R., Aguirre, J. E., Bock, J. J., Edgington, S. F., Glenn, J., Goldin, A., Haig, D., Lange, A. E., Laurent, G. T., Mauskopf, P. D., & Nguyen, H. T. 2009, ApJ, 690, 1597

Sazonov, S. Y. & Sunyaev, R. A. 1998, ApJ, 508, 1

Schneider, P., Ehlers, J., & Falco, E. E. 1992, Gravitational Lenses, ed. Schneider, P., Ehlers, J., & Falco, E. E.

Schneider, P., Kochanek, C. S., & Wambsganss, J. 2006, Gravitational Lensing: Strong, Weak and Micro, ed. Schneider, P., Kochanek, C. S., & Wambsganss, J.

Schwan, D., Ade, P. A. R., Basu, K., Bender, A. N., Bertoldi, F., Cho, H., Chon, G., Clarke, J., Dobbs, M., Ferrusca, D., Gusten, R., Halverson, N. W., Holzapfel, W. L., Horellou, C., Johansson, D., Johnson, B. R., Kennedy, J., Kermish, Z., Kneissl, R., Lanting, T., Lee, A. T., Lueker, M., Mehl, J., Menten, K. M., Muders, D., Pacaud, F., Plagge, T., Reichardt, C. L., Richards, P. L., Schaaf, R., Schilke, P., Sommer, M. W., Spieler, H., Tucker, C., Weiss, A., Westbrook, B., & Zahn, O. 2010, ArXiv e-prints

Schwan, D., Bertoldi, F., Cho, S., Dobbs, M., Guesten, R., Halverson, N. W., Holzapfel, W. L., Kreysa, E., Lanting, T. M., Lee, A. T., Lueker, M., Mehl, J., Menten, K., Muders, D., Myers, M., Plagge, T., Raccanelli, A., Schilke, P., Richards, P. L., Spieler, H., & White, M. 2003, New Astronomy Reviews, 47, 933

Scott, K. S., Austermann, J. E., Perera, T. A., Wilson, G. W., Aretxaga, I., Bock, J. J., Hughes, D. H., Kang, Y., Kim, S., Mauskopf, P. D., Sanders, D. B., Scoville, N., & Yun, M. S. 2008, MNRAS, 385, 2225

Serjeant, S., Dunlop, J. S., Mann, R. G., Rowan-Robinson, M., Hughes, D., Efstathiou, A., Blain, A., Fox, M., Ivison, R. J., Jenness, T., Lawrence, A., Longair, M., Oliver, S., & Peacock, J. A. 2003, MNRAS, 344, 887

Sheth, R. K. & Diaferio, A. 2001, MNRAS, 322, 901

Sheth, R. K., Mo, H. J., & Tormen, G. 2001, MNRAS, 323, 1

Sievers, J. L., Mason, B. S., Weintraub, L., Achermann, C., Altamirano, P., Bond, J. R., Bronfman, L., Bustos, R., Contaldi, C., Dickinson, C., Jones, M. E., May, J., Myers, S. T., Oyarce, N., Padin, S., Pearson, T. J., Pospieszalski, M., Readhead, A. C. S., Reeves, R., Shepherd, M. C., Taylor, A. C., & Torres, S. 2009, ArXiv e-prints

Silk, J. & White, S. D. M. 1978, ApJ, 226, L103

Siringo, G., Kreysa, E., De Breuck, C., Kovacs, A., Lundgren, A., Schuller, F., Stanke, T., Weiss, A., Guesten, R., Jethava, N., May, T., Menten, K. M., Meyer, H., Starkloff, M., & Zakosarenko, V. 2010, The Messenger, 139, 20

Siringo, G., Kreysa, E., Kovács, A., Schuller, F., Weiß, A., Esch, W., Gemünd, H.-P., Jethava, N., Lundershausen, G., Colin, A., Güsten, R., Menten, K. M., Beelen, A., Bertoldi, F., Beeman, J. W., & Haller, E. E. 2009, A&A, 497, 945

Skrutskie, M. F., Cutri, R. M., Stiening, R., Weinberg, M. D., Schneider, S., Carpenter, J. M., Beichman, C., Capps, R., Chester, T., Elias, J., Huchra, J., Liebert, J., Lonsdale, C., Monet, D. G., Price, S., Seitzer, P., Jarrett, T., Kirkpatrick, J. D., Gizis, J. E., Howard, E., Evans, T., Fowler, J., Fullmer, L., Hurt, R., Light, R., Kopan, E. L., Marsh, K. A., McCallon, H. L., Tam, R., Van Dyk, S., & Wheelock, S. 2006, ApJ, 131, 1163

Smail, I., Ivison, R. J., & Blain, A. W. 1997, ApJ, 490, L5+

Springel, V. & Farrar, G. R. 2007, MNRAS, 380, 911

Springel, V., White, S. D. M., Jenkins, A., Frenk, C. S., Yoshida, N., Gao, L., Navarro, J., Thacker, R., Croton, D., Helly, J., Peacock, J. A., Cole, S., Thomas, P., Couchman, H., Evrard, A., Colberg, J., & Pearce, F. 2005, Nature, 435, 629

Stanford, S. A., Eisenhardt, P. R., Brodwin, M., Gonzalez, A. H., Stern, D., Jannuzi, B. T., Dey, A., Brown, M. J. I., McKenzie, E., & Elston, R. 2005, ApJ, 634, L129

Staniszewski, Z., Ade, P. A. R., Aird, K. A., Benson, B. A., Bleem, L. E., Carlstrom, J. E., Chang, C. L., Cho, H., Crawford, T. M., Crites, A. T., de Haan, T., Dobbs, M. A., Halverson, N. W., Holder, G. P., Holzapfel, W. L., Hrubes, J. D., Joy, M., Keisler, R., Lanting, T. M., Lee, A. T., Leitch, E. M., Loehr, A., Lueker, M., McMahon, J. J., Mehl, J., Meyer, S. S., Mohr, J. J., Montroy, T. E., Ngeow, C., Padin, S., Plagge, T., Pryke, C., Reichardt, C. L., Ruhl, J. E., Schaffer, K. K., Shaw, L., Shirokoff, E., Spieler, H. G., Stalder, B., Stark, A. A., Vanderlinde, K., Vieira, J. D., Zahn, O., & Zenteno, A. 2009, ApJ, 701, 32

Sunyaev, R. A. & Zeldovich, Y. B. 1970, Ap&SS, 7, 3

—. 1972, Comments on Astrophysics and Space Physics, 4, 173

—. 1980, MNRAS, 190, 413

Swinbank, A. M., Smail, I., Longmore, S., Harris, A. I., Baker, A. J., De Breuck, C., Richard, J., Edge, A. C., Ivison, R. J., Blundell, R., Coppin, K. E. K., Cox, P., Gurwell, M., Hainline, L. J., Krips, M., Lundgren, A., Neri, R., Siana, B., Siringo, G., Stark, D. P., Wilner, D., & Younger, J. D. 2010, Nature, 464, 733

The Planck Collaboration. 2006, ArXiv Astrophysics e-prints

Tucker, W., Blanco, P., Rappoport, S., David, L., Fabricant, D., Falco, E. E., Forman, W., Dressler, A., & Ramella, M. 1998, ApJ, 496, L5+

Tucker, W. H., Tananbaum, H., & Remillard, R. A. 1995, ApJ, 444, 532

Vanderlinde, K., Crawford, T. M., de Haan, T., Dudley, J. P., Shaw, L., Ade, P. A. R., Aird, K. A., Benson, B. A., Bleem, L. E., Brodwin, M., Carlstrom, J. E., Chang, C. L., Crites, A. T., Desai, S., Dobbs, M. A., Foley, R. J., George, E. M., Gladders, M. D., Hall, N. R., Halverson, N. W., High, F. W., Holder, G. P., Holzapfel, W. L., Hrubes, J. D., Joy, M., Keisler, R., Knox, L., Lee, A. T., Leitch, E. M., Loehr, A., Lueker, M., Marrone, D. P., McMahon, J. J., Mehl, J., Meyer, S. S., Mohr, J. J., Montroy, T. E., Ngeow, C., Padin, S., Plagge, T., Pryke, C., Reichardt, C. L., Rest, A., Ruel, J., Ruhl, J. E., Schaffer, K. K., Shirokoff, E., Song, J., Spieler, H. G., Stalder, B., Staniszewski, Z., Stark, A. A., Stubbs, C. W., van Engelen, A., Vieira, J. D., Williamson, R., Yang, Y., Zahn, O., & Zenteno, A. 2010, ApJ, 722, 1180

Vieira, J. D., Crawford, T. M., Switzer, E. R., Ade, P. A. R., Aird, K. A., Ashby, M. L. N., Benson, B. A., Bleem, L. E., Brodwin, M., Carlstrom, J. E., Chang, C. L., Cho, H., Crites, A. T., de Haan, T., Dobbs, M. A., Everett, W., George, E. M., Gladders, M., Hall, N. R., Halverson, N. W., High, F. W., Holder, G. P., Holzapfel, W. L., Hrubes, J. D., Joy, M., Keisler, R., Knox, L., Lee, A. T., Leitch, E. M., Lueker, M., Marrone, D. P., McIntyre, V., McMahon, J. J., Mehl, J., Meyer, S. S., Mohr, J. J., Montroy, T. E., Padin, S., Plagge, T., Pryke, C., Reichardt, C. L., Ruhl, J. E., Schaffer, K. K., Shaw, L., Shirokoff, E., Spieler, H. G., Stalder, B., Staniszewski, Z., Stark, A. A., Vanderlinde, K., Walsh, W., Williamson, R., Yang, Y., Zahn, O., & Zenteno, A. 2010, ApJ, 719, 763

Vikhlinin, A., Voevodkin, A., Mullis, C. R., VanSpeybroeck, L., Quintana, H., McNamara, B. R., Gioia, I., Hornstrup, A., Henry, J. P., Forman, W. R., & Jones, C. 2003, ApJ, 590, 15

Voit, G. M. 2005, Reviews of Modern Physics, 77, 207

Weiß, A., Kovács, A., Coppin, K., Greve, T. R., Walter, F., Smail, I., Dunlop, J. S., Knudsen, K. K., Alexander, D. M., Bertoldi, F., Brandt, W. N., Chapman, S. C., Cox, P., Dannerbauer, H., De Breuck, C., Gawiser, E., Ivison, R. J., Lutz, D., Menten, K. M., Koekemoer, A. M., Kreysa, E., Kurczynski, P., Rix, H., Schinnerer, E., & van der Werf, P. P. 2009, ApJ, 707, 1201

Weiß, A., Kovács, A., Güsten, R., Menten, K. M., Schuller, F., Siringo, G., & Kreysa, E. 2008, A&A, 490, 77

White, D. A. & Fabian, A. C. 1995, MNRAS, 273, 72

Wilson, G. W., Hughes, D. H., Aretxaga, I., Ezawa, H., Austermann, J. E., Doyle, S., Ferrusca, D., Hernández-Curiel, I., Kawabe, R., Kitayama, T., Kohno, K., Kuboi, A., Matsuo, H., Mauskopf, P. D., Murakoshi, Y., Montaña, A., Natarajan, P., Oshima, T., Ota, N., Perera, T. A., Rand, J., Scott, K. S., Tanaka, K., Tsuboi, M., Williams, C. C., Yamaguchi, N., & Yun, M. S. 2008, MNRAS, 390, 1061

Wright, E. L. 1979, ApJ, 232, 348

Zeldovich, Y. B. & Sunyaev, R. A. 1969, Ap&SS, 4, 301

Zemcov, M., Rex, M., Rawle, T. D., Bock, J. J., Egami, E., Altieri, B., Blain, A. W., Boone, F., Bridge, C. R., Clement, B., Combes, F., Dowell, C. D., Dessauges-Zavadsky, M., Fadda, D., Ilbert, O., Ivison, R. J., Jauzac, M., Kneib, J., Lutz, D., Pelló, R., Pereira, M. J., Pérez-González, P. G., Richard, J., Rieke, G. H., Rodighiero, G., Schaerer, D., Smith, G. P., Valtchanov, I., Walth, G. L., van der Werf, P., & Werner, M. W. 2010, A&A, 518, L16+